

Evaluation of Root Zone Salinity Under Wheat Crop in Some Selected Fields in the Yuma Valley Irrigation Districts: A Modeling Study

D. Zerihun and C.A. Sanchez

dawit@ag.arizona.edu or sanchez@ag.arizona.edu

Abstract: Soil salinity can pose series limitations to crop production in irrigated soils. Mechanisms by which adverse effects of salinity are expressed include reduced root water uptake, poor soil permeability and tilth, and specific ion effects. Effective salinity management is a key component of optimal agronomic and irrigation management package in irrigated watersheds. Thus, the objective of the project reported here is to conduct a modeling study aimed at a preliminary point-scale analysis of the effectiveness of current salinity management practices in selected fields that are under wheat crop in the Yuma Valley Irrigation Districts. HYDRUS-1D - a physically based soil water flow and transport-reaction model is used here to simulate pertinent root zone soil processes. HYDRUS inputs for season-long simulation of the time-evolution of the root zone salinity of a cropped field (which include soils, crop, irrigation, meteorological, and events calendar data) were obtained from field and laboratory measurements, literature sources, HYDRUS databases, and were computed based on measured data. The measured data sets were derived from salinity data collected as part of a study conducted in the Yuma Valley Irrigation Districts in the winter and spring seasons of 2016 and 2017. From the data sets collected in these past years, two data-sets (labeled here as data sets I and II) were used in the current analysis. Results of the simulation study show that the seasonal average root zone salinity levels, expressed in terms of the electrical conductivity (EC) of the soil solution, are 2.8dS/m for data set I and 1.8dS/m for data set II. Assessment of salinity effects on crop yield suggests that, for both data sets, the average root zone salinity has no measurable adverse effect on crop yield. The seasonal average root zone sodium adsorption ratios, SAR , are $6.2\text{meq}^{0.5}/\text{L}^{0.5}$ for data set I and $5.1\text{meq}^{0.5}/\text{L}^{0.5}$ for data set II. The root zone average SAR of both data sets are not particularly high. However, a determination of the potential sodic risks, associated with the salt composition of the soil solution, based on the more rigorous criterion that takes into account the effects of the root zone average SAR and EC could not be made here. The leaching fractions, for the cropping season, are 27.1 and 50.7% for data sets I and II, respectively.

Contents

Chapter I. Introduction	6
1.1. Background and objectives	6
1.2. Method and data description	7
1.3. Results, Soil water	9
1.4. Results, Soil salinity	10
1.5. Result, Sodium adsorption ratio	11
1.6. Cumulative boundary fluxes, transpiration, and leaching fraction	12
1.7. Cautionary note	13
Chapter 2. Review: sources, effects, and management of salinity in irrigated soils	13
2.1. Salinity in irrigated soils: nature, sources, measurements, and effects on crop production	13
2.1.1. Nature and sources of salinity	13
2.1.2. Salinity indicator parameters and measurements	14
2.1.3. Effects of soil salinity on crops and soil physical properties of agronomic significance	17
2.1.3.a. Crop water stress and yield effects	17
2.1.3.b. Effects on soil permeability and tilth	18
2.1.2.c. Specific ion effect	19
2.2. Salinity management in irrigated soils	19
2.2.1. Salinity control in the crop root zone	19
2.2.2. Irrigation water quality considerations	21
2.3. Salinity modeling with HYDRUS-1D	23
2.3.1. Model Description	23
2.3.2. Model functionalities used in the current study	24
2.3.3. Soil water dynamics, equations and initial and boundary conditions	24
2.3.3.a. Equations	24
2.3.3.b. Initial and boundary conditions, soil water dynamics	26
<i>Initial conditions</i>	26
<i>Boundary conditions</i>	26
2.3.4. Coupled solute transport and reaction equations	28
2.3.4.a. Equations	28
2.3.4.b. Initial and boundary conditions, solute transport-reaction	29
<i>Initial conditions</i>	29
<i>Boundary conditions</i>	29

2.3.5. Model inputs	31
---------------------------	----

Chapter 3. A modeling study of root zone salinity in the Yuma

Valley Irrigation Districts	32
3.1. Introduction.....	32
3.2. Data Set I	34
3.2.1. Data description	34
3.2.1.a. Simulation duration and events calendar, data set I.....	34
3.2.1.b. Soils data, data set I	34
3.2.1.c. Irrigation data, data set I	39
3.2.1.d. Crop data, data set I	40
<i>Potential evapotranspiration, transpiration, and evaporation</i>	40
<i>Actual crop transpiration</i>	44
3.2.1.e. Meteorological data, data set I	46
3.2.2. Simulation results	46
3.2.2.a. Introduction	46
3.2.2.b. Soil water content, data set I.....	47
<i>Seasonal variation of root zone soil water content</i>	47
<i>Seasonal variation of root zone soil water. content in light of irrigation management</i>	50
3.2.2.c. Seasonal variation of root zone salinity and effects on crop yield, data Set I	51
<i>Seasonal variation of root zone salinity</i>	51
<i>Salinity effects on crop yield</i>	57
3.2.2.d. Sodium adsorption ratio and risk of sodicity, data set I.....	59
<i>Seasonal variability of root zone sodium adsorption ratio</i>	59
<i>Potential sodic hazard to the root zone soil profile</i>	61
3.2.2.e. Cumulative boundary fluxes, transpiration, and leaching fraction	62
<i>Cumulative boundary fluxes and transpiration</i>	62
<i>Leaching fraction</i>	63
3.2.2.f. Cautionary note	64
3.3. Data set II	65
3.3.1. Data Description	65
3.3.1.a. Simulation duration and events calendar, data set II	65
3.3.1.b. Soils data, data set II	65

3.3.1.c. Irrigation data, data set II	66
3.3.1.d. Crop data, data set II	69
3.3.1.e. Meteorological data, data set II	70
3.3.2. Simulation results, data set II	70
3.3.2.a. Introduction	70
3.3.2.b. Soil water content, data set II	72
<i>Seasonal variation of root zone soil water</i> <i>content</i>	72
<i>Seasonal variation of root zone soil water</i> <i>content in light of irrigation management</i>	74
3.3.2.c. Soil salinity and effects on crop yield, data set II	77
<i>Seasonal variation of root zone salinity</i>	77
<i>Salinity effects on crop yield</i>	80
3.3.2.d. Sodium adsorption ratio and risk of sodicity, data set II	80
<i>Seasonal variability of root zone sodium</i> <i>adsorption ratio</i>	80
<i>Potential sodic hazard to the root zone soil</i> <i>profile</i>	86
3.3.2.e. Cumulative boundary fluxes, transpiration, and leaching fraction	87
3.3.2.f. Cautionary note.....	88
 Chapter 4. Concluding remarks, summary, and cautionary note	89
4.1. Background and objectives.....	89
4.2. Method and data description.....	90
4.3. Results, Soil water.....	91
4.4. Results, Soil salinity.....	92
4.5. Result, Sodium adsorption ratio	94
4.6. Cumulative boundary fluxes, transpiration, and leaching fraction.....	95
4.7. Summary and cautionary note.....	96
 References ..	99

List of Tables

Table 1. Potential sodic hazard associated with irrigation water quality as a function of SAR_{iw} and EC_{iw}	23
Table 2. Applicable initial and boundary conditions, soil water dynamics	27
Table 3. Chemical species considered in the major-ion chemistry module of HYDRUS-1D and chemical species considered in the current study	30
Table 4. Applicable initial and boundary conditions, solute transport -reaction	31
Table 5a. Input data to the major-ion chemistry module of HYDRUS-1D, Data-set I	35
Table 5b. Input data to the major-ion chemistry module of HYDRUS-1D, Data-set I	36
Table 5c. Input data to the major-ion chemistry module of HYDRUS-1D, Data-set I	37
Table 6a. Input data to the major-ion chemistry module of HYDRUS-1D, Data-set II	67
Table 6b. Input data to the major-ion chemistry module of HYDRUS-1D, Data-set II	68
Table 6c. Input data to the major-ion chemistry module of HYDRUS-1D, Data-set II	69

List of Figures

Figure 1. (a) A comparison of the leaf area index of wheat crop calculated with Eq. 14 and measured data and (b) crop coefficient of durum wheat.....	41
Figure 2. Daily reference crop evapotranspiration, ET_o , precipitation, P , potential crop evapotranspiration, ET , potential transpiration, T , and potential evaporation, E , over the cropping season	43
Figure 3. Root water uptake stress response function (Feddes, 1978)	45
Figure 4. Seasonal variation of root zone soil water content at five observation points, data set I	49
Figure 5. Seasonal variation of root zone soil water content at five observation points superimposed on lines showing soil water constants of irrigation significance, Data set I	52
Figure 6. Seasonal variation in the electrical conductivity of the soil solution at five observation points, Data set I	54
Figure 7. Seasonal variation of root zone sodium adsorption ratio at five observation points, Data set I	60
Figure 8. Cumulative (running sum of) infiltration, transpiration, evaporation, evapotranspiration, and deep percolation fluxes.....	63
Figure 9. Daily reference crop evapotranspiration, ET_o , precipitation, P , potential crop evapotranspiration, ET , potential transpiration, T , and potential evaporation, E , over the cropping season	71
Figure 10. Seasonal variation of root zone soil water content at five observation points, data set II	73
Figure 11. Seasonal variation of root zone soil water content at five observation points superimposed on lines showing soil water constants of irrigation significance, Data set II	76
Figure 12. Seasonal variation in the electrical conductivity of the soil solution at five observation points, Data set II	78
Figure 13. Seasonal variation of root zone sodium adsorption ratio at five observation points, Data set I	81
Figure 14. Changes in the concentrations of the major cations (Ca , Mg , and Na) in the soil exchange complex and $Ca-CaCO_3$ in the upper 20cm layer of the crop root zone during the: (a) first, (b) third, and (c) fifth irrigation of data set II.....	84
Figure 15. Cumulative (running sum of) infiltration, transpiration, evaporation, evapotranspiration, and deep percolation fluxes	88

Chapter 1. Introduction

1.1. Background and objectives

Agriculture, specifically crop production, is an important sector of the local economy in Yuma, Arizona. Agriculture in the Yuma area is almost entirely dependent on irrigation water supply from the Colorado river, which contains dissolved salts. With an average electrical conductivity (EC_{iw}) of 1.1 to 1.3dS/m, the Colorado river water in Yuma can be considered a medium salinity water in terms of its suitability for crop production. In the project area, seasonal crop water requirements are typically applied, with surface or pressurized systems, in multiple irrigations distributed across cropping seasons. Because of the concentrating effects of evapotranspiration, which is particularly high in the Yuma area during the spring and summer months of the year, root zone salinity generally increases in the course cropping seasons.

Soil salinity can pose series limitations to crop production in irrigated soils. The adverse effects of salinity are expressed in terms of reduced root water uptake (owing to reduced osmotic potential of soil water), poor soil permeability and tilth associated with excess sodium in soils (leading to reduced infiltration rate, crop availability of soil water, and soil aeration), and specific ion effects (Rhoads, 1990). Thus, periodic leaching of salts from the crop root zone is widely practiced in the region to maintain favorable salt balance for optimal crop growth and yield. Effective leaching is particularly important in the Yuma area, because many crops grown in the area are sensitive to soil salinity (Sanchez and Silvertooth, 1996).

Optimal salinity management in irrigated soils, in principle, involves monitoring the salt load of irrigation water and the time evolution of salt concentrations in the root zone soil solution over a suitable time frame, such as a cropping season. A salinity management strategy that is wholly reliant on measured data is impractical, because the time and effort needed for field collection and laboratory analysis of such data and expenses incurred can be prohibitive. By comparison, a seasonal time-series data of root zone salinity with a sufficiently high resolution can be produced with a physically based coupled soil water dynamics and solute transport-reaction model (such as HYDURS-1D, Simunek et al., 2013) at a fraction of the time and effort needed if such data were to be produced through field studies. While measured data is essential, to gain insight and understanding that would inform the development and refinement of the

theories underlying mathematical models and, to calibrate and validate models; models, on the other hand, represent more flexible and inexpensive salinity evaluation, management, and research aid.

The overall objective of the project reported here is, thus, to conduct a modeling study aimed at a preliminary evaluation of the effectiveness of current salinity management practices in fields that are under wheat crop in the Yuma Valley Irrigation Districts. The specific objectives of the project are: (1) To conduct a simulation based point-scale analysis of the season-long evolution of root zone soil salinity under wheat crop in some selected fields (in the Yuma Valley Irrigation Districts) with a physically based mathematical model and (2) To assess potential adverse effects of root zone salinity, if any, on crop yield and soil physical properties of agronomic significance.

1.2. Method and data description

In the current study, HYDRUS-1D - a physically based mathematical model with the capability to simulate the coupled processes of soil water dynamics, solute transport, various soil physicochemical reactions (including complexation, cation exchange, and precipitation/dissolution of salts), and heat transport in variably saturated porous medium - is used to model pertinent root zone soil processes. The HYDRUS-1D simulation model, and its precursor UNSATCHEM (Simunek et al., 1996) were widely used to analyze the time-evolution of salinity and/or sodicity in agricultural soils and to evaluate alternative management practices (Goncalves et al., 2005; Corwin et al., 2007; Ramos et al., 2011; Oster et al., 2012; Rasouli et al., 2013) and reclamation scenarios (Simunek and Suarez, 1997).

HYDRUS-1D inputs for a season-long simulation of the time-evolution of the root zone salinity of a cropped field consists of soils, crop, irrigation, meteorological, and events calendar data. Specifically, HYDRUS input data are comprised of model parameters, initial and boundary conditions for both soil water dynamics and solute transport-reaction simulations, and limiting surface fluxes. In the current study, some of the model inputs were obtained through field and laboratory measurements and other inputs were derived from literature sources, HYDRUS databases, or were computed based on measured data. The measured salinity data, used in the simulation study presented here, was derived from data sets collected in the Yuma Valley Irrigation Districts in the winter and spring seasons of 2016 and 2017. From the data sets

collected over these past years, two data sets (labeled here as data sets I and II) were selected for use in the current analysis. Data set I is collected in a field located in the South Gila Valley and data set II is from a field in the Yuma Valley.

Both data sets I and II were collected in fields that were under (durum) wheat crop. Crop was grown in rectangular irrigation basins, measuring 650ft (198.1m) × 1250ft (381m) for data set I and 625ft (190.5m) × 895ft (272.8m) for data set II. The salinity simulation period, which is nearly the same as the length of the cropping season, spans 143 and 141 days for data sets I and II, respectively, and mainly straddled the winter and spring seasons of 2016-2017. The soils of the study sites are loam for data set I and sandy loam for data set II. Precipitation has minimal contribution to the seasonal water balance of the Yuma area, thus, irrigation is the primary source of water to meet the consumptive use needs of the crop. Seasonal crop water requirements were applied in five irrigation doses (for data set I) and six irrigations (for data set II), distributed across the cropping season.

Reference crop evapotranspiration and precipitation data, for data sets I and II, were downloaded from the Arizona Meteorological Network (AZMET) web portal for the weather stations that are closest to the study sites. Crop potential evapotranspiration was deduced from the reference evapotranspiration as a function of the crop coefficient, which vary from a minimum of 0.3 at season's end to 1.1 in the mid-season stage. The potential evapotranspiration was then partitioned into evaporation and transpiration components (which constitute separate input streams of HYDRUS-1D) as a function of the crop leaf area index (e.g., Simunek et al., 2013). HYDRUS computes actual transpiration as a function of the potential crop transpiration, the root water uptake distribution, and the crop's response to soil water and salinity stresses. In the current study, root water uptake distribution is modeled with the equation proposed by Hoffman and van Genuchten (1983) and the crop's soil water stress response is defined using the equation developed by Feddes (1978). Crop response to salinity stresses was considered here to be multiplicative to that of the soil water stress and is described with the equation presented by Maas (1990). Parameters of the soil water and salinity stress response functions were derived from HYDRUS-1D databases based on crop type.

1.3. Results, Soil water

The seasonal root zone soil water content variations, for both data sets I and II, show that irrigation events are marked by sharp increases in soil water contents, particularly in the upper soil layers of the profile. In these soil horizons, soil water contents reach saturation levels of 41cm/m (for data set I) and 38.8cm/m (for data set II) at the end of each irrigation event. By comparison, soil water contents generally decline with time, between irrigation events, due to the combined effects of crop transpiration, evaporation through the soil surface, and deep percolation through the bottom boundary of the root zone. The seasonal minima root zone soil water contents, which also occurred in the upper soil layers of the root zone profile, were 11.7cm/m for data set I and 12.2cm/m for data set II. For both data sets, relatively dry soil water contents were observed in the upper layers of the root zone early in the cropping season and toward the end of the season. The desiccation of the soil water content of the near surface soil horizons observed in the early part of the season was related to longer irrigation intervals. On the other hand, the relatively dry soil condition that occurred in the time period preceding crop harvest was due to increased evapotranspiration attributable to the warming spring weather. Overall, the simulation outputs showed that, for both data sets, soil water contents increased with depth from the soil surface.

In order to provide context for the observed seasonal variation of root zone soil water contents in light of irrigation management, the simulated soil water content data was compared with soil water constants of irrigation significance (including field capacity, wilting point, and the lower limit of the readily available soil water content). The comparison showed that, for both data sets I and II, root zone soil water contents over much of the cropping season fell within the readily available soil water range, suggesting a favorable soil water environment for crop growth. However, relatively dry soil conditions that approximate wilting point water contents (of 12.5 and 10cm/m for data sets I and II, respectively) were noted in the upper soil horizon over a period of weeks, early in the season and, prior to crop harvest. The relatively low soil water contents of the upper soil horizons in the early part of the cropping season and the resultant reduction in root water uptake, particularly for data set I, may have some effect on crop growth, if not yield, and hence may need to be looked into in follow-up studies. Furthermore, in data set

II, soil water contents well in excess of field capacity were observed in parts of the growing season, suggesting significant over irrigation.

The root zone soil water content profiles described here are results of simulation and are only partly based on measurements. It is, thus, important that the preceding observations on limited crop availability of soil water (in parts of the growing season) and its potential adverse effects on crops and the excess drainage below the crop root zone should be viewed only as cautionary notes.

1.4. Results, Soil salinity

Simulated seasonal root zone salinity profiles show that, for both data sets I and II, the soil solution electrical conductivity, *EC*, at the upper soil layers decreased sharply during irrigation events. The decline in the *EC* of the upper soil layers averaged over all irrigations of the season are 1.0 and 0.8dS/m for data sets I and II, respectively. The corresponding average *ECs* of the surface layers right after an irrigation event are 1.3dS/m (data set I) and 1.0dS/m (data sets II), respectively. Note that these values are well below the seasonal average root zone salinity of 2.8dS/m, for data set I, and 1.8dS/m, for data set II. The *EC* of the lower soil horizons showed little or no change during irrigations. The main mechanisms that led to the observed sharp decline in the *EC* of the upper soil layer of the root zone, during irrigation events, appear to be dilution of the soil solution, of the upper soil layers, by the incoming irrigation water and subsequent transport (leaching) of salts. However, computed data shows that soil physicochemical processes do have a contribution.

Overall, the root zone *EC*, for both data set I and II, showed increasing trends with time between irrigation events, typically peaking right before irrigation events. Generally, the time rate of increase in soil solution *EC* is highest in the upper soil layers and declined with depth. As a result, all root zone salinity extremes (a seasonal minimum of 1.2dS/m and maximum of 7.7dS/m for data set I and a minimum of 0.9 and a maximum of 4.2dS/m for data set II) were observed in the near surface soil horizons. The computed data also showed that the *EC* of the upper soil horizons are highly sensitive to surface fluxes and as a result the corresponding salinity profiles show occasional localized dips attributable to the dilution and leaching effects of natural precipitation events. On the other hand, precipitation events seem to have no discernible effects on the salinity of the lower lying profiles. Between irrigations, the increase in *EC* in the

upper soil horizons is mainly attributable to the concentrating effect of evapotranspiration on the soil solution. It is likely that in the lower sections of the root zone profile *EC* levels appears to be influenced more by downward transport (leaching) of salts.

Salinity effects on crop yield were evaluated here based on the seasonal average root zone *EC* that the crop encountered and the crop salt tolerance threshold. The seasonal average root zone *EC* for data set I is 2.8dS/m, which exceeds the crop salt tolerance threshold of 2.1dS/m for durum wheat (Maas, 1990) by a margin of 0.7dS/m. The corresponding relative yield calculated with the equation of Maas and Hoffman (1977) is 98.3%. By comparison, the seasonal mean root zone salinity for data set II is 1.8dS/m, which is less than the crop salt tolerance threshold. The implication is that root zone salinity of data set II had no adverse effect on crop yield. Overall, these results suggest that the average seasonal root zone salinity had no measurable adverse effects on crop yield in both fields.

1.5. Result, Sodium adsorption ratio (SAR)

For both data sets I and II, the simulated seasonal variation of the root zone sodium adsorption ratio, *SAR*, follows the same general trend with time as those of the *EC* data. Overall, the soil solution *SAR* increased between irrigation events throughout the root zone. Furthermore, the time rate of increase in *SAR* is highest in the upper soil horizons and is more pronounced toward the end of the cropping season. As a result, the seasonal maximum *SAR* of 9.2 and 7.6meq^{0.5}/L^{0.5} for data sets I and II, respectively, occurred in the upper soil layers and were observed right before crop harvest. Generally, the simulated data shows that, for both data sets, the root zone *SAR* increased during the season.

The *SAR* profile, of data set I, shows that in the upper soil horizon of the root zone, *SAR* declined slightly during each irrigation event, however, it showed no discernible change over much of the lower section of the soil profile. The average decrease in the *SAR* over the upper 20cm soil layer across all irrigations is 0.18 meq^{0.5}/L^{0.5} and the maximum decrement is 0.35meq^{0.5}/L^{0.5}. By contrast, the soil solution *SAR* in the upper soil horizon, of data sets II, showed an appreciable increase during irrigation events, with an average and maximum increments of 0.35meq^{0.5}/L^{0.5} and 0.82meq^{0.5}/L^{0.5}, respectively. The results suggest that a

complex interaction of solute transport and soil physicochemical processes underlie the changes in the soil solution *SAR* observed during irrigation events.

A closer look at the output data of HYDRUS-1D shows that, in both data sets, precipitation of calcium as calcium carbonate, during irrigation, is the most significant soil physicochemical process in terms of its effect on *SAR*. Furthermore, for both data sets the net effect of cation exchange on *SAR* was shown to be limited. Overall, the results show that the interactive effects of calcite precipitation and transport (advection and dispersion) of salts are the main determinant of *SAR* in the upper soil layers during irrigation events. Thus, the soil physicochemical reactions in concert with transport processes appeared to have led to changes in the concentration of calcium, magnesium, and sodium in the soil solution in such proportions that the resultant *SAR* decreased in data set I and increased in data set II.

The seasonal average root zone *SAR* for data set I is $6.2\text{meq}^{0.5}/\text{L}^{0.5}$. By comparison, the seasonal average root zone *SAR*, for data set II, is $5.1\text{meq}^{0.5}/\text{L}^{0.5}$. The seasonal average root zone *SAR* of both data sets are not particularly high. However, a more rigorous evaluation of sodic risks needs to take into account not only the soil solution *SAR*, but also the corresponding *EC*. Essington (2005) described a sodic soil as one with a *SAR* exceeding 13 to $15\text{meq}^{0.5}/\text{L}^{0.5}$ and an *EC* of 4dS/m or less. While the average root zone *SAR* for both data sets I and II are well under the indicated upper limit, the seasonal average root zone *EC* of 2.8dS/m (data set I) and 1.8dS/m (data set II) are, nonetheless, less than the 4dS/m lower bound by an appreciable margin. Evidently, this leaves us with a degree of uncertainty on how to characterize the potential sodic hazard posed by the root zone soil solution salt composition. However, based on the observed *SAR* and *EC* levels the potential for limited adverse effects on soil structure and hydraulic properties cannot be entirely ruled out.

1.6. Cumulative boundary fluxes, transpiration, and leaching fraction

Computed cumulative fluxes (i.e., the running sum of fluxes) that leave the crop root zone through its upper and lower boundaries and the crop canopy were examined to assess the seasonal leaching fraction. These include cumulative infiltration, evaporation, deep percolation, and transpiration fluxes. A close examination of the data shows that the seasonal cumulative infiltration fluxes accounted for 100 and 99.9% of the cumulative outgoing fluxes, from the root

zone, of data sets I and II, respectively. The corresponding seasonal leaching fractions are 27.1% for data set I and 50.7 % for data set II. Note that the large leaching fraction in data set II is consistent with the relatively low seasonal average root zone *EC* of 1.8dS/m, which is not only about two-thirds of the root zone average *EC* of data set I, but it is also well under the 2.1dS/m salt tolerance threshold of durum wheat.

1.7. Cautionary note

It is important to put the results presented here, with regard to soil salinity and sodicity risks, in perspective. Many of the model inputs were obtained through measurements. Other inputs were obtained either from literature sources, model databases, or calculated based on measurements. The seasonal *SAR*, *EC*, fluxes, and soil water distribution data used in the current analyses were derived through simulations.

In essence, the results and observations stemming from the current study are only partly based on measured data and are not complemented with crop growth and yield data. Hence, they need to be treated only as useful insights that can help in identifying potential problems and guiding future studies. Furthermore, the current study is limited to point-scale analysis and as such the results cannot be directly generalized for an entire field, without the assumption that the surface boundary conditions, initial conditions, and the soil physical and chemical parameters of the sampling node (used in the current analysis) are replicated fully or substantially across the field.

Chapter 2. Review: sources, effects, and management of salinity in irrigated soils

2.1. Salinity in irrigated soils: nature, sources, measurements, and effects on crop production

2.1.1. Nature and sources of salinity

Soil salinity refers to the occurrence of soluble salts in soils, and specifically to the concentration of salts in the soil solution. Irrigated soils, including those in the Yuma area,

generally contain soluble mineral salts to a varying degree, the common constituents being those derived from salts of the alkaline and alkaline-earth metals. The main cationic species found in the root zone solution of these soils are Ca^{2+} , Mg^{2+} , Na^+ , and K^+ and the primary anions are Cl^- and SO_4^{2-} , HCO_3^- , NO_3^- , and at higher pH, CO_3^{2-} (Jurinak, 1990, Essington, 2005). In addition, saline soils may also contain various other metals and nonmetals in trace amounts (Deverel and Fuji, 1990). Salts found in the crop root zone of these soils may originate from a combination of sources. They could be products of in-situ mineral weathering and dissolution of salts. Other sources include application of fertilizers, atmospheric deposition, and saline water intrusion into the root zone through capillary rise from a shallow saline water table, among others. Importantly, salt input through irrigation is generally considered a key factor in root zone salinity of irrigated soils.

Salinity can pose series limitations to the productivity and sustainability of irrigated agriculture. The adverse effects of salinity express themselves in terms of reduced root water uptake (osmotic effect), poor soil permeability and tilth (sodic effect), and specific ion effects. The deleterious outcomes of salinity on crop production may range from reduced vegetative growth and limited yield loss, to crop failure, and abandoned cultivated lands (Rhoades and Loveday, 1990). Thus, salinity management aimed at maintaining root zone salinity levels under a set threshold, required for optimal crop production, is an essential component of an effective agronomic and irrigation management package in irrigated watersheds.

2.1.2 Salinity indicator parameters and measurements

Salinity management in irrigated soils, in principle, involves monitoring the salt load of incoming irrigation water (salinity of irrigation water) and the time evolution of the salt concentration of the soil solution in the crop root zone (soil salinity) over a suitable time frame, such as a cropping season. Salinity indicator parameters widely used for management purposes mainly include those that measure the bulk electrolyte concentration and the concentration of the monovalent cation, sodium (Na^+), relative those of the divalent cations, calcium (Ca^{2+}) and magnesium (Mg^{2+}), in irrigation waters and in the soil solution. The total electrolyte concentration of solutions is a measure of the adverse effect of salts on root water uptake, while the concentration of Na^+ relative to those of Ca^{2+} and Mg^{2+} is used to appraise the deleterious effects of sodium on soil physical properties of agronomic significance, such as soil permeability

and tilth. Note that for convenience, sodicity (which refers to the presence of excess sodium, relative to calcium and magnesium, in the soil exchange complex) is treated here as a particular case of the more general problem of salinity.

The overall electrolyte concentration of solutions can be expressed in terms of the concentrations of total dissolved salts (*TDS*). However, electrical conductivity of solutions (*EC*), a physical property of solutions that is correlated with electrolyte concentrations and is a readily measurable quantity, is commonly used to evaluate bulk salt concentrations in irrigation water and soil solutions (Hanson et al., 2006; Tanji, 1990). Electrical conductivity of solutions are commonly measured in dS/m or mmho/cm. Functional relationships exist that can be used to relate electrical conductivities of irrigation water or soil solutions to total concentrations of dissolved salts and to correct for temperature effects, when measurements are made in nonstandard conditions (Hanson et al., 2006).

Various methods, both direct and indirect, have been developed for measuring soil salinity under field and laboratory conditions (Robbins, 1990; Corwin, 2003). Most indirect methods are used in the concurrent in-situ measurements of salinity and other soil physical parameters (mainly, water content), based on the electromagnetic properties of the liquid and solid phases of soils. Important methods in this category include the time domain reflectometry (*TDR*) and the electromagnetic induction (*EMI*) methods (Corwin, 2003). However, the most widely used method for point-scale salinity determination is one based on measurements of electrical conductivity (to ascertain bulk electrolyte concentrations) and chemical analysis of solutions extracted from the saturated paste of soil samples (to determine concentrations of specific ions). Note that the indirect methods can be used to determine only the total salt concentration of the soil and do not provide data on the concentrations of specific ions in the soil solution.

Electrical conductivity of irrigation water can be measured directly with electrical conductivity salinity sensors, while the *EC* of soil solutions is typically approximated based on measurements made on solution samples extracted from a saturated soil paste. Generally, the electrical conductivity of the saturated paste extract, *EC_e*, is different from that of the in-situ soil solution. The rule of thumb for estimating the electrical conductivity of the in-situ soil solution, *EC_{sw}*, from *EC_e* assumes that the *EC_{sw}* at field capacity water content is twice *EC_e* (e.g., Ayers and Westcot, 1985; Ramos et al., 2011).

Exchangeable sodium percentage (*ESP*, %), the percentage of the cation exchange capacity (*CEC*) of the soil exchange complex that is occupied by Na^+ , Eq. 1, is a direct measure of the sodic hazard to soil physical properties.

$$ESP = \frac{[NaX]}{CEC} 100 \quad (1)$$

where $[NaX]$ is the concentration of sodium ion on the exchange complex (*meq/kg of soil*) and *CEC* is the total concentration of adsorbed cation charge that can be displaced per unit mass of the exchange complex (*meq/kg*). Generally, the *CEC* of irrigated soils is approximated by the sum of the concentrations of the major cations (Ca^{2+} , Mg^{2+} , Na^+ , and K^+) that are predominant on the exchange complex of these soils.

Sodium adsorption ratio (*SAR*), a parameter related to *ESP* and a more readily determinable quantity, is commonly used to characterize sodic conditions in soils (Essington, 2005). *SAR* ($meq^{0.5}/L^{0.5}$), defined as the concentration of Na^+ relative to the concentrations of Ca^{2+} and Mg^{2+} in soil solutions, is expressed as

$$SAR = \frac{[Na^+]}{\left(\frac{[Ca^{2+}] + [Mg^{2+}]}{2}\right)^{0.5}} \quad (2)$$

where $[.]$ is the concentrations of Na^+ , Ca^{2+} , and Mg^{2+} ions in the soil solution (*meq/L*). Sodium adsorption ratio, *SAR*, is also used to evaluate irrigation water quality relative to potential sodic hazard.

In addition to the salinity indicator parameters of *EC* and *SAR*, concentrations of the individual ions and some of the trace elements in the soil solution may need to be determined to assess specific ion effects on crops. While the concentration of these cations in irrigation water can be directly measured with standard analytical methods, their concentrations in the soil solution is typically estimated based on measurements made on solution samples extracted from a saturated soil paste.

As will be shown in subsequent discussions, the salinity indicator parameters defined here are generally used to evaluate the potential adverse effects of salinity on crop production and soil physical properties and in establishing irrigation water quality criteria and soil salinity thresholds for use in effective management.

2.1.3. Effects of soil salinity on crops and soil physical properties of agronomic significance

The mechanisms through which the adverse effects of salinity on crop production are expressed include: salinity induced crop water stress, soil aggregate instability and clay mineral dispersion caused by the presence of excess sodium in the soil exchange complex, and specific ion effects.

2.1.3.a. Crop water stress and yield effects

Increases in soil salinity leads to reduced osmotic potential of the soil water and hence to a reduced total soil water potential. In other words, increases in soil salinity results in a diminished potential difference across the soil-water-root interface. The implication is that, all things (i.e., including the soil water pressure) being equal, the plant needs to expend more energy per unit volume of water extracted from a saline soil than would have been the case under a non-saline condition. Traditionally, soils are considered saline if the *EC* of the soil solution exceeds 4mmhos/cm (Richards, 1954). However, subsequent studies have revealed that crop response to salinity induced water stress varies and is modulated by such factors as agronomic and irrigation management and climate. Generally, most crops have a degree of tolerance to salinity and yield loss is expected to occur only when the root zone soil salinity exceeds some finite threshold (Maas, 1990). Furthermore, for soil salinity levels exceeding the crop salt tolerance threshold, yield loss was shown to be a linear decreasing function of salinity. Accordingly, a function of the form given in Eq. 3, proposed by Maas and Hoffman (1977), is widely used to express crop yield, at a specific root zone salinity level, as a percentage of the potential maximum

$$\Delta = \begin{cases} 100 & \text{for } \beta \geq \overline{EC_e} \\ \text{and} & \\ 100 - \alpha(\overline{EC_e} - \beta) & \text{for } \beta < \overline{EC_e} \end{cases} \quad (3)$$

In Eq. 3, Δ is the relative yield under a specific root zone salinity (%); $\overline{EC_e}$ (dS/m) is the root zone average electrical conductivity of the saturation extract and reflects the average root zone salinity that the crop encounters during most of the season after the crop has been well established under non-saline conditions (Hanson et al., 2006); α is the slope of the relative yield curve, i.e., percent decrease in crop yield from the maximum per unit increase in salinity in excess of β (dS/m)⁻¹; and β is crop salt tolerance, i.e., threshold root zone salinity level beyond which crop yield loss occurs (dS/m).

The relative yield equation can be used to determine yield loss that would occur when a crop is grown in a soil of specific root zone salinity, $\overline{EC_e}$, as compared to the potential maximum yield. In principle, the potential maximum yield is one that is obtainable under an equivalent non-saline condition (i.e., a root zone salinity level that is less than a threshold), in which cultural and management practices emulate those recommended for commercial production. Estimates of crop specific values of α and β for various crops were reported by Maas (1990) and Hanson et al. (2006) for use as a guideline in salinity management. Note that the relative yield equation can also be used to determine the root zone salinity level corresponding to a preset level of tolerable crop yield loss.

2.1.3.b. Effects on soil permeability and tilth

When the soil exchangeable sodium percentage, ESP , exceeds a threshold, aggregate instability (deflocculation) and clay mineral dispersion occurs. Resultant changes in the soil physical properties, such as poor permeability, will then lead to reduced infiltration, soil water movement, crop availability of soil water, and soil aeration. High ESP also results in poor soil tilth (soil friability). Traditionally, soils with an ESP exceeding 15% are designated as sodic (Richards, 1954). However, the effect of sodium on soil physical properties is confounded by many factors, including clay mineralogy of the soil and alkalinity among others, but importantly

by electrolyte concentration of the soil solution (Essington, 2005). Salinity has a moderating influence on the deleterious effects of excess sodium on soil physical properties. In other words, all things being equal, for a given *ESP*, the higher the electrolyte concentration of the soil solution (i.e., the higher the *EC*), the less destructive the effects of excess sodium would be on soil structure. Thus, the exchangeable sodium percentage at which aggregate instability and clay dispersion ensues is closely related to the salinity of the soil solution.

As noted earlier, instead of *ESP* of a soil, sodium adsorption ratio, *SAR*, of the soil solution is commonly used to characterize potential sodic risks in soils. Accordingly, Essington (2005) suggested that overall a soil with a *SAR_e* that is greater than 13 to $15\text{meq}^{0.5}/\text{L}^{0.5}$ and an *EC_e* less than 4dS/m can be considered sodic.

2.1.3.c. Specific ion effect

In addition to the adverse effects on root water uptake and soil physical properties, the occurrence of specific solutes in the soil solution in concentrations that exceed crop specific thresholds (Maas, 1990; Hanson et al., 2006) can lead to toxic effects and nutritional imbalances on crops. Sodium and chloride ions can have damaging effect on some crops if accumulated in plant tissues in toxic levels. Sodium can cause nutritional imbalances by discouraging the absorption of calcium, potassium, and magnesium. Furthermore, boron an essential plant nutrient can be toxic to crops if present in the soil solution in amounts that barely exceed the optimal concentrations (Maas, 1990). However, discussion on specific ion effects is not within the scope the current study, thus will not be considered further.

2.2. Salinity management in irrigated soils

2.2.1. Salinity control in the crop root zone

Salt input associated with irrigation is considered an important source of salinity in irrigated soils and as such irrigation water quality is generally treated as a major salinity management parameter. Generally, the concentration of soluble salts in the soil solution, particularly in the upper layers of the root zone, increases over time following irrigation events as soil water is depleted through evaporation and crop transpiration. Thus, effective salinity management practice is key to, maintaining a favorable root zone salt balance over a cropping

season and, preventing the adverse effects of salinity on crop growth and yield and on soil physical properties of agronomic significance.

Scheduled periodic leaching of soluble salts that have accumulated in the crop root zone is the primary salinity control/management method in irrigated agriculture. Typically, equations deduced under a quasi-steady state assumption are used to estimate the irrigation depth that needs to be applied (in excess of the crop consumptive use needs over a prescribed salinity management time frame) to effect adequate leaching of salts from the crop root zone. Under the quasi-steady state assumption salt influx to, efflux from, and production and loss in the crop root zone are presumed to balance out over the salinity management time frame (e.g., a cropping season). The quasi-steady state assumption was further coupled, with the notion that the contributions of salt influx pathways, other than irrigation, to the overall salt balance are negligible, and that the net effect of the interaction between the soil physicochemical processes and crop removal of salts on the electrolyte concentrations of the soil solution are marginal, to derive an equation for leaching fraction (e.g., Rhoades, 1974)

$$LF = \frac{D_{dw}}{D_{iw}} = \frac{EC_{iw}}{EC_{dw}} \quad (4)$$

In Eq. 4, LF is the fraction of the applied irrigation water that needs to pass through the root zone, during a salinity management time frame, to ensure salt balance [-]; D_{dw} is the depth of drainage water that left the root zone during the salinity management time frame [L^3]; D_{iw} is the depth of irrigation water applied during the salinity management time frame [L^3]; EC_{iw} is the electrical conductivity of irrigation water (dS/m); and EC_{dw} is the electrical conductivity of drainage water (dS/m).

Considering a scenario in which the assumptions mentioned earlier are adequately satisfied, application of the LF ensures that the average root zone salinity remains unchanged over a salinity management time frame. However, it does not necessarily lead to an average root zone salt content that is within a prescribed threshold, which is a requirement to prevent crop yield loss or limit losses within an acceptable range. Rhoades (1974) introduced an expression for the maximum allowable electrical conductivity of the drainage water, EC_{dw} , if the average

root zone electrical conductivity of the saturated extract is to remain within a prescribed threshold.

$$EC_{dw} = 5\xi - EC_{iw} \quad (5)$$

where ξ is the threshold root zone average electrical conductivity of the saturation extract that does not adversely impact crop yield. As noted earlier, ξ can be set to a level that limits yield loss to a degree considered tolerable or to the crop salt tolerance threshold, β . Substituting Eq. 5 in 4 yields an expression for the leaching requirement, LR :

$$LR = \frac{EC_{iw}}{5\xi - EC_{iw}} \quad (6)$$

where LR is the minimum LF needed to maintain a root zone salinity that does not adversely impact potential crop yield [-].

Threshold root zone salinity levels for ensuring potential crop yield, expressed in terms of the average EC of the root zone saturation extracts, vary from 1.5dS/m for sensitive to 10dS/m for tolerant crops (Essington, 2005). As can be noted from Eqs. 4 to 6, both salt build up in the crop root zone and leaching requirement are functions of irrigation water quality, EC_{iw} , which underlines the significance of irrigation water quality as a salinity management parameter.

While salinity control in irrigated agriculture generally requires the provision of adequate leaching and drainage in combination with suitable agronomic practices, the mitigation of sodic effects may, on the other hand, require the application of chemical amendments, specifically gypsum and calcite (e.g., Simunek and Suarez, 1997). However, remediation of sodic soils in irrigated fields is outside the scope of the current study. Furthermore, sodic conditions are not common in the Yuma area.

2.2.2. Irrigation water quality considerations

As noted earlier, irrigation water quality is an important consideration in salinity management of irrigated soils. From the standpoint of salinity, the quality of water supplies for irrigation use is assessed based on the potential risks for soil salinization and sodification. The bulk concentration of salts, (expressed in terms of EC) and the concentration of the sodium ion

relative to those of calcium and magnesium ions (defined in terms of *SAR*) are the two key irrigation water quality indicator parameters. However, quality assessments of irrigation water, or development of an irrigation water quality metrics, for a specific application needs to consider the *EC* and *SAR* of the irrigation water along with crop variety, soil type, irrigation and agronomic management practices, and climatic factors. Ayers and Westcot (1985), for instance, examined the relationship between irrigation water salinity level, *LF*, and crop sensitivity to salinity assuming a 40-30-20-10% vertical distribution of root water uptake by crops. The results showed that for any given crop increasing the leaching fraction would allow the use of relatively marginal quality water for irrigation without causing adverse effects on crop yield. Similar results were presented by Rhoades (1982) on the relationships between EC_{iw} , *LF*, and crop sensitivity to salinity under conditions of high frequency irrigation. These observations underscore the significance of effective salinity management in mitigating the potential risks, of using relatively poor-quality irrigation water, to crop production,

A general guideline that can be used to make preliminary assessment of the potential salinity risk to crop production associated with the use of saline irrigation waters is provided by the University of California Committee of Consultants (1974). Accordingly, irrigation water with *EC* that is less than 0.7dS/m is deemed a low-salinity water and no restriction is recommended with regard to the type of crop it can be used to irrigate. Medium salinity water, with *EC* ranging between 0.7 and 3dS/m is considered to have detrimental effects on salt sensitive crops, thus require careful management. Irrigation water supplies with *EC* exceeding 3dS/m are treated as waters of high salinity with sever potential problems to cope, hence they can be used only with salt tolerant crops. Classification of crops according to their tolerance to salts in the soil solution can be found in the salinity literature (e.g., Maas, 1990; Hanson et al., 2006).

There exists a broad guideline that uses the *EC* and *SAR* of irrigation water to assess irrigation water quality as related to potential sodic hazard (e.g., Ayars and Westcot, 1985). A summary of this guideline is presented in Table 1. Overall, the guideline shows that irrigation water with relatively high sodium adsorption ratio, SAR_{iw} , can be used safely for irrigation purposes (i.e., without impacting soil physical properties adversely), if the electrolyte concentration of the irrigation water, EC_{iw} , is also sufficiently high.

Table 1. Potential sodic hazard associated with irrigation water quality as a function of SAR_{iw} and EC_{iw}

SAR_{iw} ($meq^{0.5}/L^{0.5}$)	Sodic risk		
	None	Slight to moderate	Severe
	EC_{iw} (dS/m)		
0-3	>0.7	0.7-0.2	<0.2
3-6	>1.2	1.2-0.3	<0.3
6-12	>1.9	1.9-0.5	<0.5
12-20	>2.9	2.9-1.3	<1.3
20-40	>5	5.0-2.9	<2.9

2.3. Salinity modeling with HYDRUS-1D

As noted earlier, effective salinity management in irrigated soils requires monitoring the salt load of irrigation water and the time evolution of salt concentrations in the root zone soil solution over a suitable time frame, such as a cropping season. A salinity management strategy that is entirely dependent on measured data is impractical, because the required time and effort and expenses incurred can be prohibitive. Although measured data is essential, to gain insight and understanding on pertinent soil processes and to calibrate and validate models; models, on the other hand, represent more flexible and inexpensive salinity evaluation, management, and research aid. Accordingly, HYDRUS-1D (Simunek et al., 2013) - a mathematical model with the capability to simulate the coupled processes of soil water dynamics, solute transport and various soil physicochemical process, and heat transport in variably saturated porous medium – was used in the modeling study reported here.

2.3.1. Model Description

The soil water dynamics module of HYDRUS-1D can simulate steady and transient flows, under equilibrium and nonequilibrium conditions, accounting for root water uptake as modulated by soil water pressure and osmotic potential. HYDRUS can also model the transport of solutes involving uncoupled sequential chain reactions and plant solute uptake. Solute transport and reaction takes place in the aqueous, solid, and gas phases. HYDRUS can also

simulate carbon dioxide transport and production in the soil profile and its effects on major-ion chemistry.

Important soil physicochemical processes simulated with the major-ion chemistry module of HYDRUS-1D include complexation in the soil solution, precipitation/dissolution of mineral salts, and cation exchange involving major cations found in soils as a function of soil physical and chemical properties. It also has provisions to model the net effect of those processes on the potential development of sodic conditions as it relates to soil hydraulic properties.

The model is capable of simulating heat transport through the soil profile, producing soil temperature distribution profiles as a function time, which is then used to correct for temperature effects on reaction rate and equilibrium constants and hydraulic conductivities during each computational time step.

In the current study, however, only a limited subset of the capabilities of HYDRUS-1D was used.

2.3.2. Model functionalities used in the current study

The soil physical processes considered in the study reported here consist of transient flow in variably saturated porous medium and chemical reactions that are important in the chemistry of salt affected soils, generally described in the HYDRUS-1D literature as major-ion chemistry. Soil water dynamics simulations account for surface fluxes (infiltration and evaporation) along with crop root water uptake and drainage through the bottom boundary of the simulation domain. Flow and transport in soils were treated as physical equilibrium processes. Gas phase transport of constituents as well as carbon dioxide production and transport were not considered. Instead, carbon dioxide concentration was assumed constant through the soil profile at the same level as the partial pressure of carbon dioxide in the atmosphere. Flow and solute transport were treated as isothermal processes taking place at standard conditions (i.e., heat transport is not simulated).

2.3.3. Soil water dynamics, equations and initial and boundary conditions

2.3.3.a. Equations

The soil water dynamics module of HYDRUS-1D (Simunek et al., 2013), which simulates soil water movement and retention in variably saturated soils, is based on a numerical

solution of the one-dimensional form of Richards' equation with a sink term that accounts for root water uptake. Assuming isothermal conditions and negligible vapor flow, the equation is given as

$$\frac{\partial \theta}{\partial t} = \frac{\partial}{\partial x} \left(K(h) \left(\frac{\partial h}{\partial x} + \cos \phi \right) \right) - S \quad (7)$$

In Eq. 7, θ is soil water content [L^3/L^3]; t is time [T]; x is distance [L]; h is soil water pressure head [L]; $K(h)$ is the unsaturated hydraulic conductivity [L/T]; ϕ is the angle between the vertical and the flow direction (*rad*); and S is the sink term accounting for root water uptake [$L^3/L^3/T$].

HYDRUS provides multiple options to model the soil water retention curve, $\theta(h)$. However, the van Genuchten model, Eq. 8, is used in the current study

$$\theta = \begin{cases} \theta_r + \frac{\theta_s - \theta_r}{(1 + |\alpha h|^n)^m} & \text{for } h < 0 \\ \theta = \theta_s & \text{for } h \geq 0 \end{cases} \quad (8)$$

were θ_r and θ_s are residual and saturation moisture contents [L^3/L^3], respectively; and α , n , and m are empirical parameters. The unsaturated hydraulic conductivity, $K(h)$, is then described in terms of the van Genuchten-Mualem model

$$K(h) = K_s (S_e)^l \left(1 - \left(1 - (S_e)^{\frac{1}{m}} \right)^m \right)^2 \quad (9)$$

The root water uptake or actual transpiration term in Eq. 7 is related to the potential transpiration with an expression of the form

$$S(h(x), h_\phi(x)) = \delta(h(x), h_\phi(x)) b(x) T_p \quad (10)$$

In Eq. 10, $S(h(x), h_\phi(x))$ is the actual transpiration rate, i.e., the rate at which the crop transpires after accounting for soil water availability as modulated by soil water and osmotic pressures $[T^{-1}]$; h_ϕ is the osmotic pressure $[L]$; δ represents the root water uptake stress functions, which accounts for crop water stress due to soil water and osmotic pressures $[-]$; $b(x)$ is the root water uptake distribution function, which is a function of root density distribution in the crop root zone $[L^{-1}]$; and T_p is the potential transpiration rate, which is the atmospheric consumptive use demand under conditions of unlimited water supply $[L/T]$.

2.3.3.b. Initial and boundary conditions, soil water dynamics

Equation 7 is solved numerically subject to applicable and site specific initial and boundary conditions.

Initial condition

HYDRUS-1D allows specification of initial conditions in the soil profile in terms of a prescribed soil water pressure, $h_i(x)$, or soil water content, $\theta_i(x)$, profile (Table 2).

Boundary conditions

HYDRUS-1D accommodates various kinds of boundary conditions. Surface boundary conditions include infiltration through a surface inundated with a constant or variable depth. Alternatively, infiltration may occur under a constant/variable flux, in which the net precipitation rate is less than soil intake rate. Infiltration can also take place under a scenario in which there is precipitation excess leading to a surface water buildup or one in which instantaneous removal of the precipitation excess can be assumed.

Evaporation from bare soil surface or a combination of evaporation and precipitation may represent the surface boundary conditions under which soil water flow occurs between irrigations. Boundary conditions at the bottom of the flow domain can be specified in terms of flux (e.g., in a field with tile drainage system) or a constant head equal to zero under a scenario where the lower limit of the simulation domain is a shallow water table. Drainage through the bottom boundary of the simulation domain can also be assumed to occur under a unit hydraulic gradient.

Table 2. Applicable initial and boundary conditions, soil water dynamics

Description	Irrigation method	Initial and boundary conditions	Type of boundary condition	Applicable condition
Initial conditions	Basin and sprinkler irrigation	$h(x,t) = h_i(x)$ at $t = 0$, for $0 < x < L$	Not applicable	Initial condition specified in terms of soil water pressure
		$\theta(x,t) = \theta_i(x)$ at $t = 0$, for $0 < x < L$		Initial condition specified in terms of soil water content
Boundary conditions	Sprinkler irrigation	$-K(h)(\partial h/\partial x + 1) = q_0(t) - dh/dt$ at $x = L$	Surface boundary condition	Net precipitation could exceed infiltration rate
		$\partial h/\partial x = 0$ at $x = 0$	Bottom boundary condition	Deep, homogeneous, and well-drained soil
	Basin irrigation	$h(x,t) = h_0(t)$ at $x = L$	Surface boundary condition	Flow depth hydrograph
		$\partial h/\partial x = 0$ at $x = 0$	Bottom boundary condition	Deep, homogeneous, and well-drained soil
	Time interval between irrigation events	$-K(h)(\partial h/\partial x + 1) = q_0(t) - dh/dt$ at $x = L$	Surface boundary condition	Net precipitation could exceed infiltration rate
		$\partial h/\partial x = 0$ at $x = 0$	Bottom boundary condition	Deep, homogeneous, and well-drained soil

where: $h_i [L]$ and $\theta_i [L^3/L^3]$ are prescribed soil water pressure head and soil water content functions of x , at $t = 0$; and L is distance of the soil surface from the bottom of the simulation domain. Note: the set of boundary conditions presented here consists of a list that applies to the study presented here and is not a complete list of all the boundary conditions that can be accommodated by the HYDRUS-1D model. Furthermore, water table in the study sites is sufficiently deep for capillary rise to have appreciable effect on root zone soil water dynamics.

The boundary conditions pertinent to the current study are a limited subset of the alternatives provided in HYDRUS-1D. They consist of typical surface and bottom boundary conditions that occur under basin and sprinkler irrigation events and those pertinent to the time intervals spanning consecutive irrigation events and are summarized in Table 2.

2.3.4. Coupled solute transport and reaction equations

2.3.4.a. Equations

HYDRUS-1D models the movement, sequestration, and transformation of solutes in variably saturated porous medium as a coupled multiphase (liquid, solid, and gas phase) transport-reaction processes. As noted earlier, gas phase transport is not considered in the current study. Advection and dispersion are the main mechanisms of solute transport in the liquid phase, while the liquid-solid phase interactions are modeled based on equilibrium relationships. With regard to soil reactions, the interest here is on the chemistry of major-ions prevalent in salt affected soils. Accordingly, the 1D form of the advection-dispersion-reaction equation with a sink term, implemented in HYDRUS-1D (Simunek et al., 2013), can be expressed as

$$\frac{\partial(\theta c_i^l)}{\partial t} + \rho \frac{\partial c_i^s}{\partial t} = \frac{\partial}{\partial x} \left(\theta D_i \frac{\partial c_i^l}{\partial x} \right) - \frac{\partial(q c_i^l)}{\partial x} + \Gamma_i - \Phi_i \quad \text{for } i \in [1, I] \quad (11)$$

In Eq. 11, C_i^l is the concentration of the i th solute in the liquid phase [M/L^3]; C_i^s is the concentration of the i th solute in the solid phase [M/M]; ρ is bulk density of the soil [M/L^3], D_i is the hydrodynamic dispersion coefficient of the porous medium [L^2/T]; q is soil water flux [L/T]; Γ_i is reaction term for the i th solute; Φ_i is the sink term that represents passive root uptake of the i th solute, and I is the number of chemical species considered. Note that root water uptake of major-ions is often considered negligible (e.g., Rhoades, 1974) and is treated as such in HYDRUS-1D.

The chemical species and parameters considered in the major-ion chemistry module of HYDRUS-1D consist of the cations (Ca^{2+} , Mg^{2+} , Na^+ , and K^+) and anions (Cl^- , SO_4^{2-} , and

NO_3^-). The soil physicochemical processes considered significant in determining the distribution of the major-ions in the aqueous and solid phase of the soil system are: complexation in the soil solution, cation exchange, and precipitation/dissolution.

Overall, HYDRUS-1D considers thirty-seven ions and molecules, which occur either in the aqueous and/or solid phase of the soil system, as the primary chemical species involved in the major-ion chemistry processes of the unsaturated zone. A list of the ionic and other chemical species is provided in Table 3. A discussion on the system of equations that constitute the reaction term, r_i , in Eq. 11 are provided by Simunek et al. (2013). This includes expressions describing mass balance, charge balance, alkalinity, and equilibrium relationships (consisting of cation exchange based on Gapon's formulation, precipitation/ dissolution, and complexation reactions).

2.3.4.b. Initial and boundary conditions, solute transport-reaction

The solute transport-reaction equation, Eq. 11, is solved numerically after having been coupled with applicable initial and boundary conditions.

Initial conditions

The initial concentration of each chemical species, both in the aqueous, C_i^l , and solid, C_i^s , phases needs to be specified. In the major-ion chemistry module of HYDRUS-1D, the initial concentration of each chemical species is specified in the *Selector.IN* input data file and is defined as a constant over each distinct soil layer, with a defined soil physical and chemical properties, or over the entire root zone. A more formal description of the initial conditions is provided in Table 4.

Boundary conditions

The solute concentration or flux can be specified as boundary conditions at the surface or bottom of the problem domain. Alternatively, concentration gradient can be set to zero, with the implication that the dispersive component of the total boundary flux is zero. HYDRUS also have provisions for specification of surface boundary conditions for volatile solutes. However, solutes

Table 3. Chemical species considered in the major-ion chemistry module of HYDRUS-1D and chemical species considered in the current study

Liquid phase				Solid phase	
Chemical species considered in the major-ion chemistry module of HYDRUS-1D					
Free ions that are none CO_2 - H_2O species	Complexes	CO_2 - H_2O species	Silicate species	Precipitated species	Adsorbed species
Number of species in each category					
7	10	7	3	6	4
Ca^{2+} , Mg^{2+} , Na^+ , K^+ , SO_4^{2-} , Cl^- , NO_3^-	$CaCO_3^0$, $CaHCO_3^+$, $CaSO_4^0$, $MgCO_3^0$, $MgHCO_3^+$, $MgSO_4^0$, $NaCO_3^-$, $NaHCO_3^0$, $NaSO_4^-$, KSO_4^-	$CO_{2(g)}$, $H_2CO_3^*$, CO_3^{2-} , HCO_3^- , H^+ , OH^- , H_2O	H_4SiO_4 , $H_3SiO_4^-$, $H_2SiO_4^{2-}$	$CaCO_3$, $CaSO_4 \cdot 2H_2O$, $MgCO_3 \cdot 3H_2O$, $Mg_5(CO_3)_4(OH)2 \cdot 4H_2O$, $Mg_2Si_3(OH)3H_2O$, $CaMg(CO_3)_2$	Ca^{2+} , Mg^{2+} , Na^+ , K^+
Chemical species considered in the current study					
Free ions that are none CO_2 - H_2O species	Complexes	CO_2 - H_2O species	Silicate species	Precipitated species	Adsorbed species
Number of species in each category					
6	10	7	0	1	4
Ca^{2+} , Mg^{2+} , Na^+ , K^+ , SO_4^{2-} , Cl^-	$CaCO_3^0$, $CaHCO_3^+$, $CaSO_4^0$, $MgCO_3^0$, $MgHCO_3^+$, $MgSO_4^0$, $NaCO_3^-$, $NaHCO_3^0$, $NaSO_4^-$, KSO_4^-	$CO_{2(g)}$, $H_2CO_3^*$, CO_3^{2-} , HCO_3^- , H^+ , OH^- , H_2O	-	$CaCO_3$	Ca^{2+} , Mg^{2+} , Na^+ , K^+

Note: $H_2CO_3^*$ is the sum total of hydrated carbon dioxide, $CO_2 \cdot H_2O$ and H_2CO_3 present in the soil solution. H_4SiO_4 is silicic acid and is considered important in the dissolution reactions of silicates (Simunek et al., 2013)), however, it is not considered in the current study. Note: the upper half of the table shows a list of the processes and ions and molecules that are considered in the major-ion chemistry module of HYDRUS-1D. The lower half, on the other hand, shows the chemical species considered in the current study, which represent a subset of those considered in the major-ion chemistry module of HYDRUS.

considered in the current study are nonvolatile, hence related boundary condition is not relevant here. A description of the boundary conditions applicable to the current study are summarized in Table 4.

2.3.5. Model inputs

Inputs to the HYDRUS-1D model consist of general model parameters, including specification of pertinent soil physical and chemical processes to be modeled, profile geometry, simulation duration, and output formatting. The input data also includes soil water retention and conductivity parameters, crop data, soil water and salinity stress function parameters, events calendar data, meteorological data, solute transport-reaction parameters, and applicable initial and boundary conditions. A more detailed discussion on this is provided in *Section 3.1*.

Table 4. Applicable initial and boundary conditions, solute transport-reaction

Initial/ boundary conditions	Applicable initial and boundary conditions	Type of boundary condition	Description
Initial conditions	$C_i^l(x,t) = C_{i,in}^l(x)$ at $t = 0$, for $0 < x < L$	Not applicable	Aqueous phase
	$C_i^s(x,t) = C_{i,in}^s(x)$ at $t = 0$, for $0 < x < L$		Solid phase
Boundary conditions	$-\theta D(\partial C/\partial x) + qC = q_0(t)C_{i,o}^l(t)$, at $x = L$	Surface boundary condition	Flux boundary
	$\partial C(x,t)/\partial x = 0$ at $x = 0$	Bottom boundary condition	Zero concentration gradient

$C_{i,in}^l$ is the initial concentration profile of the i th solute in the liquid phase $[M/L^3]$; $C_{i,in}^s$ is the initial concentration profile of the i th solute in the solid phase $[M/M]$; and $C_{i,o}^l(t)$ is the concentration of the i th solute in irrigation water or precipitation $[M/L^3]$. Note: $C_{i,in}^l$ and $C_{i,in}^s$ are defined for each distinct soil layer or for the entire root zone, thus they are not continuous function of depth. The boundary and initial conditions listed here are those pertinent to the current study only.

CHAPTER 3. A MODELING STUDY OF ROOT ZONE SALINITY IN THE YUMA VALLEY IRRIGATION DISTRICTS

3.1. Introduction

This chapter presents a modeling study on the time-evolution of point-scale root zone salinity, over the growing season of a wheat crop, in selected growers' fields in the Yuma Valley Irrigation Districts. As noted earlier, the coupled soil water dynamics, solute transport, and reaction model used in the current study is HYDRUS-1D. A concise review of the theoretical basis, computational capabilities, and input data requirements of the model is presented in *Section 2.3*. HYDRUS-1D has been successfully used to analyze and assess potential risks of salinity and sodicity in irrigated soils. For instance, Goncalves et al. (2005) applied HYDRUS-1D to evaluate soil salinization and sodification risks associated with the multi-season use of irrigation waters of different quality in lysimeters. HYDRUS-1D was also used to study the potential risks of salinity and excess sodium under irrigated field conditions (Ramos et al., 2011). The precursor of HYDRUS-1D, known as UNSATCHEM (Simunek et al., 1996), was extensively used to analyze the time-evolution of saline and/or sodic conditions in agricultural soils and alternative management practices (Corwin et al., 2007; Oster et al., 2012; Rasouli et al., 2013) as well as reclamation scenarios (Simunek and Suarez, 1997).

The specific input data requirements of HYDRUS-1D for a season-long simulation of the root zone salinity of a cropped field consist of soils, irrigation, crop, meteorological, and events calendar data. The soils data include both physical and chemical parameters, initial soil water content profile, and the concentrations of major-ions in the soil solution and the solid phase. Solid phase concentrations refer to concentrations of major-cations in the soil exchange complex and molecules present in the form of participates, taking part in precipitation/dissolution reactions.

Irrigation related data include irrigation schedule (i.e., the number and timing of irrigations in a season) and duration of irrigations. Furthermore, the precipitation rates (of sprinkler irrigation) or flow depth hydrographs (of basins irrigation events) need to be specified

as the surface boundary condition for infiltration events associated with irrigation. In addition, the chemical composition of the irrigation water, which provides the surface boundary condition for the simulation of the solute transport and major-ion chemistry processes, is also a model input.

Crop data includes crop type, root water uptake distribution profile, parameters of soil water and salinity stress functions, potential transpiration, potential evaporation through the cropping season. Meteorological data relevant to the current study relates to the timing and depth of natural precipitation events. Finally, events calendar, particularly dates of soil sampling, planting, and harvesting are needed to set the simulation duration.

In the current study, many of the inputs, including initial soil water content, initial concentrations of major-ions in the soil solution and in the irrigation water, irrigation timing, and rate of applications (constituting surface boundary conditions), soil textural class, and weather data were determined through measurements. Other inputs such as soil bulk density, soil hydraulic and solute transport parameters, potential transpiration and evaporation, soil water and salinity stress response function parameters, cation exchange capacity of soils, initial concentration of cations on the exchange complex, and cation exchange selectivity coefficients were obtained from literature sources, HYDRUS databases, or were computed based on measured data.

The measured salinity data used in the modeling study presented here was derived from data sets collected as part of a salinity evaluation project conducted, by Dr. Charles Sanchez, in the Yuma Valley Irrigation Districts since 2016. As noted earlier, the data collected in the field and laboratory studies include soil physical parameters, soil water content, concentrations of major-ions in the soil solution, irrigation, crop, and events calendar. In each field, the salinity data was collected at multiple sampling nodes suitably spread over the field. Although the data was collected at the beginning of the growing season of wheat crop and several weeks following harvest, only the data measured days prior to the planting of the wheat crop is used in the simulation study presented here. This data provides the initial conditions for soil water and solute transport-reaction modeling.

From the salinity data sets collected over the past years, two data sets among those obtained during the winter spring seasons of 2016 and 2017 were selected for use in the current analysis. These data sets are labeled here as data sets I and II. Data set I was collected in a field

located in the South Gila Valley and data set II was from a field in the Yuma Valley. Descriptions of the input data and simulation results on the seasonal evolution of point-scale root zone salinity along with characterization of potential effects on crops and soil physical properties will now be presented for both data sets.

3.2. Data Set I

3.2.1. Data description

3.2.1. a. Simulation duration and events calendar, data set I

Data set I was collected in a field that was under (durum) wheat crop. The wheat field consists of a 650ft (198.1m) wide and 1250ft (381m) long rectangular basin with an area of 18.7Acre (7.55ha). The planting and harvest dates were December 14, 2016 and May 5, 2017, respectively. The pre-plant soil sampling was undertaken on December 12, 2016. The initial conditions for the simulation study (which requires specification of the soil water content and concentration of major-ions in the soil) were set based on soil conditions on the day of the pre-plant soil sampling. Thus, the start date for the simulation is set to December 12, 2016 and the cropping season is assumed to have ended on the last full day that the crop was on the field (i.e., the last full day of the season during which soil water loss attributable to transpiration has occurred), which is May 4, 2017. It then follows that the length of the salinity simulation period for data set I is equal to 143 days. Note that for convenience the phrases salinity simulation period and cropping season are used interchangeably in subsequent discussions.

3.2.1.b. Soils data, data set I

For data set I, soil salinity data was collected over twelve sampling points distributed over the basin. At each sampling node, four soil samples were collected at increments of 1ft (30.48cm) up to a depth of 4ft (121.9cm), which is equal to the effective rooting depth of the crop (Table 5a). Soil samples were then preserved for subsequent analysis in the laboratory. Gravimetric soil water contents, for each sampling layer, were determined by oven drying extracts from the samples for 48 hours at 110°C. The differences between the wet and dry sample weights were then used to determine the antecedent soil water content right before planting. In

Table 5a. Input data to the major-ion chemistry module of HYDRUS-1D, Data-set I

Descriptions of data items		Unit	Value	Comment		
General input data						
<i>Processes</i>						
Water flow		N/A	Yes			
Solute transport-reaction (major-ion chemistry)		N/A	Yes			
Root water uptake		N/A	Yes	<i>Root growth is not considered</i>		
<i>Profile and geometry</i>						
Number of materials		-	1	<i>Soil is considered homogeneous through the root zone</i>		
Number of layers		-	1			
Effective crop root depth		cm	121.9			
<i>Time information</i>						
Simulation duration		day	143			
Soils data						
<i>Soil physical properties</i>	<i>Soil texture</i>		<i>Clay</i>	%	21.7	<i>Soil is Loam</i>
			<i>Silt</i>	%	40	
			<i>Sand</i>	%	38.3	
	<i>Bulk density</i>			<i>g/cm³</i>	1.5	
	<i>Soil water content</i>	<i>Soil sampling depth</i>	<i>0-30.48cm</i>	<i>cm³/cm³</i>	14.57	
			<i>30.48-60.96cm</i>	<i>cm³/cm³</i>	18.98	
			<i>60.96-91.44cm</i>	<i>cm³/cm³</i>	29.60	
			<i>91.44-121.9cm</i>	<i>cm³/cm³</i>	26.44	
	<i>Soil water retention/conductivity function parameters</i>					
	<i>van Genuchten – Mualem model, root zone soil</i>		θ_r	<i>cm³/cm³</i>	0.0658	<i>No dual porosity, no hysteresis</i>
			θ_s	<i>cm³/cm³</i>	0.4109	
			α	<i>1/cm</i>	0.0096	
			n	-	1.4936	
			m	-	0.3305	
			l	-	0.5	
		K_s	<i>cm/day</i>	9.63		
<i>Solute transport parameters</i>						
<i>Longitudinal dispersivity</i>			<i>cm</i>	25.8		
<i>Molecular diffusion coefficient</i>			<i>cm²/day</i>	2		
<i>Soil chemical properties, root zone average</i>	<i>Initial concentration of ions in the soil solution</i>		Ca^{2+}	<i>meq/L</i>	15.28	
			Mg^{2+}		5.99	
			Na^+		17.87	
			K^+		0.66	
			Cl^-		11.38	
			SO_4^{2-}		14.82	
			<i>Alkalinity</i>		5.87	

Table 5b. Input data to the major-ion chemistry module of HYDRUS-1D, Data-set I

<i>Soils data</i>							
Description of data items				Unit	Value	Comment	
<i>Chemical properties, root zone average</i>	<i>Cation exchange reaction parameters</i>	<i>Concentrations on the soil exchange complex</i>	Ca^{2+}	<i>meq/kg</i>	63.5		
			Mg^{2+}		33.75		
			Na^{+}		2.5		
			K^{+}		0.25		
	<i>Gapon's selectivity coefficients</i>	Ca/Mg	-	1.4			
		Ca/Na	-	6.38			
		Ca/K	-	0.36			
<i>Precipitation/dissolution reaction</i>	<i>Concentration in the solid phase</i>	<i>Calcite</i>	<i>meq/kg</i>	0.6	<i>Calcite is the only salt precipitate considered in the study</i>		
<i>Irrigation data</i>							
<i>Irrigation method and calendar</i>	<i>Sprinkler</i>	<i>1st irrigation</i>	<i>12/14/2016</i>	<i>N/A</i>	<i>N/A</i>	<i>Flux boundary condition</i>	
	<i>Basin</i>	<i>2nd irrigation</i>	<i>02/14/2017</i>		<i>N/A</i>	<i>N/A</i>	<i>Pressure (flow depth) boundary condition</i>
		<i>3rd irrigation</i>	<i>03/09/2017</i>				
		<i>4th irrigation</i>	<i>03/26/2017</i>				
		<i>5th irrigation</i>	<i>04/11/2017</i>				
<i>Chemical properties of irrigation water</i>	<i>Concentration of ions in the irrigation water</i>	Ca^{2+}		<i>meq/L</i>	4.09		
		Mg^{2+}			2.63		
		Na^{+}			5.62		
		K^{+}			0.15		
		Cl^{-}			3.68		
		SO_4^{2-}			5.30		
		<i>Alkalinity</i>			6.46		
<i>Crop data</i>							
<i>Crop coefficient, Kc</i>	<i>Initial</i>			<i>-</i>	0.45	<i>Variable Kc values are shown in Figure 1b</i>	
	<i>Development</i>				<i>Variable, Figure 1b</i>		
	<i>Mid-season</i>				1.1		
	<i>Late season</i>				<i>Variable, Figure 1b</i>		
	<i>End of season</i>				0.3		
<i>Root water uptake</i>							
<i>Feddes' soil water stress response function parameters</i>	h_1			<i>cm</i>	0	<i>Data was obtained from the HYDRUS database for wheat</i>	
	h_2				-1		
	h_{3H}				-500		
	h_{3L}				-900		
	h_4				-16000		
	r_{3H}			<i>cm/day</i>	0.5		
	r_{3L}			0.1			

Table 5c. Input data to the major-ion chemistry module of HYDRUS-1D, Data-set 1

<i>Crop data</i>				
Root water uptake, salinity stress response function				
Description of data items	Unit	Value	Comments	
<i>Multiplicative salinity stress response function</i>	β	<i>l/cm</i>	0.0000328	<i>Data was obtained from HYDRUS database for durum wheat</i>
	$h_{\phi t}$	<i>cm</i>	-1549.7	
	<i>Osmotic coefficient</i>	<i>cm(L/meq)</i>	1	<i>Recommended value, HYDRUS-1D</i>
<i>Solute transport and major-ion chemistry</i>				
<i>Number of distinct solutions</i>	-	3	<i>#1 is soil solution #2 is irrigation water #3 is natural precipitation</i>	

Notations used in Tables 5a-5c:

Number of materials is the number of soil layers, with distinct soil physical and chemical properties, into which the root zone profile is divided for HYDRUS simulations (-);

Number of layers is the number of layers the root zone profile is divided for water balance calculations (-);

θ_r is residual soil water content (cm^3/cm^3);

θ_s is saturation soil water content (cm^3/cm^3);

α , n , and m are parameters of the van Genuchten soil moisture characteristics function;

K_s is saturated hydraulic conductivity (cm/day);

l is parameter of the van Genuchten-Mualem conductivity function parameter (-);

Ca/Mg , Ca/Na , Ca/K indicates that the forward half of the cation exchange reaction is one in which Ca^{2+} replaces Mg^{2+} , Na^+ , and K^+ from the soil exchange complex;

h_1 is soil water pressure below which water uptake begins;

h_2 is the maximum of the soil water pressure range in which soil water uptake is optimal and hence root water uptake equals potential transpiration;

h_{3L} is the lower end of the soil water pressure range in which soil water uptake is optimal when the transpiration rate is equal to r_{3L} ;

h_{3H} is the lower end of the soil water pressure range in which soil water uptake is optimal when the transpiration rate is equal to r_{3H} ;

h_4 is the soil water pressure below which root water uptake ceases (cm);

β (*l/cm*) is the slope of the salinity stress response function;

the current study, the root zone soil is assumed to have homogeneous chemical and physical properties.

Soil textural class is an important soil physical property, based on which various physical and chemical parameters of the root zone soil were derived. On the average, the root zone soil is composed of 21.7% clay, 40% silt, and 38.3% sand and the corresponding soil textural class is loam. The soil water retention and conductivity parameters, Eqs. 8 and 9, were computed with the Rosetta module of HYDRUS-1D (Table 5a) based on soil textural data.

Extracts from a saturated paste, obtained from each soil sample, were analyzed in the laboratory to determine the approximate concentrations of major-ions (Ca^{2+} , Mg^{2+} , Na^+ , K^+ , SO_4^{2-} , CO_3^{2-} , Cl^-) in the soil solution using ion chromatography. Although the analytical concentrations of carbonate species in the soil solution is reported here in terms CO_3^{2-} concentration, because of the near neutral pH of the soil solution HCO_3^- is the dominant carbonate species in the soil. In its major-ion chemistry module, HYDRUS-1D does not have a provision for specifying the concentration of CO_3^{2-} or HCO_3^- at the input, however, their effects can be specified in terms of soil solution alkalinity. Thus, initial alkalinity of the soil solution, *Alkalinity* (Table 5a), is calculated here with Eq. 12 assuming irrigation water with a neutral pH .

$$Alkalinity = 2CO_{3T} + HCO_{3T} + [OH^-] - [H^+] \quad (12)$$

In Eq. 12, CO_{3T} (meq/L) and HCO_{3T} (meq/L) are total concentration of carbonate and bicarbonate species, respectively (i.e., both free ion and complex forms).

The mean cation exchange capacity of the crop root zone soil was set to 100meq/kg. A trial and error procedure involving a series of HYDRUS simulations was used to determine the initial concentrations of major cations (Ca^{2+} , Mg^{2+} , Na^+ , and K^+) on the exchange complex such that the corresponding initial *EC* profile of the soil solution is sufficiently close to the measured profile. Note that the soil solution *EC* reported in this document is calculated as the sum of the (equivalent) concentrations of the dissolved cations, computed with HYDRUS-1D, divided by 10 (Essington, 2005).

Gapon's selectivity coefficients for cation exchange reactions, shown in Table 5b, are those reported by Robbins et al. (1980) and Robbins and Carter (1983) for Penyor loam, a soil with close physicochemical characteristics as that of the field considered in this study (Table 5b). It is generally assumed that in irrigated arid lands soils the soil exchange complex has preference for Ca^{2+} to those of Mg^{2+} , Na^+ , and K^+ . Thus, the forward half of the cation exchange reactions considered here are those in which Ca^{2+} replaces each of the other three cations from the exchange complex, which is represented in Table 5b with the notation *Ca/Mg*, *Ca/Na*, and *Ca/K*. Furthermore, the average root zone calcite concentration was estimated to be 0.6meq/kg of soil (Table 5b). The molecular diffusion coefficient of major-ions in the soil solution is set to $2cm^2/day$ and the longitudinal dispersivity coefficient is set to 25cm, based on experience with

earlier salinity studies (PC-Progress, 2020). The maximum permissible concentration of major ions absorbed by the crop (which refers to passive absorption) is set to zero, implying that root uptake of salts is negligible.

While the electrical conductivity of the saturation extract, EC_e , for each of the soil samples was determined through measurements, the corresponding sodium adsorption ratio, SAR_e , was calculated from the measured concentrations of calcium, magnesium, and sodium (Eq. 2). As mentioned earlier in *Section 2.1.2*, it ought to be noted that the EC_e and SAR_e are only approximations of the in-situ soil water EC , EC_{sw} , and SAR , SAR_{sw} . Note that EC_e and SAR_e are not HYDRUS inputs.

Because a basin was used to apply irrigation, the surface boundary condition changed from flux to pressure head and vice-versa through the cropping season. Numerical difficulties were encountered in our HYDRUS simulations for scenarios involving mixed flux and pressure head boundary conditions (*Section 3.2.2.a*). As a result, the entire cropping season could not be simulated in a single sweep. To obviate these difficulties an alternative approach that is robust, but more demanding in terms of the required time and effort was implemented in the current study. Thus, to keep the required simulation time and effort to a practical level, the current study was limited to point-scale analysis of the seasonal evolution of root zone salinity (i.e., the study is not a comprehensive field-scale assessment of salinity). In other words, the initial condition used to initiate the simulation study was based on measurements made on soil samples collected from only one of the sampling nodes in the field. The sampling node used in the study is the one closest to the geometric center of the field. The idea is that the seasonal evolution of root zone salinity obtained for the mid-field point can have some degree of field-wide relevance.

3.2.1.c. Irrigation data, data set I

In data set I, irrigation accounts for, by far, the largest input of water and for a considerable amount of the seasonal salt influx into the root zone profile. The precipitation rates of sprinkler irrigations and the depth hydrographs of basin irrigations provide the surface boundary conditions for infiltration processes occurring during irrigation events. As shown in Table 5b, the seasonal irrigation requirements were applied in five events distributed over the cropping season. The early season irrigation was applied using a sprinkler system on 12/14/2016 following planting of the wheat crop. The rest of the irrigations were applied on 02/14/2017,

03/09/2017, 03/26/2017, and 04/11/2017 with the basin method. The concentration of major-ions in the irrigation water is given in Table 5b.

3.2.1.d. Crop data, data set I

The crop grown in the study site during the simulation period is durum wheat. As noted in Section 2.3.3.a, HYDRUS-1D computes the actual crop transpiration from the potential transpiration as a function of the root water uptake distribution and the crop response to soil water and salinity stresses (Eq. 10). Thus, potential transpiration and evaporation need to be specified as separate input streams to the HYDRUS-1D model. This section describes the steps followed in the determination of potential crop transpiration and evaporation from the potential crop evapotranspiration.

Potential evapotranspiration, transpiration, and evaporation

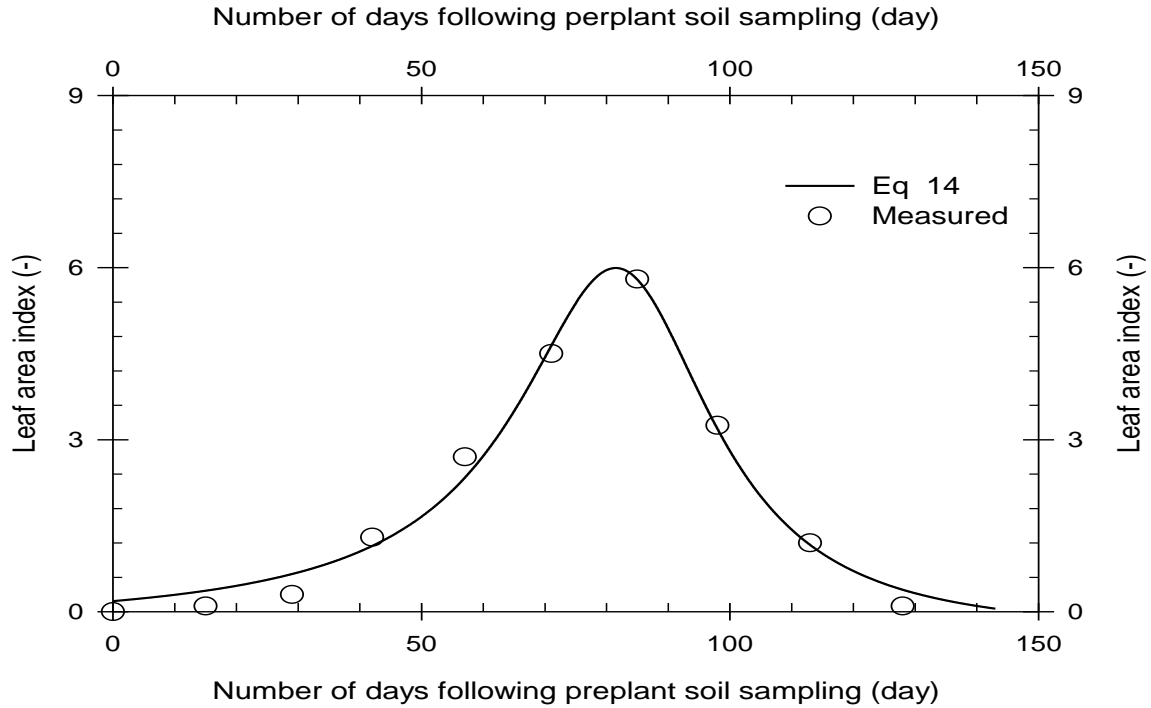
Potential crop transpiration, T , and evaporation, E , were computed from the potential evapotranspiration, ET , based on the crop leaf area index, LAI (-), with the following expressions

$$\left. \begin{aligned} T &= ET(1 - \exp(-k * LAI)) \\ E &= ET \exp(-k * LAI) \end{aligned} \right\} \quad (13)$$

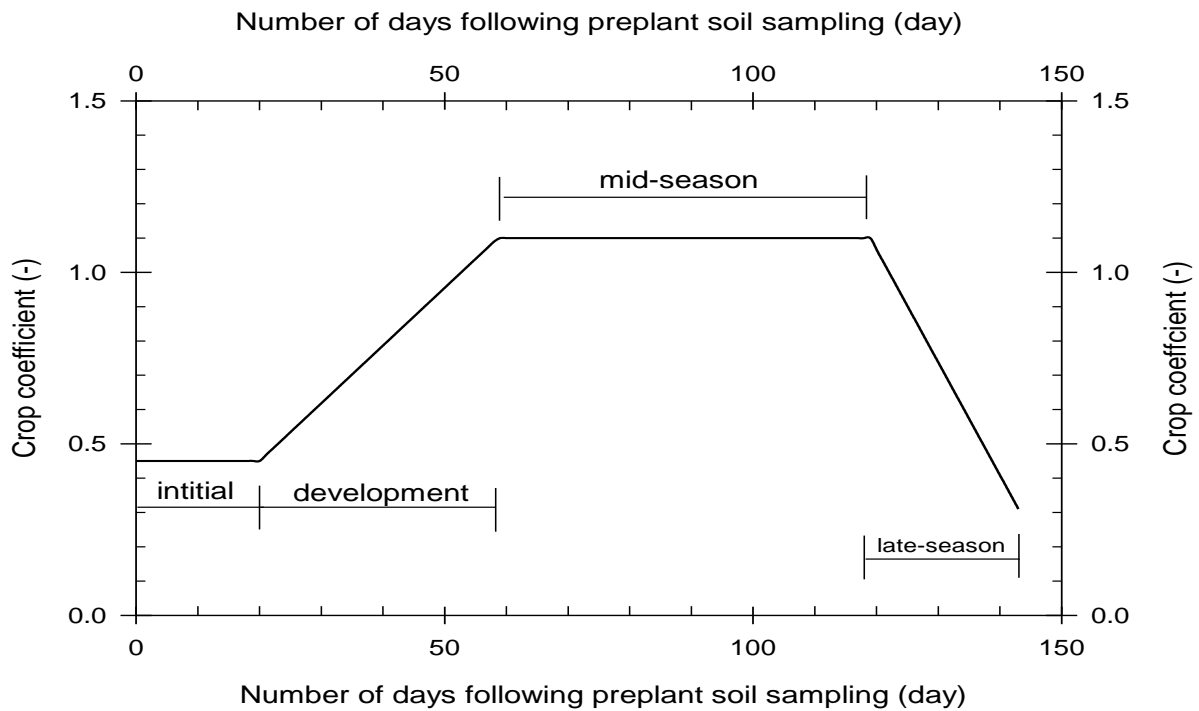
where k [-] is a constant accounting for the radiation extinction by crop canopy, which is a function of sun angle, plant distribution and arrangement of leaves (e.g., Simunek et al, 2013). It varies between 0.5 to 0.75 and was set to 0.65 in the current study.

An empirical crop leaf area index function was obtained through regression (with $r^2 = 0.99$, Figure 1a) by fitting a rational function of the form given in Eq. 14 to a measured LAI data for a wheat crop grown in the Yuma area. The LAI data used in the regression was obtained from Hunsaker et al. (2017).

$$LAI = \frac{a + b(d)}{1 + c(d) + e(d)^2} - 0.31 \quad (14)$$



(a)



(b)

Figure 1. (a) A comparison of the leaf area index of wheat crop calculated with Eq. 14 and measured data and (b) Crop coefficient of durum wheat

In Eq. 14, d is time referenced from date of planting (day) and a (-), b (day^{-1}), c (day^{-1}), and e (day^{-2}) are empirical coefficients, where $a = 0.4972$, $b = -0.0021day^{-1}$, $c = -0.0229day^{-1}$, and $e = 0.00014 day^{-2}$. The seasonal ET is calculated from the reference crop evapotranspiration, ET_o , with the function

$$ET = K_c ET_o \quad (15)$$

where K_c [-] is the crop coefficient. Seasonal ET_o , computed with the Penman-Monteith equation, was obtained from the Arizona Meteorological Network (AZMET) web portal for the North Gila meteorological station. North Gila meteorological station was used in preference to other stations because it is the closest to the study site and hence condition there are considered to be representative of those in the study site. Based on personal communication with Dr. Douglas Hunsaker of the USDA-ARS Arid Lands Agricultural Research Center, K_c values used in the current study are 0.45 for the initial stage (which accounts for 14% of the cropping season), 1.1 for the mid-season stage (covering 42% of the growing period), and 0.3 at season's end. It was further assumed that the development and late season stages account for 27 and 17% of the cropping season, respectively (Figure 1b). The K_c values for the development and late-season stages vary linearly with time and were calculated as a function of the duration of the respective growth stages and the limiting K_c values for the initial and mid-season stages and at season's end. Figure 1b depicts the K_c values used in the current study for the four stages of the cropping season.

The seasonal reference evapotranspiration, ET_o , the potential wheat crop evapotranspiration, ET , (Eq. 15) along with the seasonal potential transpiration, T , and evaporation, E , (Eq. 13) are depicted in Figure 2. A closer look at Figure 2 shows that the reference crop evapotranspiration, ET_o , exceeds the potential evapotranspiration of the wheat crop, ET , in the initial, development, and late-season growth stages of the crop. However, ET exceeds ET_o in the mid-season stage, because the crop coefficient for this stage is greater than 1. Although ET shows appreciable daily variations, which could possibly be attributed to variabilities in meteorological parameters, the overall seasonal trend is that ET increases in the initial and development stages and the early part of the mid-season stage. It then stays nearly

constant, in the average sense, over the later part of the mid-season stage and exhibits a relatively steep decline in the late-season stage. Overall, transpiration shows a similar trend in time as that of ET over the initial, development, and early part of the mid-season stages, but it begins to decline well before the end of the mid-season stage and continue through the late-season stage. Note that this is related to the trends in the leaf area index function of the crop. Evaporation accounts for a significantly larger fraction of ET in the initial stage, the early part of the development stage, and the later part of the mid-season and the entire late season growth stages. Transpiration exceeds evaporation by a significant margin in the later part of the development and the early part of the mid-season stages, where both K_c and LAI are either increasing or are at their maximum value.

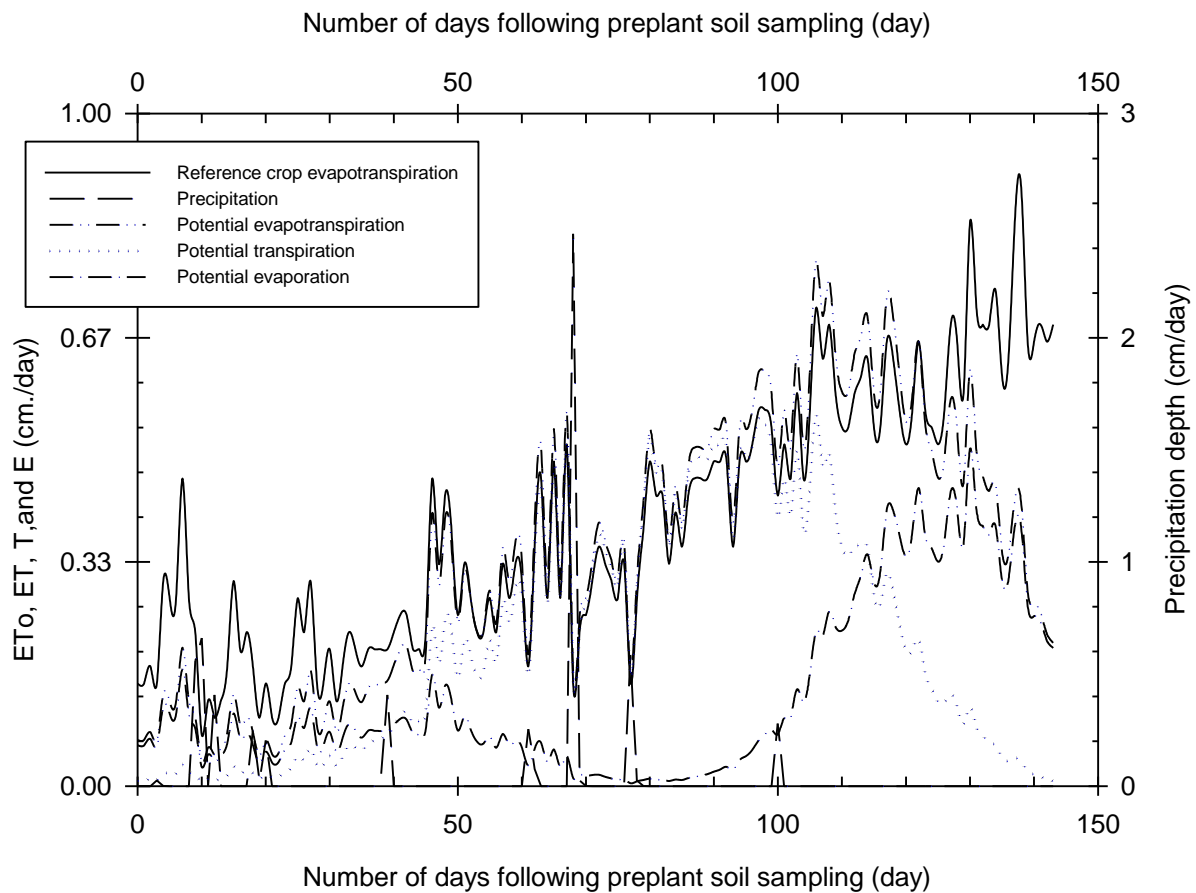


Figure 2. Daily reference crop evapotranspiration, ET_o , precipitation, P , potential crop evapotranspiration, ET , potential transpiration, T , and potential evaporation, E , over the cropping season

Actual crop transpiration

As noted earlier, HYDRUS computes the actual transpiration rate (i.e., the root water extraction rate, represented in Eq. 7 in terms of the sink term) as a function of the root water uptake distribution and the crop response to soil water and salinity stresses (Eq.10). In the current study, the root water uptake distribution function (which is related to the density distribution of feeder roots) is modeled using the Hoffman and van Genuchten (1983) equation, given as

$$b(x) = \begin{cases} \frac{1.667}{L_r} & \text{for } x > L - 0.2L_r \\ \frac{2.0833}{L_r} \left(1 - \frac{L-x}{L_r}\right) & \text{for } x \in [L - L_r; L - 0.2L_r] \\ 0 & \text{for } x < L - L_r \end{cases} \quad (16)$$

In Eq. 16, $b(x)$ is the root water uptake distribution function [-], L_r is the crop root depth [L], x is the vertical distance of a point from the lower boundary of the simulation domain [L], and L is the distance of the soil surface from the reference datum [L]. Note that Eq. 16 describes a root water uptake profile with a trapezoidal distribution, in which maximum absorption occurs over the upper 20% of the root zone at a uniform rate, followed by a linearly decreasing root water uptake with depth.

Furthermore, the soil water stress response function used in the current study is that of Feddes (1978) and is given as

$$\alpha_w(h) = \begin{cases} 0, & \text{for } h_1 < h \leq 0 \\ \frac{h-h_1}{h_2-h_1} & \text{for } h_2 < h \leq h_1 \\ 1, & \text{for } h_3 < h \leq h_2 \\ \frac{h-h_3}{h_4-h_3} & \text{for } h_4 < h \leq h_3 \end{cases} \quad (17)$$

Feddes' model considers a trapezoidal root water uptake stress response function (Figure 3).

Root water uptake is set to zero between a threshold soil water pressure, h_1 , and saturation ($h =$

0). As the soil water pressure falls below h_1 , root water uptake increases linearly reaching the potential transpiration rate, T_p (i.e., $\alpha_w(h) = 1$) at $h = h_2$. Root water uptake stays constant at T_p (i.e., $\alpha_w(h) = 1.0$) in the interval $h \in (h_3, h_2]$, it then declines linearly over the interval $h \in (h_4, h_3]$, and ceases as h falls under a minimum threshold soil water pressure, h_4 . Note that the values of Feddes' soil water stress function parameters, Eq. 17, used in the current study (Table 5b) were obtained from HYDRUS-1D database for wheat crop (Wesseling, 1991).

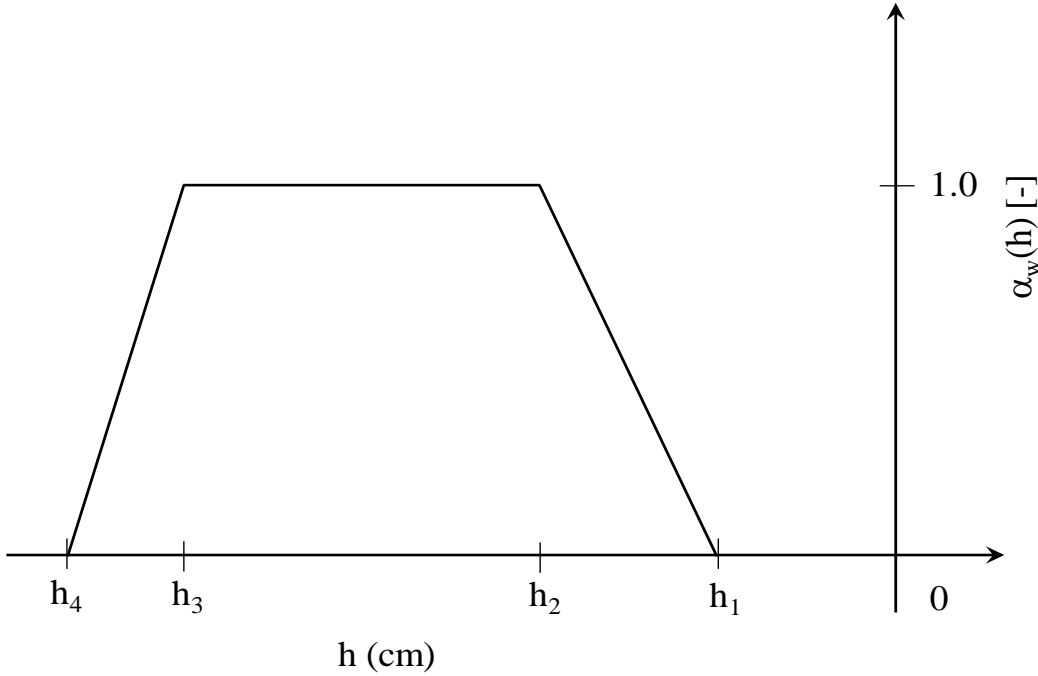


Figure 3. Root water uptake stress response function (Feddes, 1978)

The salinity stress response function is considered here to be multiplicative to the effect of soil water stress. The function used to quantify the salinity stress response is the threshold-slope equation of Maas (1990), which is given as

$$\gamma(h_\phi) = 1 + \zeta(h_\phi - h_{\phi t}) \quad \text{for } h_\phi > h_{\phi t} \quad (18)$$

where $\gamma(h_\phi)$ is the salinity stress response function [-], ζ [1/L] is the slope of the function, which represents the rate of decrease in root water uptake per unit increase in osmotic pressure, h_ϕ [L], in excess of the threshold osmotic pressure, $h_{\phi t}$ [L]. The soil water osmotic pressure, h_ϕ ,

corresponding to a given salinity level is estimated in HYDRUS-1D assuming an osmotic coefficient of 1.0. The ζ and h_{ϕ_t} values for durum wheat were obtained from HYDRUS database.

3.2.1.e. Meteorological data, data set I

In the current study, the only meteorological data that constitutes a direct input to HYDRUS-1D simulations is natural precipitation. Recorded daily precipitation depths, P , for the North Gila meteorological station, covering the simulation period were downloaded from the AZMET web portal (Figure 2).

Precipitation events are not only rare in the Yuma area, when they occur they are generally light showers of limited depth. Out of the 143 days of the cropping season, only sixteen days have recorded precipitation events. Apart from the maximum daily precipitation depth, which is 2.5cm, the recorded daily precipitation depths are generally less than 0.5cm through the season and the seasonal average is 0.04cm. Thus, precipitation has negligible contribution to the overall water balance of the area, and hence the study site.

3.2.2. Simulation results

3.2.2.a. Introduction

Although the early season irrigation was applied with a sprinkler system, the next four irrigations were applied with the basin method. In addition, natural precipitation and evaporation from bare soil surface, between irrigation events, involve flux boundary conditions. As a result, the surface boundary condition used in the seasonal simulation changes from flux (during the sprinkler irrigation and between irrigations) to pressure head boundary condition (during the surface irrigation events). Numerical difficulties were encountered in our HYDRUS-1D simulations when sharp changes occur in the boundary conditions, i.e., in both the flux and depth boundary conditions. To circumvent the numerical problems, associated with the handling of boundary conditions, the variable flux and pressure head surface boundary condition data (which is specified in the *Atmosph.In* input data file of HYDRUS-1D) was partitioned into segments. With this approach, each data segment would be consisting of a uniform boundary condition, i.e., either flux or pressure head. This resulted in the partitioning of the season long simulation (spanning 143 days) into nine distinct time intervals, each simulated separately in chronological

order. The implication is that the soil water and major-ion concentration profiles at the last time step of each simulation form the initial conditions for the simulation that follows immediately.

The approach used here (i.e., segmentation of the seasonal simulation into intervals with uniform surface boundary condition) would have no effect on the seasonal water flow simulation, because HYDRUS allows specification of the exact soil water content profile, from the last time step of a simulation, as an initial soil water content for the simulation that follows. However, the initial conditions related to the concentrations of major-ions (both in the liquid and solid phases) can be specified only as root zone averages or averages over a couple of distinct horizons that make up the root zone, instead of the actual simulated root zone profiles. Thus, partitioning of the data will have some effect on the accuracy of the root zone salinity profile obtained in each simulation subsequent to the first and the error might get somewhat compounded with time through the season. Results show that this can be appreciable in the surface soil layer. However, it is of limited significance in a large part of the lower section of the root zone profile.

Results of HYDRUS simulation on the seasonal evolution of the root zone salinity for data sets I and II obtained using the approach described above are presented in subsequent sections. The results consist of the seasonal variabilities of soil water content in the root zone. It also includes seasonal variation in root zone salinity as measured by the salinity indicator parameters: electrical conductivity and sodium adsorption ratio of the soil solution. The discussion concludes with a description of the seasonal variations in the computed cumulative boundary fluxes (infiltration, evaporation, and deep percolation) and crop transpiration.

3.2.2.b. Soil water content, data set I

Seasonal variation of root zone soil water content

The seasonal simulation start date is the pre-plant soil sampling date, which is December 12, 2016. The average initial soil water contents for the four soil sampling layers vary between a minimum of 14.6cm/m (in the 0-30.48cm layer) and a maximum of 29.6cm/m (in the 60.96 - 91.4cm layer), Table 5a. The soil water variability data, which is obtained by aggregating the results from the nine individual simulations is depicted in Figure 4. The curves in Figure 4 correspond to simulated soil water content data at five observation points in the root zone: 1.2,

29.3, 56.1, 87.8, and 119.6cm depth from the soil surface. The first irrigation was applied with a sprinkler system and it was started on the third day of the simulation period (Figure 4). The rest of the irrigations were applied with the basin method on the 64th, 87th, 104th, and 120th day from the pre-plant soil sampling date.

As can be noted from Figure 4, irrigation events are marked by a spike in soil water content. Between irrigations, however, soil water content generally decreases with time due to crop transpiration, evaporation from the soil surface, and deep percolation through the bottom boundary of the root zone. The soil water contents do not show a steady decline between irrigation events, instead it is punctuated by localized increases attributable to natural precipitation events.

In the time interval spanning the first two irrigations of the season, soil water content decreased from a maximum of 41cm/m (corresponding to the upper most observation point) right at the end of the first irrigation to 14.6cm/m immediately before the second irrigation (Figure 4). During the second irrigation, which occurred on 02/14/2017, soil water content for the upper most observation point again rose from a low of 14.6cm/m to a maximum of 41.1cm/m (which is the saturation water content). Soil water content then declined, overall, between the second and third irrigations reaching a minimum of 24cm/m (in the upper soil layer) just before the start of the third irrigation. It then rose to saturation at the end of the third irrigation. As can be noted from Figure 4, cycles of sharp rises in soil water content, during irrigation events, alternating with gradual decline with time between irrigations are repeated over the rest of the season.

A closer look at Figure 4 shows that the sensitivity of the root zone soil water contents to surface fluxes during irrigation and in between irrigation events vary between observation points. The closer the observation point is to the soil surface, the stronger the effects of surface fluxes (irrigation, precipitation, and evaporation) and crop transpiration are on soil water contents. Although both irrigation and precipitation events cause a sharper rise in the water contents of the upper soil horizons, the effect of irrigation is generally much more pronounced than those of the much lighter precipitation, which is typical of the study area. By comparison, transpiration and

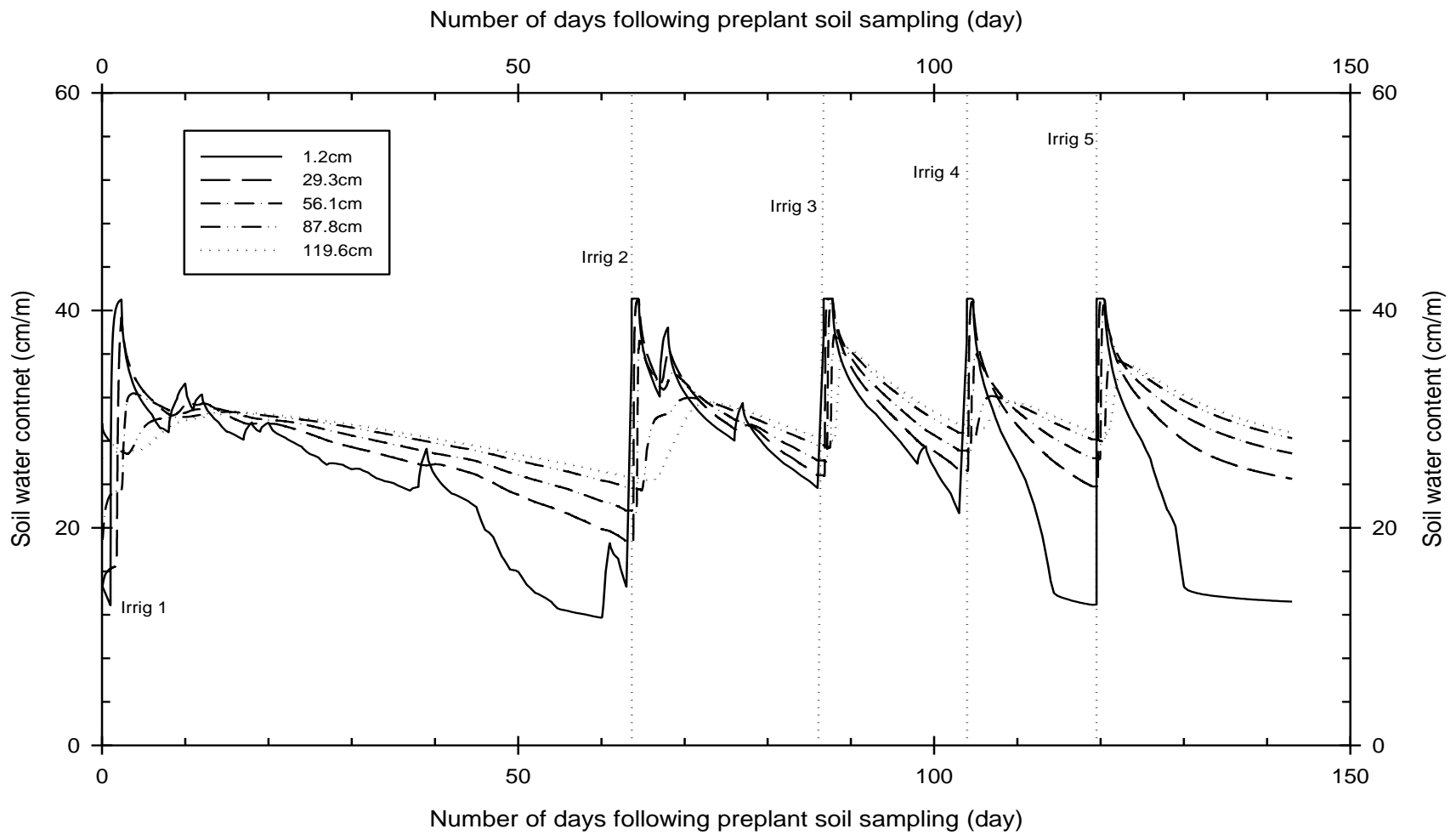


Figure 4. Seasonal variation of root zone soil water content at five observation points, data set I

evaporation, which mainly occur between irrigation events and whose effects are mostly felt in the soil horizon closer to the surface than the deeper layers, have a more gradual effect on soil water contents. Overall, Figure 4 shows that root zone soil water contents increased with depth from the surface.

Because of the sensitivity of the water contents of the near surface soil layer to surface fluxes and transpiration, all root zone soil water content extremes occur at the upper most observation point. As noted earlier, water contents of the upper most soil layer consistently rose to a seasonal maximum of 41.1cm/m following each irrigation event. Furthermore, water content at the upper most observation point fell to a seasonal minimum of 11.7cm/m days before the second irrigation event. The dry surface soil condition here appears to be related to the long irrigation interval (about two months) between the first and second irrigations. Soil water content at the upper most observation point also fell to the second lowest root zone water content level of the season, about 12.5cm/m, right before the last irrigation and weeks afterwards. The low soil water content right before the fifth irrigation event and afterwards are mainly due to the high evapotranspiration rate (averaging about 0.5cm/day), which was likely caused by the warming spring weather (with an average maximum daily temperature of 89°F) that occurred toward the end of the cropping season.

Seasonal variation of root zone soil water content in light of irrigation management

To provide practical context for the observed variation in seasonal soil water content, the seasonal root zone soil water variability curves are compared with irrigation management related soil water constants. The irrigation management related soil water constants considered here include: field capacity (*FC*), wilting point (*WP*), and the lower limit of the readily available soil water (*LLRAW*). The field capacity and wilting point soil water contents for loam soil were set at 35 and 12.5cm/m, respectively (based on suggested recommendation by the North East Region Certified Crop Advisors, 2020). Assuming 50% of the available soil water is readily available to the crop, the lower limit of the readily available water content (*LLRAW*) was set to 23.8cm/m (Figure 5). The root zone average initial soil water content (*AIWC*), calculated based on measured data is 22.4cm/m, which is less than the *LLRAW*.

Overall, the soil water contents through much of the cropping season and over a large fraction of the root zone profile fell within the readily available soil water content range

(between *LLRAW* and *FC*), which in practice is considered a favorable soil water environment for optimal crop growth and yield. However, soil water content over a significant fraction of the root zone appears to have fallen well under the *LLRAW* over a period of weeks prior to the second irrigation event (Figure 5). In addition, the water contents of the surface soil layer hovered slightly above the *WP* water content and fell well under the *LLRAW* over a period of a week and a half right before the last irrigation event and in the three week period that precede crop harvest. However, at this late stage of the cropping season, seeds were likely fully formed and crop was in senescence phase, hence the effect of limited crop availability of soil water may have no effect on crop yield. In any case, compensatory root water uptake from the lower horizons of the soil profile might, at least partly, offset the reduction in root water uptake from the upper soil layer. By comparison, the relatively low soil water content of the upper soil layer, in the weeks leading up to the second irrigation (Figure 5), in theory, may have some adverse effect on crop growth, if not yield. It appears that the irrigation interval, of about two months between the first and second irrigations, was perhaps a bit too long.

The seasonal soil water profiles depicted in Figures 4 and 5 were only partly based on measured data. Furthermore, they are not complemented with data on vegetative growth and crop yield. Thus, the observation noted above in regard to crop water stress should only be viewed as a cautionary note.

3.2.2.c. Seasonal variation of root zone salinity and effects on crop yield, data Set I

Seasonal variation of root zone salinity

Introduction: The simulated seasonal variation of root zone salinity, expressed in terms, of electrical conductivity is depicted in Figure 6. Each curve in Figure 6 represents the soil solution *EC* at one of the five observation points in the root zone. Generally, *EC* falls sharply during an irrigation event at each of the observation points, although to a varying degree. The average decline in *EC* at the upper most observation point during irrigations is about 1.0dS/m. The corresponding average soil solution *EC* is about 1.3dS/m, almost the same as the *EC* of the irrigation water (1.2dS/m). A closer examination of the computed *EC* data reveals that, the soil solution *EC* generally increases with depth during irrigation events. Furthermore, the data shows

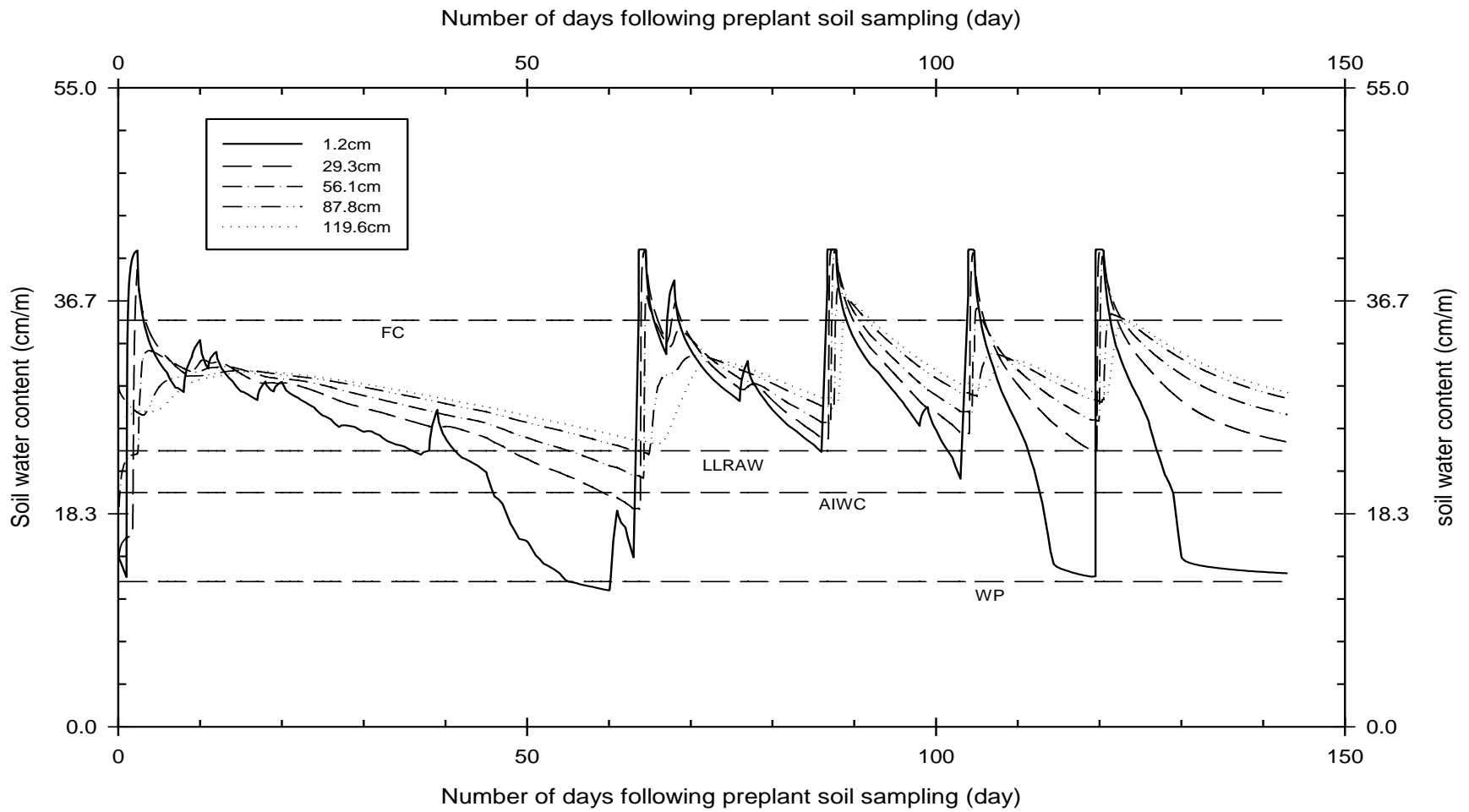


Figure 5. Seasonal variation of root zone soil water content at five observation points superimposed on lines showing soil water constants of irrigation significance, Data set I

that the *EC* in the upper soil layers decreased with time, possibly due to dilution of the soil solution and downward transport (leaching) of salts, while the *EC* in the lower sections of the root zone remains nearly constant with time.

By contrast, soil solution *EC* generally increased with time between irrigations at all observation points and typically peaked just before irrigation events (Figure 6). However, it ought to be noted here that the steady rise in *EC* between irrigation events is occasionally disrupted by localized dips, particularly in the upper soil layer. Note that the sharp increase in the *EC* of the upper soil layer, between irrigations, is consistent with the general trend of decreasing soil water content with time (Figure 4), which in this soil horizon is attributable to evapotranspiration.

Description of salinity profile behaviors: As can be noted from Figure 6, over the first half of the time interval spanning the first and second irrigations, the soil solution *EC* increased with depth from the soil surface. The root zone salinity trend remained largely the same in the second half of the irrigation interval, except that the *EC* for the upper most observation point increased at a much faster pace with time than was the case for all the other observation points. As a result, the *EC* for the upper most observation point exceeded the *EC* of all of the other observation points over the two-week period that preceded the second irrigation.

A closer look at the salinity profile data, for the first half of the time interval spanning the first and second irrigations, shows that the soil solution *EC* throughout the root zone profile was less than or equal to the *EC* at the start of the season. Note that the same holds true for the second half of the interval, except for the salinity profile of the upper most observation point. This observation suggests that dilution of the soil solution by the incoming irrigation water and subsequent downward transport (leaching) of ions is likely an important mechanism for the observed distribution of cations over much of the root zone profile. Note that the trend in *EC* variability with depth, observed in this part of the cropping season, is in sharp contrast with those observed over much of the season (Figure 6). A question that may arise here is ‘what is the explanation for the difference between the root zone *EC* profile of the first irrigation interval and those of the other irrigation intervals of the cropping season?’ An examination of the computed boundary flux data shows that the deep percolation amounts during the first irrigation interval and those of the other irrigation intervals of the season are comparable, which suggests that

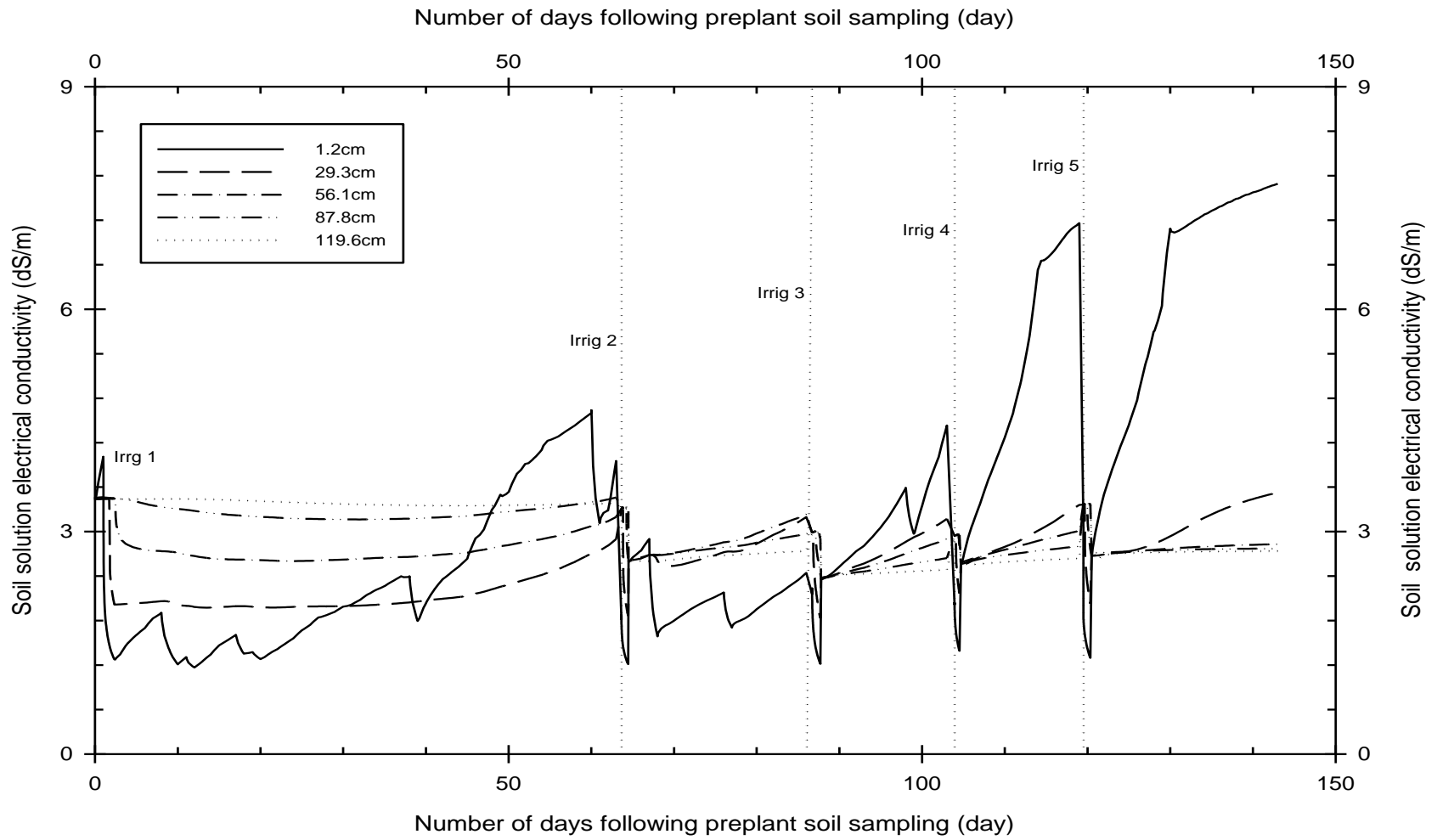


Figure 6. Seasonal variation in the electrical conductivity of the soil solution at five observation points, Data set I

differences in deep percolation amounts are not contributory factors. The main difference here is that the first irrigation was applied with a sprinkler system, while the rest of the irrigations were applied with a basin. The unsaturated flow condition that generally occurs during and following sprinkler irrigations might have contributed to the more enhanced leaching of salts observed in the first irrigation interval (e.g., Essington, 2005).

In the interval between the second and third irrigation events, the minimum root zone *EC* occurred at the upper most observation point. This is due to the relatively heavy precipitation events (of 2.5 and 0.6cm/day) that occurred during this part of the season, which led to leaching of salts from the surface soil layer to the underlying layers. By contrast, in the interval between the third and fourth irrigations, the spatial variability trends of root zone salinity was completely reversed and root zone salinity decreased with depth from a maximum at the upper most observation point. This trend was then maintained throughout the remaining part of the cropping season.

Generally, the salinity of the upper soil layer of the root zone profile is more sensitive to occasional large fluxes (mainly irrigation, but also to relatively heavy precipitation events) than those of the lower sections of the root zone profile. It can be observed from Figure 6 that the *EC* curve of the upper most observation point shows localized dips attributable to the effects of precipitation events. By comparison, natural precipitation events seem to have negligible effect on the salinity levels of the lower sections of the root zone, while major surface fluxes such as irrigation have discernible effects on the salinity of the lower lying soil layers.

Furthermore, the root zone minimum and maximum *ECs* of 1.2dS/m and 7.7dS/m, respectively (which occurred immediately following the second irrigation and at the end of the season, respectively), were both observed at the upper soil layer. It is likely that increased evapotranspiration, toward the end of cropping season (*Section 3.2.2.b*), have led to sharp rises in salt concentrations and hence to the observed increase in the soil solution *EC* of the upper soil layer.

Effects of evapotranspiration and leaching on root zone salinity profiles: Evapotranspiration, between irrigation events, creates relatively steeper gradients in the soil water potential of the biologically active near surface soil layers, which drives the movement of soil water (and the transport of dissolved salts) upwards to these soil horizons from the adjacent lower lying soil

layers. As the depletion of soil water in the near surface soil horizon and its partial replenishment from lower layers continue during an irrigation interval, salts in the surface layers become increasingly more concentrated with time.

Evidently, changes in salt concentration of the liquid phase disrupts the equilibrium, extant in the soil system, between the free-ions in the soil solution, on the one hand, and the complexes (in solution), the cations on the soil exchange complex, and calcite precipitate, on the other. The resultant physicochemical reactions would then lead to new equilibrium. In practice, however, it is likely that major-ion chemistry of the root zone soil is typically in a quasi-equilibrium, constantly adjusting to the changing concentrations in the soil solution, mainly because of the transient nature of soil water flow and transport processes under typical field conditions. This implies that, between irrigations, the distribution of ions in the liquid and solid phases of the upper soil layer of the root zone is determined by the net effect of the interaction between the physical processes of (upward movement of water and salts and the concentrating effect of evapotranspiration) and the attendant soil physicochemical processes of (complexation, cation exchange, and calcite precipitation/dissolution). A closer examination of the computed data shows that while soil physical processes have significant effect, physicochemical reactions can have appreciable influence, on the observed liquid and solid phase distribution of salts in these soil horizons.

By comparison, simulated results show that, between irrigations, the lower sections of the root zone have relatively high soil water contents and hence the downward movement of water and transport (or leaching) of salts might continue for a longer period following irrigations, although at a diminished rate, than is the case with the upper soil horizons. As a result, between irrigations, salinity in the lower sections of the root zone soil profile appears to be influenced more by leaching and to a much lesser degree by evapotranspiration. A closer look at the computed data on the liquid-solid phase distribution of major-ions, in the lower sections of the root zone, suggests that soil physicochemical processes might have negligible effect compared to the physical processes of water movement and salt transport.

It is important to note here that salt leaching generally occurs over the entire root zone, but much of salt leaching, in the upper horizon, occurs in a relatively shorter time following irrigation compared to the span of a typical irrigation interval and then attenuates more rapidly with time. By contrast, the concentrating effect of evapotranspiration on the soil solution of the

upper soil layers occurs over an entire irrigation interval and does not necessarily diminish with time. As a result, the reduction in the salt load of the soil solution in the upper soil horizons (attained in the early part of an irrigation interval through leaching) would, to some degree, be reversed over time by the effects of evapotranspiration. In the lower layers of the root zone profile, however, the concentrating effect of evapotranspiration is not as significant and drainage (and hence leaching) may continue, albeit at a diminished rate, for a longer time following irrigation. Thus, it is likely that leaching of salts have a more significant effect on salinity levels in the lower sections of the root zone than evapotranspiration.

Effects of resetting initial conditions for simulations that follow irrigation events: A closer look at Figure 6 shows that immediately following each irrigation event, the *EC* of the upper most observation point shows a sudden spike. The sharp rise in *EC* following an irrigation event represents the transition in the *EC* curve from the simulated condition at the end of irrigation to one representing the initial condition for the subsequent simulation. As noted in *Section 3.2.2.a*, the *EC* at the end of irrigation is calculated based on simulated distribution of major-ions in the root zone profile, while the *EC* corresponding to the initial condition, for the next simulation, is determined based on the root zone average concentrations of the major-ions. The soil solution *ECs* calculated based on root zone average ion concentrations are appreciably greater than the *ECs* of the surface soil horizons right at the end of an irrigation event and that is the reason for the observed jump in the *EC* of these horizons immediately following an irrigation event (Figure 6). In other words, these spikes in *EC* in the upper soil layer, immediately following irrigation events, are simply artifacts of the way the initial conditions for each segment of the seasonal simulation are formulated, rather than being a representation of simulated conditions in the surface horizons. This observation suggests that the simulation approach adopted in the current study (*Section 3.2.2.a*) may, to a degree, lead to an overestimation of the *EC* of the upper soil layer. However, over much of the root zone profile the effect of averaging, to reset initial conditions prior to each simulation, appears to be not as significant.

Salinity effects on crop yield

The relative crop yield equation, Eq. 3, and the data that it was based on are in principle applicable to crops grown under uniform root zone salinity and conditions that emulate

recommended cultural and management practices for commercial production (Maas, 1993). However, in practice salinity varies with depth in the root zone and also through the cropping season. Thus, seasonal root zone averages are used here to obtain an estimate of the salinity level encountered by the crop and its effect on crop yield.

Furthermore, relative yield estimates are made based on the electrical conductivity of the saturation extract. By comparison, the salinity profiles produced by HYDRUS, in principle, represent the in-situ root zone salinity. This implies that the computed *EC* profiles may need to be adjusted, to equivalent electrical conductivities of the saturation extracts, before they can be used in relative yield estimates. However, the initial conditions (mainly, estimates of the initial concentrations of ions in the soil solution and corresponding salinity level) used in HYDRUS modeling were derived through measurements made on the saturation extracts. Thus, it is reasoned here that the resultant seasonal root zone *EC* profiles, predicted by HYDRUS, would have tracked the *EC* of the saturation extracts more closely than the electrical conductivities of the in-situ soil solution, if concurrent measurements were to be made through the season. Accordingly, the seasonal average of the computed root zone electrical conductivity profiles was used here, without adjustment, to calculate relative yield.

The seasonal root zone average *EC* for data set I was 2.8dS/m, which exceeded the crop salt tolerance *EC* of 2.1dS/m for durum wheat (Maas, 1990) by a margin of 0.7dS/m. The crop salt tolerance data for durum wheat also shows that crop yield decreases by 2.5% from the maximum for every 1.0dS/m increase in soil solution *EC* in excess of the threshold. It can thus be readily calculated with Eq. 3 that the corresponding relative yield for data set I is 98.3%, which amounts to a theoretical yield reduction of 1.7% from the maximum. Given the very small reduction in yield, only 1.7%, it is reasonable to assume here that the mean seasonal root zone salinity has no measurable adverse effect on crop yield. However, the relatively high *EC* in the surface soil horizon, during parts of the second half of the cropping season, suggests that its effects on crop yield may need to be looked into in future studies.

Although the seasonal average root zone salinity was used to calculate relative yield, it is generally known that the sensitivity of crop yield to salinity varies through the season (Mass and Poss, 1989; Mass, 1990; Mass 1993). Mass and Poss (1989) showed the effect of salinity stress on grain yield is the highest during vegetative and early reproductive stage of durum wheat crop and appears to diminish as the season progresses. Furthermore, root zone salinity generally

varies with depth and it is likely that crops are most sensitive to higher salinity levels in the near surface soil horizons where much of the root water and nutrient uptake takes place. Thus, an analysis that compares the average salinity within the near surface soil horizon, for each crop growth stage, with the crop salt tolerance threshold may yield useful insights that can complement the relative yield calculated here.

3.2.2.d. Sodium adsorption ratio and risk of sodicity, data set I

Seasonal variability of root zone sodium adsorption ratio

Seasonal variation of the simulated sodium adsorption ratio of the soil solution for data set I is depicted in Figure 7. The soil solution *SAR* for much of the root zone, except the upper most soil layer, shows limited variation through the cropping season. The average *SAR* for the lower four observation points increased by a maximum of $0.5\text{meq}^{0.5}/\text{L}^{0.5}$ over the cropping season, from a value of $5.9\text{meq}^{0.5}/\text{L}^{0.5}$ at the start of the season to $6.4\text{meq}^{0.5}/\text{L}^{0.5}$ at season's end.

Overall, *SAR* for each of the lower four observation points of the root zone remained nearly unchanged in the time period spanning the start of the season and the second irrigation. In contrast to the lower horizons, the *SAR* curve for the upper most observation point exhibits significant variations ranging between a minimum soil solution *SAR* of $5.3\text{meq}^{0.5}/\text{L}^{0.5}$ occurring on the twelfth day of the cropping season to a local peak of $6.6\text{meq}^{0.5}/\text{L}^{0.5}$ just before the second irrigation. Note that during this period, the soil solution *SAR* for the upper soil layer fell well below the *SAR* of the lower sections of the root zone. Following the second irrigation the *SAR* curve for the upper most observation point began to rise, however, because of two precipitation events (one of them a relatively heavy rain fall of 2.5cm/day) it fell significantly below the *SAR* curves of the lower soil layers. It then recovered gradually peaking at $5.9\text{meq}^{0.5}/\text{L}^{0.5}$ just before the third irrigation.

For the rest of the cropping season, the soil solution *SAR* at the upper most observation point generally showed an increasing trend between irrigations, except for a localized dip in the interval between the third and fourth irrigations, which is due to a rainfall event. Furthermore, the soil solution *SAR* in the upper most observation point increased with time at a much faster pace toward the end of the cropping season than in the earlier parts of the season. As a result, the

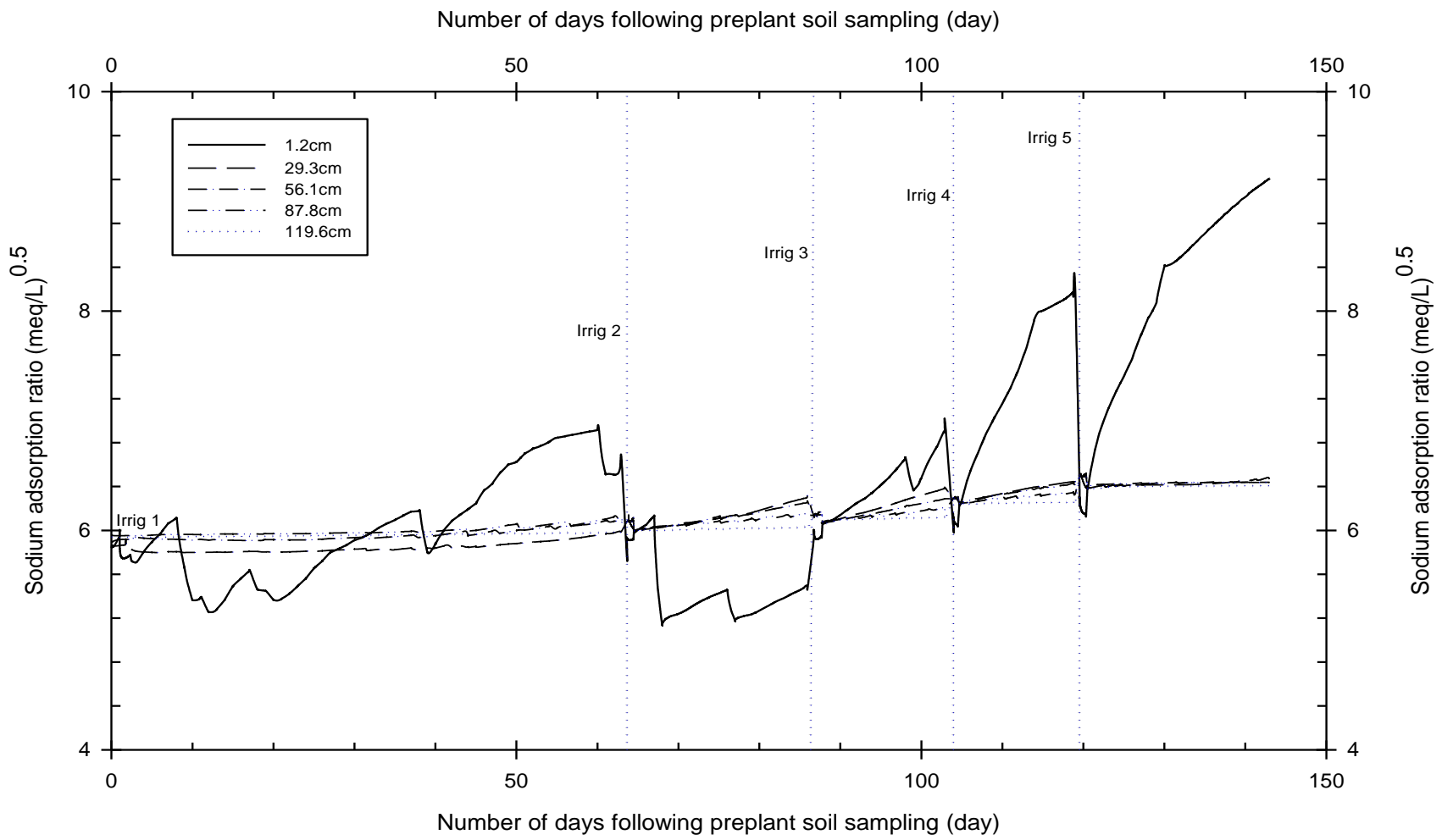


Figure 7. Seasonal variation of root zone sodium adsorption ratio at five observation points, Data set I

seasonal maximum SAR of $9.2\text{meq}^{0.5}/\text{L}^{0.5}$ occurred at the upper most observation point and right before harvesting. Note that the occurrence of high SAR in the upper soil layer coincides with the low water content observed there during the same time period (Figure 4). Thus, increased salt concentration in the surface layer, due to evapotranspiration, and the attendant soil physicochemical processes are the likely explanatory factors.

A closer look at Figure 7 and the SAR profile data shows that the SAR for the upper most observation point declined slightly during each irrigation event, which is the result of the net effect of leaching of salts to lower lying soil layers (Section 3.2.2.c) by the incoming irrigation water and the ensuing physicochemical processes. A more detailed discussion on this is provided in *Section 3.3.2.d*.

It can be observed from Figure 7 that the vertical distribution of SAR in the surface layer of the root zone broadly follows the same trend as that of EC (Figure 6). In the first half of the season, soil solution SAR of the surface layer fell below those of the lower horizons. As the season progresses, SAR near the soil surface rose sharply in between irrigation events. Over much of the season, the time rate of increase in SAR decreases sharply with depth from the surface. As was the case with salinity, it is likely that SAR in the surface soil layer was mainly affected by evapotranspiration, while the SAR of the lower sections of the root zone was more influenced by leaching effects.

Potential sodic hazard to the root zone soil profile

The seasonal average root zone SAR for data set I is $6.2\text{meq}^{0.5}/\text{L}^{0.5}$ and the maximum, which occurred at the end of the cropping season, and in the upper most observation point, is $9.2\text{meq}^{0.5}/\text{L}^{0.5}$. The seasonal average root zone SAR is not particularly high. Nonetheless, as noted in *Section 2.1.3.b*, assessment of potential sodic risks need to consider not only soil solution SAR , but also soil salinity levels, i.e., soil solution EC . The problem, it appears that there is no clear-cut criterion that takes into account both soil solution SAR and EC to characterize potential sodic risks. Essington (2005) described a sodic soil as one having a SAR exceeding 13 to $15\text{meq}^{0.5}/\text{L}^{0.5}$ and an EC of 4dS/m or less. Although the average root zone SAR for data set I is well under the indicated upper limit, the seasonal average root zone soil solution EC of 2.8dS/m is less than the 4dS/m lower bound by an appreciable margin, which leaves us with a degree of uncertainty on how to evaluate the potential sodic hazard of the soil solution salt composition of

data set I. Thus, authors could not make a definitive determination here regarding the potential effects of sodium on soil physical properties of agronomic significance. Consequently, possible subtle effects cannot be ruled out.

Nota that over the later part of the cropping season *SAR* of the upper soil layer soared to $8.2\text{meq}^{0.5}/\text{L}^{0.5}$ just before the last irrigation and $9.2\text{meq}^{0.5}/\text{L}^{0.5}$ right before harvesting. However, sodic risk in the upper most soil layer might not be as high, because the corresponding *ECs* of 7.2 and 7.7dS/m were quite high as well.

3.2.2.e. Cumulative boundary fluxes, transpiration, and leaching fraction

Cumulative boundary fluxes and transpiration

Figure 8 depicts the cumulative fluxes (i.e., the running sum of fluxes) that leave the crop root zone through its upper and lower boundaries and in the form of transpiration through the crop canopy. These include cumulative infiltration, evaporation, deep percolation, and transpiration fluxes. In order to provide a direct measure of irrigation adequacy, Figure 8 depicts the cumulative evapotranspiration curve in addition to the cumulative evaporation and transpiration fluxes. The computed seasonal cumulative infiltration, transpiration, evaporation, evapotranspiration, and deep percolation are 66.1, 28.9, 14.9, 43.8, and 17.9cm respectively. Cumulative infiltration is shown in Figure 8 as a step function that rise sharply immediately following irrigation, which then level-off and stays nearly constant in between irrigations, except for occasional slight bumps associated with precipitations. Cumulative transpiration, evaporation, and evapotranspiration are all relatively smooth increasing functions of time. Cumulative deep percolation also is an increasing function of time, but increases at a faster pace immediately following irrigations, when a significant fraction of the root zone is likely saturated or near saturation, and then it slows down with time. As can be noted from Figure 8, cumulative infiltration flux exceeds cumulative evapotranspiration throughout the season by a wide margin, suggesting a significant level of over-irrigation.

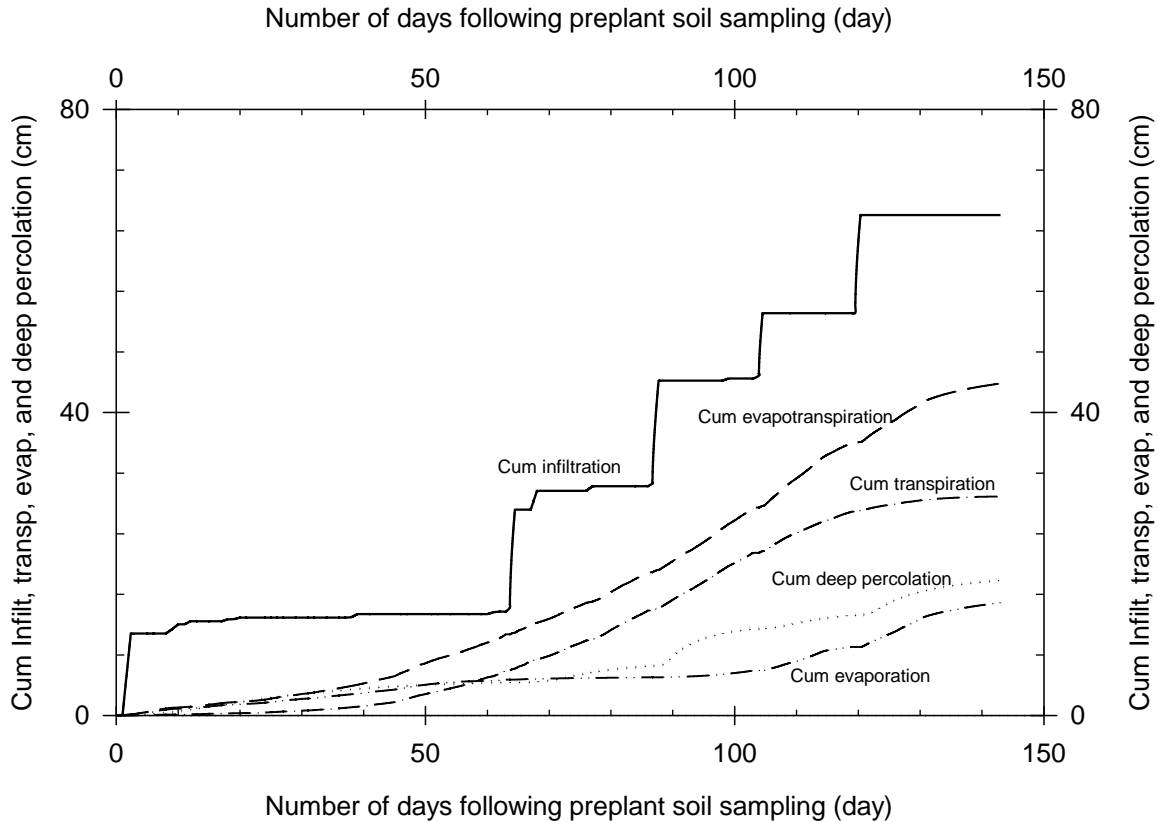


Figure 8. Cumulative (running sum of) infiltration, transpiration, evaporation, evapotranspiration, and deep percolation fluxes

Leaching fraction

Leaching fraction, for the cropping season, can be calculated as a function of the seasonal cumulative deep percolation and infiltration (due to natural precipitation and irrigation). However, the entire seasonal cumulative deep percolation flux could not necessarily be attributed to infiltration in all circumstances. Instead, depending on irrigation management related variables (such as irrigation intervals and applied irrigation depths), soil hydraulic properties, initial soil water content, and a host of other factors, there can arise a situation in which at least some of the deep percolation water may come from the soil water extant in the root zone at the start of the irrigation season (i.e., soil water carried over from the preceding season). In principle, the volume of deep percolation originating from the carryover soil water, if any, need to be determined and subtracted from the total deep percolation volume to determine the fraction that

need to be used in the calculation of leaching fraction for a cropping season or any other applicable time frame.

The point here is that although the fraction of the carryover root zone soil water content, that becomes deep percolation, contributes to salt leaching from the root zone, it, nonetheless, is not leaching that can directly be attributed to seasonal water input to the root zone and hence should not be taken into account in the calculation of leaching fraction. However, the problem is that there is no precise mechanism for differentiating between the deep percolation water that comes from the initial root zone soil water and that is from infiltration. Thus, the seasonal water balance is used here as an indicator of the relative significance of initial soil water versus infiltration as the source of deep percolation.

The seasonal root zone water balance showed that cumulative infiltration exceeded the cumulative outgoing fluxes, from the root zone, by 4.3cm. In other words, the root zone soil water content showed a net gain of 4.3cm by season's-end. These results point to a fact that the seasonal infiltration flux was not only sufficient to meet crop consumptive use needs, but also fully accounted for the drainage water and added some more water to the initial soil water content of the root zone. Thus, based on this observation it is deemed reasonable to assume here that the entire seasonal deep percolation depth of, 17.9cm, can be attributed to infiltration. It then follows, based on Eq. 4, that the leaching fraction for data set I is equal to 27.1%.

Note that the data presented here is derived based on simulations considering unsteady soil water flow and major-ion chemistry processes (including complexation, cation exchange, and calcite precipitation/dissolution reactions), thus the inverse relationship between concentrations and depths given in Eq. 4 is not applicable here. In other words, with the current data, leaching fraction can be calculated only based on the ratios of the drainage and irrigation water depths, not based on concentrations. Furthermore, the leaching requirement equation, Eq. 6, is not directly applicable to the data presented here.

3.2.2.f. Cautionary note

It is important to put the results presented here, with regard to soil salinity and sodicity risks, in perspective. As noted in *Section 3.2.1*, many of the model inputs were obtained through field and laboratory measurements. Other inputs were derived either from literature sources, or

from HYDRUS databases, or calculated based on measurements. The seasonal *SAR*, *EC*, fluxes, and soil water distribution data used in the current analyses were derived through simulations.

In essence, the results and observations stemming from the current study are not entirely based on measured data, hence they need to be treated only as useful insights that can help in identifying potential problems and guiding future studies. Furthermore, the current study is limited to point-scale analysis and as such the results cannot be directly generalized for an entire field, without the assumption that the surface boundary conditions, initial conditions, and the soil physical and chemical parameters of the sampling node (used in the current analysis) are replicated fully or substantially across the field.

3.3. Data set II

3.3.1. Data Description

3.3.1.a. Simulation duration and events calendar, data set II

Data set II was also collected in a field that was under (durum) wheat crop. Wheat was grown in a rectangular irrigation basin with an area of 12.8Acre (5.2ha), which is 625ft (190.5m) wide and 895ft (272.8m) long. The planting and harvest dates were January 11, and June 1, 2017, respectively. The salinity simulation start date was set to January 10, 2017 (i.e., the date of the pre-plant soil sampling) and the cropping season was assumed to have ended on the last full day that the crop was on the field, which is May 31, 2017. It thus follows that the salinity simulation period for data set II spans 141 days.

3.3.1.b. Soils data, data set II

For data set II, soil salinity data was collected over twelve sampling points distributed over the basin. At each sampling node, four soil samples were collected at increments of 1ft (30.48cm) up to a depth of 4ft (121.9cm), which is the effective crop rooting depth. Various physical and chemical parameters of the root zone soil profile were derived based on soil texture. The root zone soil is composed of 18.0% clay, 21.8% silt, and 60.2% sand and the corresponding soil textural class is sandy loam. Soil textural data was used to determine the soil water retention and conductivity parameters, Eqs. 8 and 9, with the Rosetta module of HYDRUS-1D (Table 6a).

The root zone soil of the study site was assumed to have homogeneous chemical and physical properties.

Soil water contents of the root zone, concentrations of the major-ions (Ca^{2+} , Mg^{2+} , Na^+ , K^+ , SO_4^{2-} , CO_3^{2-} , Cl^-) in the soil solution, and soil solution alkalinity were determined following the approach described in relation to data set I (*Section 3.2.1.b*). Related data is summarized in Table 6a. The corresponding *ECe* was measured and *SAR_e* was calculated based on the measured concentrations of pertinent cations.

The mean cation exchange capacity of the root zone was 60meq/kg. The initial concentrations of major cations (Ca^{2+} , Mg^{2+} , Na^+ , and K^+) on the exchange complex were determined, following the same approach as that described in relations to data set I (*Section 3.2.1.b*) and, are summarized in Table 6b. The soil of data set II is not so different from that of data set I, hence the Gapon selectivity coefficients for cation exchange reactions (involving replacement of Mg^{2+} , Na^+ , and K^+ from the exchange complex by Ca^{2+}) were set at the same level as those used in data set I (Table 6b). Furthermore, the average root zone calcite concentration, the molecular diffusion coefficient of major-ions, and the soil longitudinal dispersivity coefficient were set at the same level as those of data set I (Table 6a). The maximum permissible concentration of major-ions in the soil water absorbed by the crop is assumed zero.

As was the case with data set I, in data set II as well, simulation of the coupled soil water movement and solute transport and reaction processes was conducted only for a single sampling node. The sampling node that is closest to the geometric center of the field is used in the current study with the notion that the simulated salinity of the mid-field point can have some degree of field-wide relevance.

3.3.1.c. Irrigation data, data set II

Irrigation represents by far the single largest input of water into the root zone of data set II. The seasonal irrigation requirements were applied in six events distributed over the cropping season. All irrigations were applied using basin method. Thus, measured depth hydrographs provide the surface boundary condition for infiltration occurring during irrigation events. Irrigations were applied on 01/25/2017, 03/04/2017, 03/18/2017, 04/04/2017, 04/14/2017, and 04/27/2017. Data on the irrigation schedule, irrigation method, and the chemical composition of the irrigation water is summarized in Table 6b.

Table 6a. Input data to the major-ion chemistry module of HYDRUS-1D, Data-set II

Description of data items		Unit	Value	Comment		
General input data						
<i>Processes</i>						
<i>Water flow</i>		N/A	Yes			
<i>Solute transport-reaction (major-ion chemistry)</i>		N/A	Yes			
<i>Root water uptake</i>		N/A	Yes	<i>Root growth is not considered</i>		
<i>Profile and geometry</i>						
<i>Number of materials</i>		-	1	<i>Soil is considered homogeneous through the root zone</i>		
<i>Number of layers</i>		-	1			
<i>Profile/root zone depth</i>		cm	121.9			
<i>Time information</i>						
<i>Simulation duration</i>		day	141			
Soils data						
<i>Soil physical properties</i>	<i>Soil texture</i>		<i>Sand</i>	%	60.2	<i>Soil is Sandy Loam</i>
			<i>Silt</i>	%	21.8	
			<i>Clay</i>	%	18.0	
	<i>Bulk density</i>			g/cm ³	1.55	
	<i>Initial soil water content</i>	<i>Soil sampling depth</i>	<i>0-30.48cm</i>	cm ³ /cm ³	25.67	
			<i>30.48-60.96cm</i>	cm ³ /cm ³	20.99	
			<i>60.96-91.44cm</i>	cm ³ /cm ³	24.16	
			<i>91.44-121.9cm</i>	cm ³ /cm ³	28.6	
	<i>Soil water retention/conductivity function parameters</i>					
	<i>van Genuchten – Mualem model, root zone soil</i>		θ_r	cm ³ /cm ³	0.0562	<i>No dual porosity, no hysteresis</i>
			θ_s	cm ³ /cm ³	0.3876	
			α	1/cm	0.0262	
			n	-	1.3675	
			m	-	0.2687	
			l	-	0.5	
K_s			cm/day	21.33		
<i>Solute transport parameters</i>						
<i>Longitudinal dispersivity</i>		cm	25.8			
<i>Molecular diffusion coefficient</i>		cm ² /day	2			
<i>Soil chemical properties, root zone average</i>	<i>Initial concentration of ions in the soil solution</i>	<i>Ca²⁺</i>	<i>meq/L</i>	9.15		
		<i>Mg²⁺</i>		3.57		
		<i>Na⁺</i>		12.40		
		<i>K⁺</i>		0.48		
		<i>Cl⁻</i>		7.34		
		<i>SO₄²⁻</i>		9.08		
		<i>Alkalinity</i>		8.75		

Table 6b. Input data to the major-ion chemistry module of HYDRUS-1D, Data-set II

<i>Soils data</i>						
Description of data items				Unit	value	Comment
<i>Chemical properties, root zone average</i>	<i>Cation exchange reaction parameters</i>	<i>Concentrations on the soil exchange complex</i>	Ca^{2+}	<i>meq/kg</i>	39.25	
			Mg^{2+}		20.1	
			Na^+		0.5	
			K^+		0.15	
		<i>Gapon's selectivity coefficients</i>	Ca/Mg	-	1.4	
			Ca/Na	-	6.38	
		Ca/K	-	0.36		
	<i>Precipitation/dissolution reaction</i>	<i>Concentration in the solid phase</i>	$CaCO_3$	<i>meq/kg</i>	0.6	<i>Calcite is the only salt precipitate considered in the study</i>
<i>Irrigation data</i>						
<i>Irrigation method, and calendar</i>	<i>Basin</i>	<i>1st irrigation</i>	01/25/2017	<i>N/A</i>	<i>N/A</i>	<i>Pressure (flow depth) boundary condition</i>
		<i>2nd irrigation</i>	03/04/2017			
		<i>3rd irrigation</i>	03/18/2017			
		<i>4th irrigation</i>	04/04/2017			
		<i>5th irrigation</i>	04/14/2017			
		<i>6th irrigation</i>	04/27/2017			
<i>Chemical properties of irrigation water</i>	<i>Concentration of ions in the irrigation water</i>	Ca^{2+}		<i>meq/L</i>	4.09	
		Mg^{2+}			2.63	
		Na^+			5.62	
		K^+			0.15	
		Cl^-			3.68	
		SO_4^{2-}			5.30	
		<i>Alkalinity</i>			6.46	
<i>Crop data</i>						
<i>Evapotranspiration</i>						
<i>Crop coefficient, K_c</i>	<i>Initial</i>			<i>-</i>	0.45	<i>Variable K_c values are shown in Figure 1b</i>
	<i>Development</i>				<i>Variable, Figure 1b</i>	
	<i>Mid-season</i>				1.1	
	<i>Season's end</i>				<i>Variable, Figure 1b</i>	
	<i>End of season</i>				0.3	
<i>Root water uptake</i>						
<i>Feddes' soil water stress response function parameters</i>	h_1			<i>cm</i>	0	<i>Data was obtained from the HYDRUS database for wheat</i>
	h_2				-1	
	h_{3H}				-500	
	h_{3L}				-900	
	h_4				-16000	
	r_{3H}			<i>cm/day</i>	0.5	
	r_{3L}				0.1	

Table 6c. Input data to the major-ion chemistry module of HYDRUS-1D, Data-set II

<i>Crop data</i>				
Root water uptake, salinity stress function				
Description of data items	Unit	Value	Comment	
<i>Multiplicative salinity stress response function</i>	β	<i>l/cm</i>	0.0000328	<i>Data was obtained from HYDRUS database for durum wheat</i>
	h_{ϕ_r}	<i>cm</i>	-1549.7	
	<i>Osmotic coefficient</i>	<i>Cm(L/meq)</i>	1	<i>Recommended value, HYDRUS-1D</i>
<i>Solute transport and major-ion chemistry</i>				
<i>Number of distinct solutions</i>	-	3	<i>#1 is soil solution #2 Irrigation water #3 Rainfall</i>	

Notations used in Table 6a-6c

Number of materials is the number of soil layers, with distinct soil physical and chemical properties, into which the root zone profile is divided for HYDRUS simulations (-);

Number of layers is the number of layers the root zone profile is divided for water balance calculations (-);

θ_r is residual soil water content (cm^3/cm^3);

θ_s is saturation soil water content (cm^3/cm^3);

α , n , and m are parameters of the van Genuchten soil moisture characteristics function;

K_S is saturated hydraulic conductivity (cm/day);

l is parameter of the van Genuchten-Mualem conductivity function parameter (-);

Ca/Mg , Ca/Na , Ca/K indicates that the forward half of the cation exchange reaction is one in which Ca replaces Mg , Na , and K from the soil exchange complex;

h_1 is soil water pressure below which water uptake begins;

h_2 is the maximum of the soil water pressure range in which soil water uptake is optimal and hence root water uptake equals potential transpiration;

h_{3L} is the lower end of the soil water pressure range in which soil water uptake is optimal when the transpiration rate is equal to r_{3L} ;

h_{3H} is the lower end of the soil water pressure range in which soil water uptake is optimal when the transpiration rate is equal to r_{3H} ;

h_4 is the soil water pressure below which root water uptake ceases (cm);

β (*l/cm*) is the slope of the salinity stress response function

3.3.1.d. Crop data, data set II

As noted earlier in *Section 3.3.1.a*, the crop grown in the study site during the simulation period is durum wheat. The root water uptake distribution pattern of the crop is assumed here to follow Eq. 16 and the soil water stress response function is described by Eq. 17. Furthermore, the salinity stress response is modeled with the threshold-slope equation, Eq. 18. The soil water and salinity stress function parameters were obtained from HYDRUS database for wheat.

The seasonal potential crop transpiration, T , and evaporation, E , were determined with Eq. 13 from the crop potential evapotranspiration, ET , as a function of the crop leaf area index, LAI (Eq. 14). The seasonal crop ET is calculated from the reference crop evapotranspiration, ET_o , with Eq. 15. The seasonal ET_o , computed with the Penman-Monteith equation for the Yuma Valley meteorological station (a station closest to the study site), was downloaded from the AZMET web portal. The crop type and cropping season are the same for data sets I and II. In addition, the field study sites are located in the same general area (i.e., Yuma Valley Irrigation Districts), thus the K_c values used in data set II are the same as those used in data set I (Figure 1b). The seasonal ET , ET_o , T , and E for data set II are depicted in Figure 9.

3.3.1.e. Meteorological data, data set II

In the current study, the only meteorological data that constitutes a direct input to HYDRUS-1D simulations is precipitation, P , data. Records of daily precipitation depths covering the simulation period, from the Yuma Valley meteorological station, were downloaded from the AZMET web portal. Out of the 141 days of the cropping season, 9 days have recorded precipitation events. Apart from the maximum daily precipitation of 1.7cm, the recorded daily precipitation depths are generally less than 0.5cm through the season and the seasonal average is 0.03cm (Figure 9). Thus, precipitation has negligible contribution to the overall water balance of the study site.

3.3.2. Simulation results, data set II

3.3.2.a. Introduction

Irrigation water was applied in six doses distributed over the season. The surface boundary condition changes from pressure head (i.e., flow depth) during irrigation events to flux in between irrigation events. As noted earlier in relation to data set I (*Section 3.2.2.a*), sharp changes in boundary conditions have led to numerical problems in HYDRUS-1D simulations, which was particularly more pronounced for simulations involving mixed boundary conditions. To obviate the numerical difficulty, the same approach as that used to simulate data set I was applied here as well. Accordingly, the season long simulation, consisting of 141 days, was

divided into thirteen segments each consisting of uniform boundary conditions. This include six irrigation events, for which depth boundary conditions apply, and seven additional segments consisting of irrigation intervals and parts of the cropping season that come before the first irrigation and that followed the last irrigation (for which flux boundary condition apply). Simulations over each of these time intervals were conducted separately in chronological order. For each simulation subsequent to the first, initial conditions were reset based on the root zone soil water content profile, and the average root zone concentrations of the major-ions, computed in the last time step of the preceding simulation. As noted earlier in relation to data set I (*Section 3.2.2.a*), this approach entailed a level of approximation in the computed ion distribution profile and the resultant electrical conductivity and sodium adsorption ratio profiles.

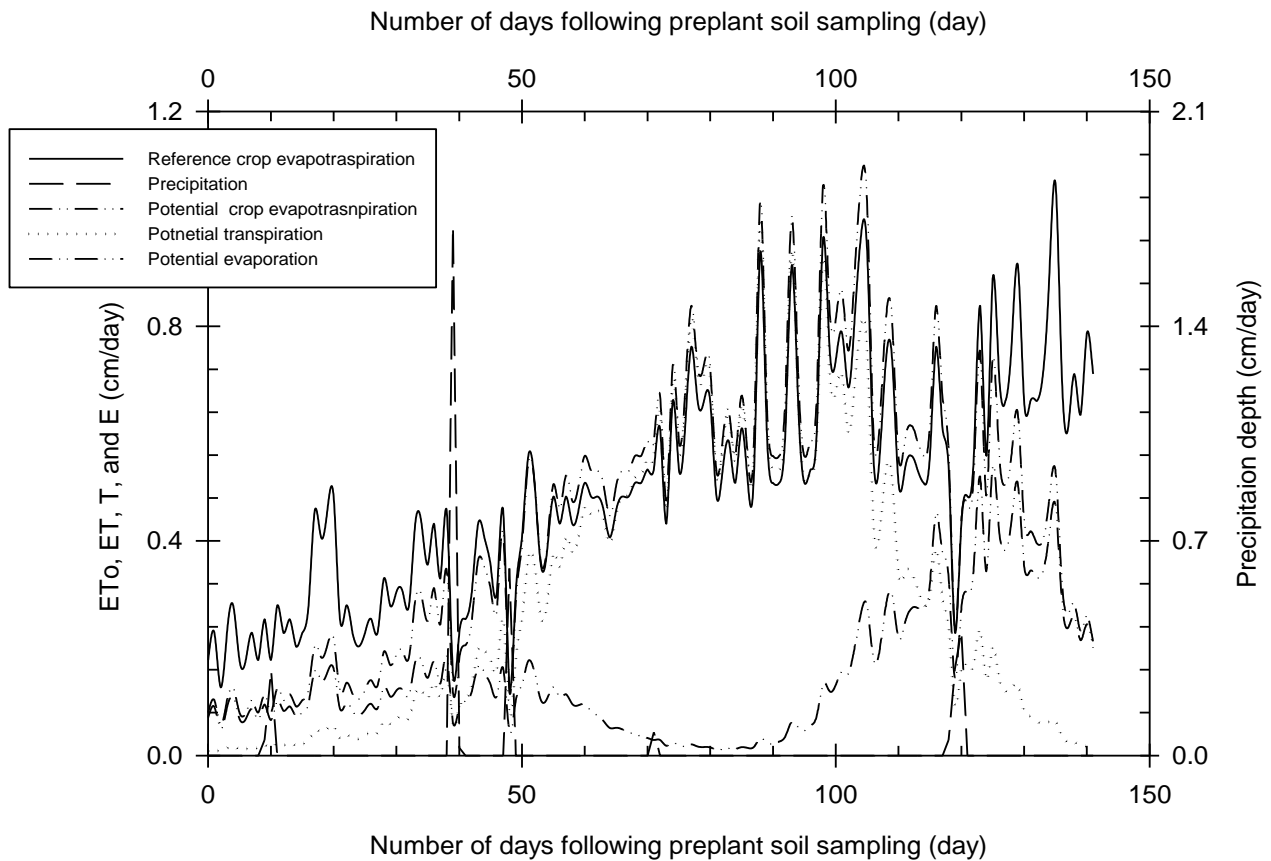


Figure 9. Daily reference crop evapotranspiration, ET_o , precipitation, P , potential crop evapotranspiration, ET , potential transpiration, T , and potential evaporation, E , over the cropping season

3.3.2.b. Soil water content, data set II

Seasonal variation of root zone soil water content

The simulation start date, which is the pre-plant soil sampling date, is January 10, 2017. The root zone soil water content determined based on samples from four sampling depths vary from a minimum of 21.0cm/m (in the 30.48-60.96cm soil layer) to 28.6cm/m (in the 91.44-121.92cm soil layer), Table 6a. The seasonal soil water content variation at five observation points, obtained by aggregating the computed profiles from each simulation, is depicted in Figure 10. The observation points are located at 1.2, 29.3, 56.1, 87.8, and 119.6cm depths from the surface. Irrigations were applied on the 15th, 53rd, 67th, 84th, 94th, and 107th days from the pre-plant soil sampling date.

As can be noted from Figure 10, irrigation events are marked by a sharp rise in soil water contents. Between irrigations, however, soil water contents generally decrease with time through the combined effects of transpiration through the crop canopy, evaporation from the soil surface, and deep percolation through the bottom boundary of the root zone. Note that at the upper most observation point, the general trend of decreasing soil water content with time over irrigation intervals is punctuated by occasional spikes that are attributable to natural precipitation events.

Considering the time interval spanning the start of the season and the first irrigation event, it can be noted that the soil water content at the upper most observation point declined over time to a root zone minimum of 17.3cm/m (Figure 10). It then rose sharply throughout the root zone profile, during the first irrigation event, reaching a root zone maximum of 38.8cm/m (saturation water content) at the upper most observation point. Between the first and second irrigations, root zone soil water content decreased with time to a minimum of 12.9cm/m just before the second irrigation. Soil water content then rose sharply, during the second irrigation event, again reaching saturation at the upper most observation point. As can be observed from Figure 10, cycles of root zone recharge (during irrigation) alternating with root zone depletion due to evapotranspiration and deep percolation (in between irrigation events) continue over the rest of the cropping season.

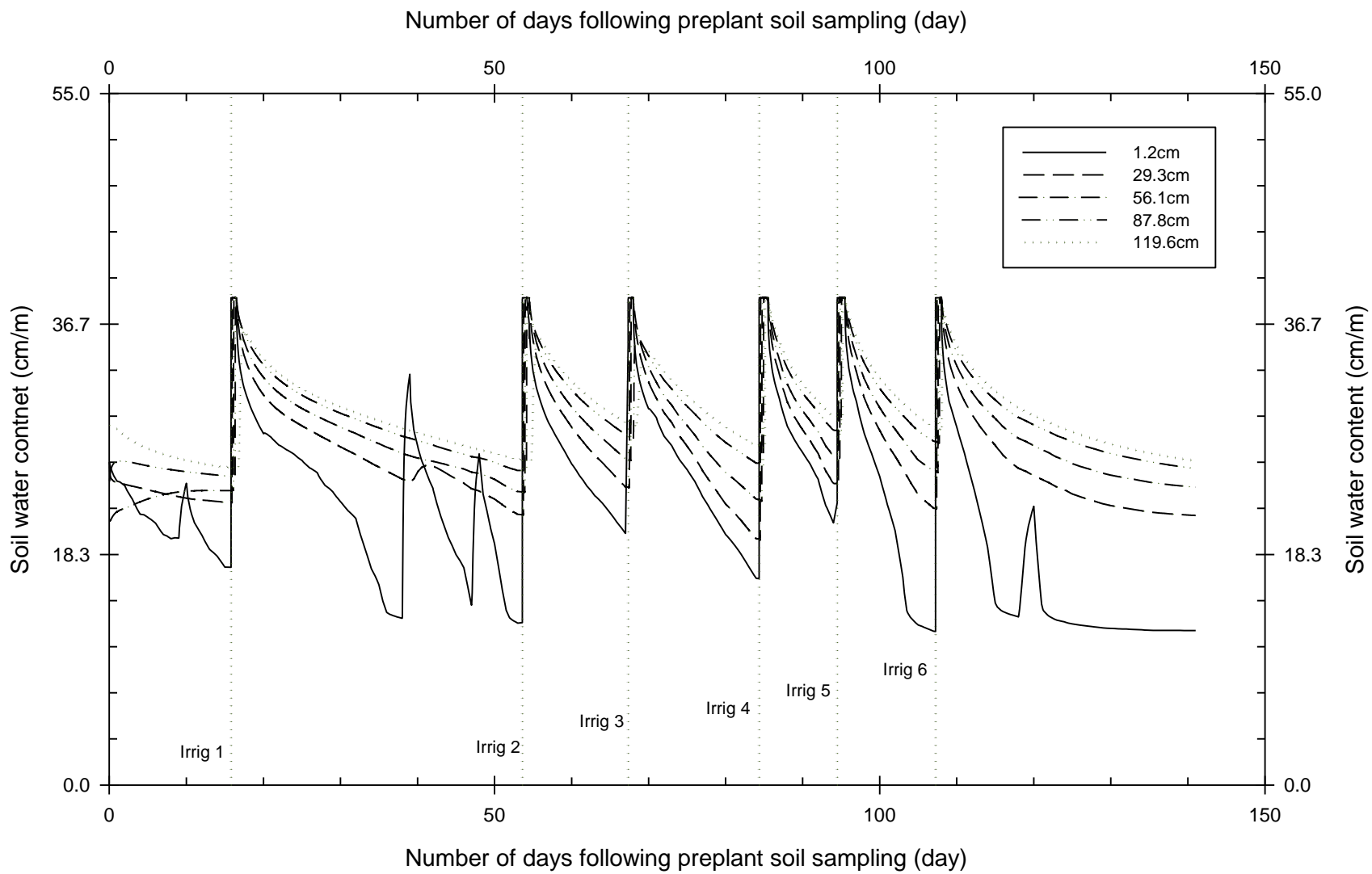


Figure 10. Seasonal variation of root zone soil water content at five observation points, data set II

Surface fluxes, such as irrigation, have a significant effect on the soil water content of the entire root zone profile. However, soil water contents in the lower soil horizons were virtually insensitive to the relatively smaller surface fluxes associated with natural precipitation (which generally consist of light showers in the study area). Evapotranspiration effects, which mainly occurred between irrigation events, have a gradual effect with time on soil water contents and were most felt in the surface layers compared to the lower lying horizons. As noted earlier, this observation is consistent with the fact that in a well-watered soil profile, such as that considered here, the most dynamic section of the root zone is the biologically active upper layer where most of the feeder roots are concentrated and much of the root water extraction, to meet evapotranspiration demands, takes place.

Notably, the upper most soil layer appears to be desiccated occasionally (Figure 10). Soil water content at the upper most observation point fell to a local minimum of 12.9cm/m just before the second irrigation event. Furthermore, in the time interval between the fifth and six irrigations and in the time period that followed the last (i.e., the sixth) irrigation, soil water content at the upper most soil layer fell sharply (from saturation right after the irrigation events) to a seasonal minimum of about 12.2cm/m. The low water content of the surface layer just before and subsequent to the last irrigation event is attributable to the relatively high evapotranspiration (an average of 0.6cm/day), occurring due mainly to the warming spring weather condition (with an average temperature of 93°F) toward the end of the cropping season. On the other hand, the low water content of the surface horizon, just before the second irrigation event, was likely related the relatively long irrigation interval, of 37 days, between the first and second irrigation events.

Seasonal variation of root zone soil water content in light of irrigation management

To provide context for the observed seasonal root zone soil water content variability in light of crop availability, the soil water content curves are superimposed on lines showing irrigation management related soil water constants (Figure 11). Soil water constants of irrigation importance considered here include: *FC*, *WP*, and *LLRAW*. The *FC* and *WP* soil water contents were set at 30 and 10cm/m, respectively (approximated based on guidelines proposed by the North East Region Certified Crop Advisors, 2020). Assuming the readily available soil water is

50% of the total crop available water, the *LLRAW* is set to 20cm/m (Figure 11). The *AIWC* calculated based on measured soil water contents, is 24.9cm/m, which is well above the *LLRAW*.

Overall, the soil water content of the root zone over much of the cropping season varied within the readily available soil water content range (between *LLRAW* and *FC*), which in practice is considered a favorable soil water environment for crop growth and yield. However, over a part of the cropping season an appreciable fraction of the root zone soil profile has water contents that are well in excess of the *FC* soil water content, suggesting significant over irrigation.

Soil water contents in the upper most soil layer of the root zone profile have fallen under the *LLRAW* water content in a couple of occasions through the season (Figure 11). Most significant declines in the soil water contents of the upper most soil layer, however, were observed in the days preceding the last irrigation event and over a period of weeks that followed the last irrigation event. The relatively low soil water content of the surface soil layer just before and following the last irrigation might not have appreciable effect on crop yield, because at this late stage of the cropping season seeds are likely fully formed and the crop should have matured and hence the effect of limited crop availability of soil water may have little or no effect on crop yield. In any case, compensatory root water uptake from the rather wet lower lying soil horizons could, at least partly, help offset the reduction in water uptake from the upper soil layer.

Figure 11 also shows that there are brief periods in the weeks leading up to the second irrigation where the soil water content of the upper soil layer is under the *LLRAW* water content, which in theory, may have some adverse effect on crop growth. However, it appears that these potential effects were, to a degree, mitigated by the precipitation fluxes of 1.7 and 0.6cm/day that occurred toward the end of the irrigation interval. Note that the seasonal soil water content profiles depicted in Figure 11 are derived through simulations and are not entirely based on measurements. Thus, the preceding observations on crop water stress and potential adverse effects should be viewed only as a cautionary note.

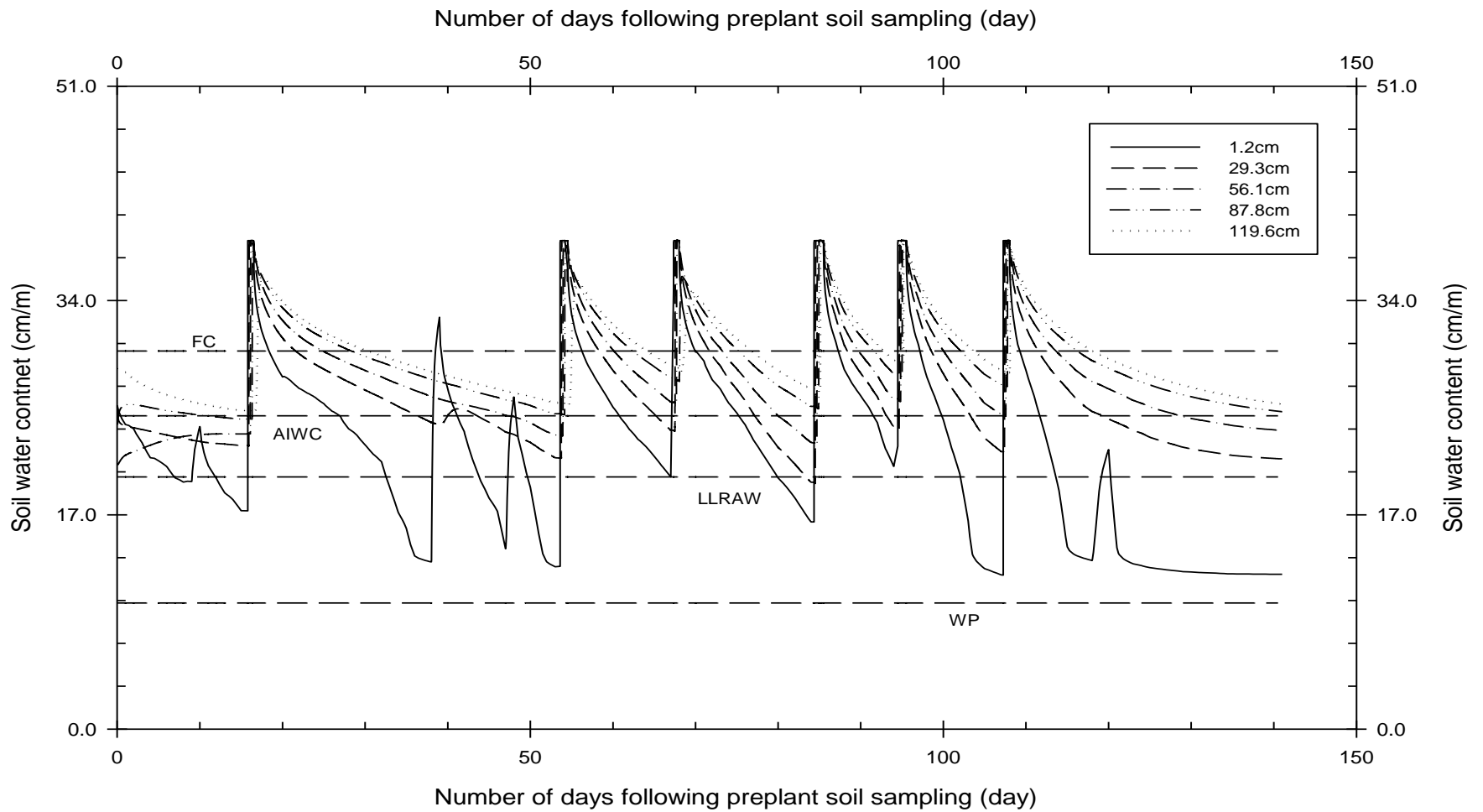


Figure 11. Seasonal variation of root zone soil water content at five observation points superimposed on lines showing soil water constants of irrigation significance, Data set II

3.3.2.c. Soil salinity and effects on crop yield, data set II

Seasonal variation of root zone salinity

Simulated seasonal variability of root zone salinity at the five observation points, described earlier, is depicted in Figure 12. Generally, the soil solution *EC* at the near surface soil horizons show sharp decline during each irrigation event. The decrease in the *EC* of the upper most observation point averaged over all irrigations of the cropping season is 0.8dS/m. The corresponding average *EC* of the upper most observation point following irrigation events is 1.0dS/m. Generally the root zone *EC* increased with depth during irrigation events. This suggests that dilution of the soil solution in the upper soil layers by the incoming irrigation water (which has an *EC* of 1.2dS/m compared to a seasonal root zone average soil solution *EC* of 1.8dS/m) and leaching of salts to lower lying layers are the main mechanisms that explain the observed trend in *EC* variability with depth during irrigation events. However, a closer look at the simulated data shows that the attendant soil physicochemical processes have also contributed to some extent (*Section 3.3.2.d*).

Figure 12 also shows that root zone salinity generally increased with time between irrigation events. Throughout the cropping season (not considering irrigation events), the *EC* of the upper most observation point increased at a much faster pace than is the case for the lower four observation points and the time rate of increase in *EC* generally declined with depth. As noted earlier (*Section 3.2.2.c*), the increasing trend in soil solution *EC* of the upper soil layer (Figure 12) was mainly driven by evapotranspiration, while drainage effects have more influence on the salinity of the lower sections of the root zone profile.

Figure 12 also shows that the steady increase in the soil solution *EC* of the upper most observation point, between irrigations, was punctuated by localized dips attributable to fluxes associated with natural precipitation events. By comparison, in the lower soil horizons the effect of major fluxes such as irrigation is noticeable, but natural precipitation events seem to have negligible effect on salinity levels. In addition, root zone salinity extremes (a seasonal minimum

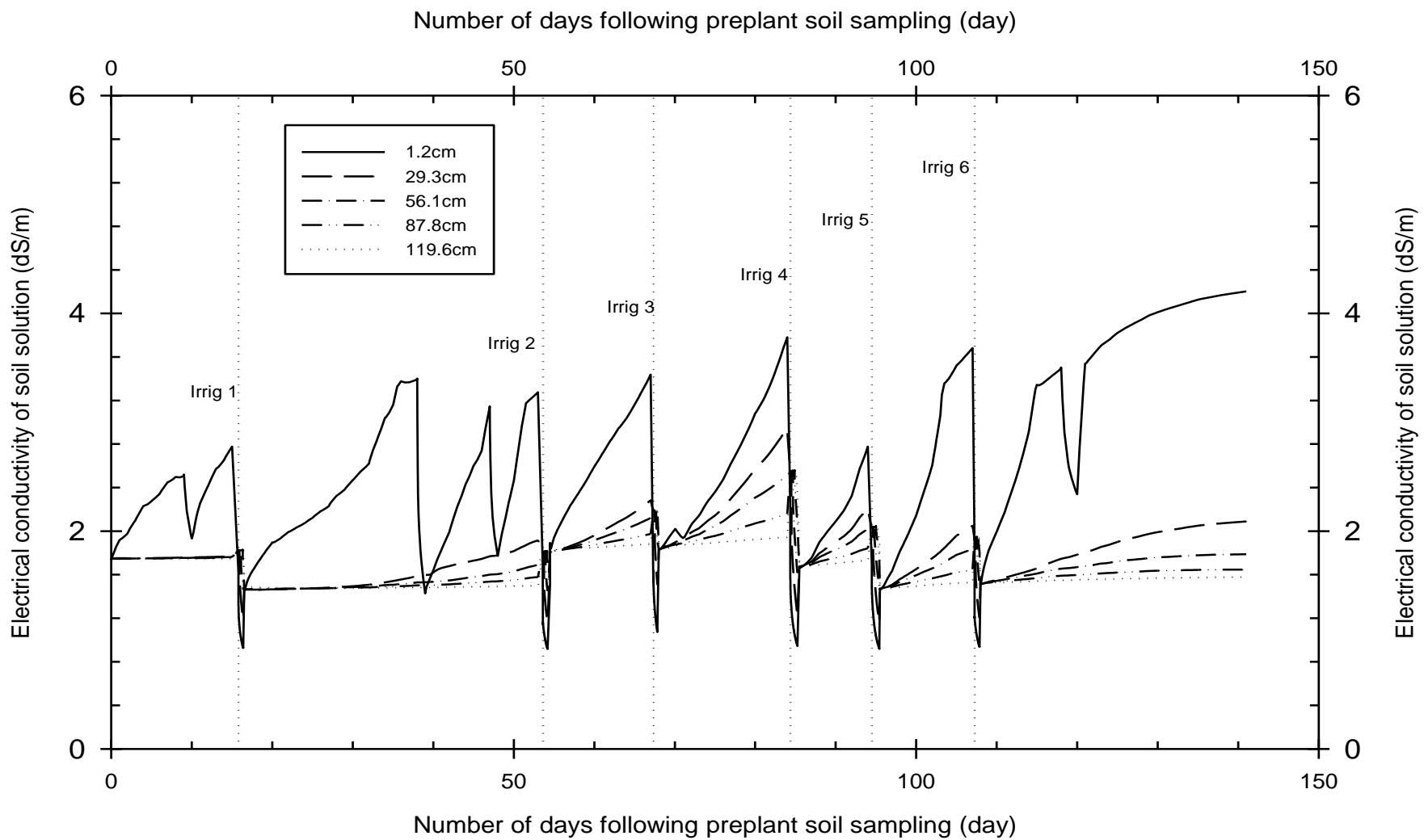


Figure 12. Seasonal variation in the electrical conductivity of the soil solution at five observation points, Data set II

EC of about 0.9dS/m and a maximum of 4.2dS/m, which were observed right before the start of the second irrigation event and at harvesting, respectively) occurred in the upper soil layer (Figure 12). Note that these results are mainly related to the sensitivity of the salinity of the upper soil horizon to surface fluxes and evapotranspiration.

Notably, the smallest increase in the *EC* of the upper most observation point, during an irrigation interval, occurred in the period that spans the fourth and fifth irrigation events (Figure 12). As can be noted from Figure 11, the fifth irrigation was applied while the root zone soil water content was relatively high. In fact, when the fifth irrigation occurred, the soil water content at the upper most observation point is greater than the *LLRAW* water content and the water content of the lower most observation point was slightly under the *FC* water content, with the water contents of the intermediate observation points falling in between. In other words, the 10day interval between the fourth and fifth irrigation events (the shortest irrigation interval of the season) was relatively short for evapotranspiration losses to have a significant effect on the soil solution concentrations of the root zone profile in general and the surface layer in particular (Figure 12). The implication is that the soil solution of the upper horizon was much less concentrated than it would have been if the irrigation interval was a bit longer, which explains the relatively modest rise in the *EC* of the upper most observation point during the time period of interest, compared to the other irrigation intervals.

A closer look at Figure 12 also shows that soon after an irrigation event is over, the root zone *EC*, especially the *EC* for the upper most observation point, increased sharply. As noted earlier (*Section 3.2.2.c*), this sudden jump in *EC* following the end of each irrigation event represents the transition from the *EC* (calculated based on the simulated major-ion concentration profiles) to the *EC* determined based on root zone average ion concentrations (which are used to reset the initial conditions for each subsequent simulation). Thus, they are artifacts of the way the initial conditions for each segment of the seasonal simulation are formulated than being a representation of the simulated salinity conditions in the root zone. Generally, the average root zone *EC* is appreciably larger than the *EC* computed, in the preceding simulation, at the upper most observation point. Thus, in simulations subsequent to the first, it is likely that there is a degree of overestimation in the computed *EC*s of the upper soil horizons. However, the error in

the simulated *EC* for the lower observation points should be relatively limited, because the root zone average *ECs* are closer to the computed *EC* values at these observation points.

Salinity effects on crop yield

As noted in *Section 3.2.2.c*, it is assumed here that the root zone electrical conductivity profiles computed by HYDRUS would have closely approximated those of the saturation extract, if such measurements were to be made concurrently through the season. Hence, in the current study, the root zone electrical conductivity profiles produced by HYDRUS were used directly (i.e., without adjustment) to calculate relative yield. The seasonal root zone average *EC* of data set II is 1.8dS/m, which is well under the crop salt tolerance threshold for durum wheat (2.1dS/m). It can, thus, be deduced from Eq. 3 that the corresponding relative yield is 100%, which implies that the seasonal average root zone salinity had no adverse effect on crop yield.

The root zone salinity of data set II varies with time through the cropping season (Figure 12). Furthermore, root zone salinity of data set II reaches its maximum value in the upper soil layer. Crop sensitivity to salinity generally varies with depth through the soil profile and is considered to be at its maximum in the near surface horizon of the root zone. Thus, comparing the salinity levels of the upper soil horizon, during the most sensitive crop growth stages, with the crop salt tolerance threshold may yield some useful insights that can complement the relative yield data presented earlier.

3.3.2.d. Sodium adsorption ratio and risk of sodicity, data set II

Seasonal variability of root zone sodium adsorption ratio

Seasonal variation of the simulated sodium adsorption ratio of the soil solution for data set II is depicted in Figure 13. The root zone *SAR* tends to increase with time between irrigation events at each of the observation points, although to a varying degree. Between irrigations, the *SAR* of the upper most soil layer increased at a much faster pace with time than the lower four observation points. As a result, the root zone *SAR*, typically, peaked right before irrigation events and the peak invariably occurred at the upper most observation point. However, the time interval between the first and second irrigations is an exception to this observation in that the corresponding maximum *SAR* occurred in the middle of the interval, right before a relatively

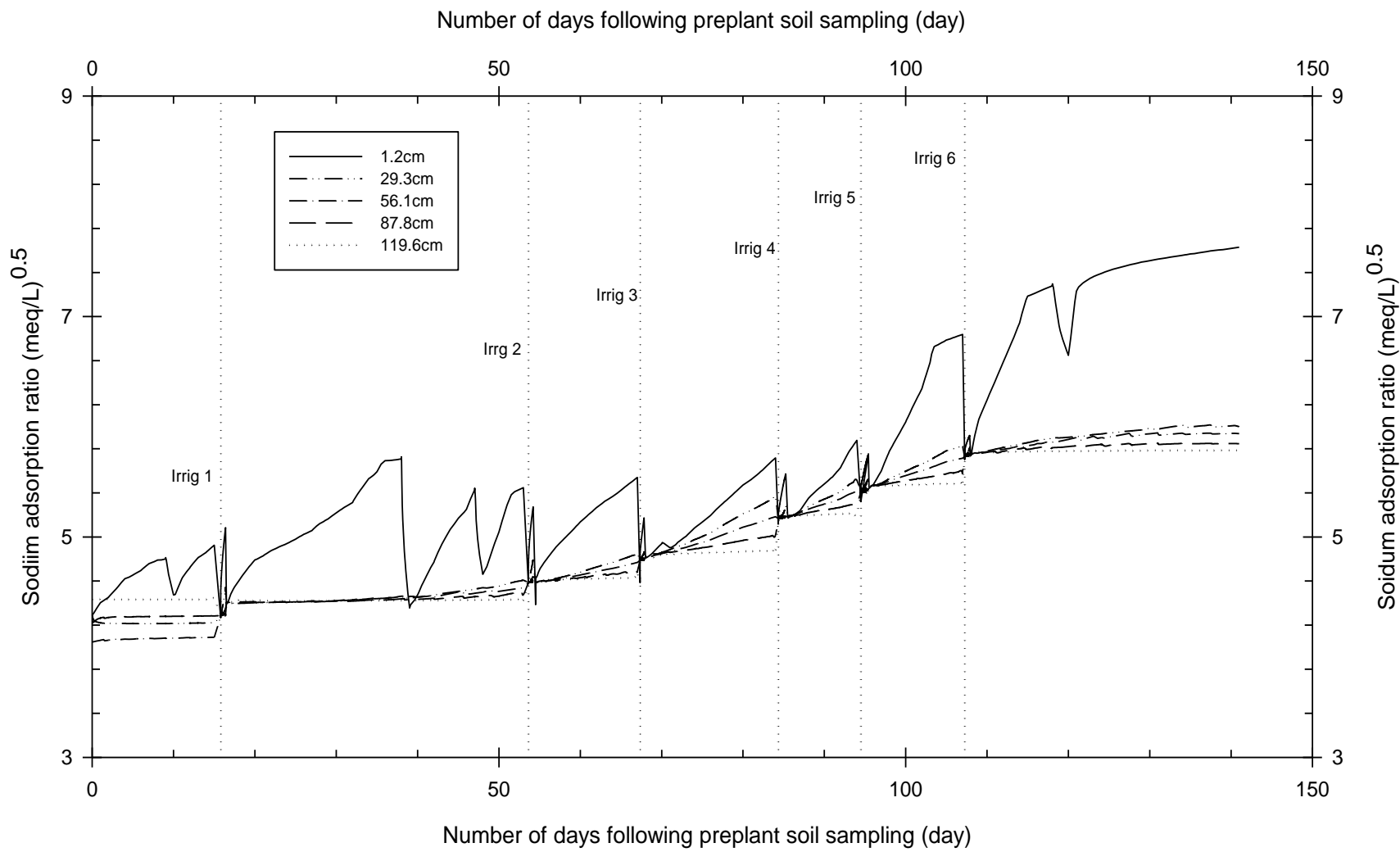


Figure 13. Seasonal variation of root zone sodium adsorption ratio at five observation points, Data set I

major precipitation event of 1.7cm, which led to a sharp decline in the *SAR* of the upper soil layer. Although *SAR* over much of the root zone profile increased steadily during irrigation intervals, that is not necessarily the case for the rather more sensitive upper soil layer, which is punctuated by localized dips due to natural precipitation events.

While evapotranspiration is the main factor that drives the observed general increases in soil solution *SAR* between irrigations, dilution of the soil solution by (the nearly distilled water from) precipitation and subsequent downward transport of salts are the main cause of the sharp localized decline in *SAR* following precipitation events. However, in both situations the attendant soil physicochemical processes have played a role in determining the relative concentrations of sodium, calcium, and magnesium in the soil solution and the corresponding *SAR*.

The seasonal minimum soil solution *SAR* was equal to $4.1\text{meq}^{0.5}/\text{L}^{0.5}$ and it occurred in the middle of the soil profile and at the beginning of the season (Figure 13). Furthermore, the seasonal maximum *SAR* of $7.6\text{meq}^{0.5}/\text{L}^{0.5}$ occurred at the upper most observation point and right before crop harvest, the time at which soil water content of the upper soil layer fell to the seasonal minimum (Figure 11). Overall, soil solution *SAR* showed an increasing trend with time through the cropping season, with an average increment of about $1.98\text{meq}^{0.5}/\text{L}^{0.5}$ over the season. A closer look at Figure 13 shows that the *SAR* of the upper most observation point fell sharply right before each irrigation event, it then showed a steep rise during irrigations, and declined abruptly immediately after each irrigation event. A closer examination of the root zone *SAR* profile data reveals that the sudden decrease in *SAR* prior to and following an irrigation event are artifacts of the way the initial conditions are set for each segment of the cropping season, which involves averaging the root zone profile concentrations of the major-ions (*Section 3.2.2.a*).

While averaging the root zone concentration profiles of the ions has limited effect on much of the root zone, it appears to have appreciable effect on the surface layer concentration profiles and the resultant *SAR*. As can be noted from Figure 13, the average root zone *SAR* used to reset the initial conditions, for each simulation subsequent to the first, are less than the *SAR* computed at the upper most observation point in the preceding simulation. Thus, its net effect is likely to be underestimation of the *SAR* at the upper most observation point, in subsequent simulations.

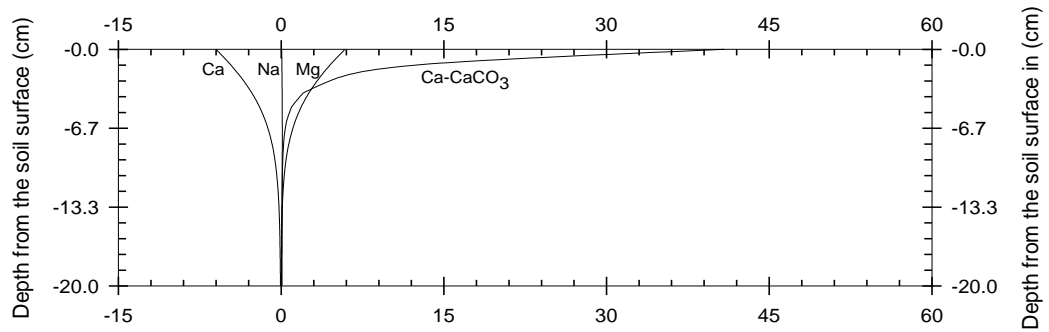
An important observation among those noted in the preceding paragraph is the increase in *SAR* during irrigation events, particularly in the upper soil layer of the root zone. As noted earlier, the changes in the concentrations of the individual cations in the soil solution and the corresponding *SAR* during each irrigation event is determined by the net interactive effect between solute transport (dispersion/mixing and advection) and soil physicochemical processes (complexation, cation exchange, and precipitation/dissolution of calcite).

A closer look at the computed aqueous phase concentrations of major cations in the upper 20cm layer of the root zone profile (which is provided in the *Conc.Out* file of HYDRUS-1D) reveals that in the surface soil layer the concentrations of all pertinent cations decreased and the corresponding *SAR* have invariably increased during each irrigation event. The decrement in the concentrations of *Ca*, *Mg*, and *Na* in the soil solution of the upper 20cm layer, averaged over all irrigations of the season, are 5.45, 0.71, and 3.97meq/L, respectively. The corresponding average increase in *SAR*, during an irrigation event, is $0.35\text{meq}^{0.5}/\text{L}^{0.5}$ and the maximum increment in *SAR* is $0.82\text{meq}^{0.5}/\text{L}^{0.5}$ and it occurred in the first irrigation event.

To assess the contributions of the individual soil physiochemical pathways to the observed changes in the liquid phase concentrations of pertinent cations during irrigations, the changes in the computed solid phase concentrations of calcium, magnesium, and sodium over the upper 20cm soil layer of the root zone (which is provided in the *Solid.Out* file of HYDRUS-1D) were examined. The changes in the concentration profiles of the cations, *Ca*, *Mg*, and *Na*, on the exchange complex and that of calcium-as-calcium-carbonate, *Ca-CaCO₃*, precipitate during irrigations #1, 3, and 5 are depicted in Figures 14a-14c. Note that in Figure 14, the negative algebraic sign indicates a decrease in the solid phase concentration of a chemical species during an irrigation event, while a positive algebraic sign shows an increase. The same pattern was observed for irrigation #2, 4, and 6 as those shown in Figure 14, thus for brevity only the data for irrigations #1, 3, and 5 are shown here.

As can be noted from Figures 14a-14c, the concentrations of each ion on the exchange complex and that of *Ca-CaCO₃* precipitate show maximum deviation from the initial conditions at the soil surface and then steadily approaches the initial condition with depth, reaching it at about 10 to 15cm depth from the surface (note that in Figure 14, the 0-0 line represents a scenario where there is no change in concentrations from the initial condition). The concentration of *Ca* in the soil exchange complex is invariably reduced, while that of magnesium, *Mg*, is

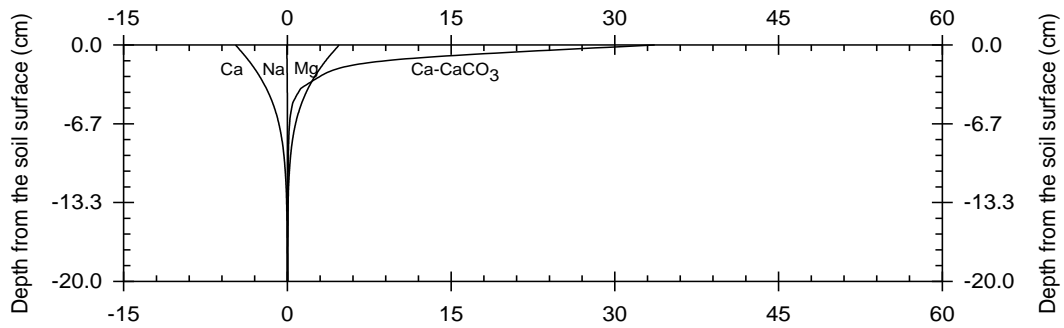
Change in the concentrations of Ca, Mg, and Na ions in the soil exchange complex and Ca-CaCO₃ (meq/Kg)



Change in the concentrations of Ca, Mg, and Na ions in the soil exchange complex and Ca-CaCO₃ (meq/Kg)

(a)

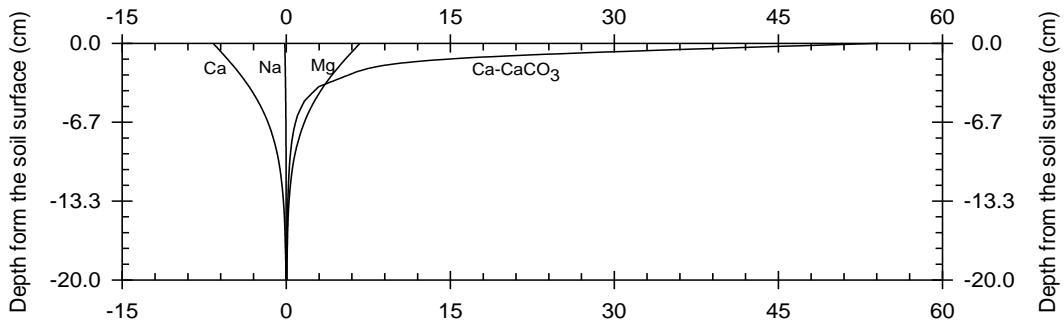
Change in concentrations of Ca, Mg, and Na ions in the soil exchange complex and Ca-CaCO₃ (meq/Kg)



Change in the concentrations of Ca, Mg, and Na in the soil exchange complex and Ca-CaCO₃ (meq/Kg)

(b)

Change in the concentrations of Ca, Mg, and Na ions in the soil exchange complex and Ca-CaCO₃ (meq/Kg)



Change in the concentrations of Ca, Mg, and Na ions in the soil exchange complex and Ca-CaCO₃ (meq/Kg)

(c)

Figure 14. Changes in the concentrations of the major cations (Ca^{2+} , Mg^{2+} , and Na^{+}) in the soil exchange complex and $Ca-CaCO_3$ in the upper 20cm layer of the crop root zone during the: (a) first, (b) third, and (c) fifth irrigation of data set II (*Note: the cations considered here are those pertinent to the determination of the sodium adsorption ratio of the soil solution*)

increased by roughly the same amount during each irrigation event, Figures 14a-14c. This may appear counter intuitive, given that calcium is the preferred ion by the exchange complex than magnesium. This might, perhaps, be due to the competitive effect of calcite precipitation on calcium concentration in the soil solution and indirectly on the exchange complex. One should also need to acknowledge here that complexation reactions, in principle, may also have an effect on the solubility of calcium and hence on its equilibrium concentration in the soil solution and the exchange complex. By comparison, sodium concentration in the exchange complex increased during the first irrigation and decreased during the third and fifth irrigations, but only by trace amounts (Figures 14a-14c) and mainly in the upper most soil layer. The implication is that the observed appreciable decline in sodium concentration of the soil solution, during irrigation events, is likely (for the most part) the product of transport processes.

As can be noted from Figures 14a-14c, cation exchange has contributed to an increase in the concentration of *Ca* and a decrease in the concentration of *Mg* in the soil solution of the upper soil layer of the root zone (during irrigation events), which appears to be particularly significant near the soil surface. On the other hand, the data (Figures 14a-14c) shows that precipitation of calcite is far more important physicochemical process, than cation exchange, in terms of its effect on the soil solution concentration of calcium during irrigations. It is likely that calcium immobilization through calcite precipitation accounted for a significant fraction of the net decrease in *Ca* concentration of the soil solution. These observations suggest that the decrease in soil solution *SAR*, during irrigations are likely the results of the interactive effects of mainly calcite precipitation (on the concentration of *Ca* in the soil solution), solute transport processes and cation exchange (on the concentration of *Mg* in the soil solution), and mainly solute transport processes (on the concentration of *Na* in the soil solution).

It is important to note here that this is only an explanation of the simulated data and should not necessarily imply an exact characterization of the actual soil physicochemical processes of the study site. Recognizing that the soil physicochemical processes considered here are not exhaustive and that the results presented here are not entirely based on field and laboratory measurements, it is conceivable that the actual field processes could differ from the description provided here.

Notably, the increase in soil solution *SAR* during irrigation events observed in data set II, contrasts with the result for data set I, where such a spike in *SAR* during irrigation events is not discernible in Figure 7. An examination of the computed data in the upper 20cm layer of the root zone, of data set I, revealed that the total liquid phase concentrations of *Ca*, *Mg*, and *Na* have decreased during each irrigation events (*Section 3.2.2.d*), as was the case with data set II. However, unlike data set II, the corresponding *SAR* as well decreased slightly during each irrigation. The average decrease in the *SAR* of the upper 20cm soil layer across all irrigations is $0.18 \text{ meq}^{0.5}/\text{L}^{0.5}$. The maximum decrease in the *SAR* is $0.35 \text{ meq}^{0.5}/\text{L}^{0.5}$ and it occurred during the fifth irrigation.

A closer look at the effects of the different soil physicochemical pathways on the computed concentration distributions of the major-cations (both on the solid and liquid phases) during irrigation events shows a similar pattern for data set I as those described above for data set II (Figure 14a-14c). The concentration of calcium is reduced and that of magnesium is increased in the soil exchange complex by about the same amount during irrigations. The concentration of sodium in the exchange complex of the upper most soil horizon decreased during irrigations, but by a much smaller amounts than the changes observed for calcium and magnesium.

A close examination of the solid phase solute data showed that calcite precipitation is the most dominant physicochemical process, in data set I as well, in terms of its effect on the liquid phase calcium concentration of the surface soil horizon. However, the scale of calcite precipitation, in data set I, is much smaller than that observed in data set II. Overall, sodium concentration in the soil solution of data set I decreased in such proportions to those of calcium and magnesium that the corresponding *SAR* was less than the *SAR* at the start of irrigations.

Potential sodic hazard to the root zone soil profile

The seasonal average root zone *SAR* is $5.1 \text{ meq}^{0.5}/\text{L}^{0.5}$ and the maximum which occurred at the end of the cropping season and in the upper most observation point is $7.6 \text{ meq}^{0.5}/\text{L}^{0.5}$. Based on the criterion described by Essington (2005), which combines root zone *SAR* and *EC* levels to characterize sodic risks, it can be observed that the average and maximum root zone *SAR* of data set II are well under the indicated upper limit of 13 to 15 $\text{meq}^{0.5}/\text{L}^{0.5}$. However, the seasonal average root zone soil solution *EC* of 1.8dS/m is less than the proposed lower bound of 4dS/m by

a significant margin. This leaves us with a degree of uncertainty as to how to characterize the potential sodic hazard of the soil solution salt composition of data set II. Authors, therefore, could not make a definitive determination here regarding the potential effects of sodium on soil physical properties

The *SAR* of the surface soil layer in the period following the last irrigation is relatively high, ranging between $6.8\text{meq}^{0.5}/\text{L}^{0.5}$ right before the last irrigation and $7.6\text{meq}^{0.5}/\text{L}^{0.5}$ at season's end. However, the corresponding soil solution *EC* was also higher (varying between 3.7dS/m right before irrigation and 4.2dS/m at harvest), which suggests that the adverse effects, if any, of the larger *SAR* would have been, to some degree, mitigated by the larger *EC*.

3.3.2.e. Cumulative boundary fluxes, transpiration, and leaching fraction

For data set II, the seasonal running sum of fluxes leaving the crop root zone (i.e., cumulative infiltration, transpiration, evaporation, evapotranspiration, and deep percolation) are depicted in Figure 15. The simulated seasonal cumulative infiltration, transpiration, evaporation, evapotranspiration, and deep percolation, for data set II, are 104.7, 39.6, 12.1, 51.7, and 53.6cm respectively. Each of the cumulative boundary fluxes and crop transpiration, computed for data set II, show exactly the same functional behavior as those observed in relation to data set I (*Section 3.2.1.e*). Cumulative infiltration flux exceeded cumulative evapotranspiration throughout the season by a wide margin (Figure 15), suggesting over irrigation.

As noted in *Section 3.2.2.e*, the seasonal root zone soil water balance was used as an approximate indicator of the relative significance of initial soil water content versus infiltration as the source of deep percolation water. The root zone soil water content showed a net decrease of 0.5cm over the cropping season. This observation suggests that although the seasonal cumulative infiltration flux of 104.7cm was significantly larger than that of the crop consumptive use need of 51.7cm; it, nonetheless, fell short of covering the entire deep percolation flux of 53.6cm, by 0.5cm. In other words, the drainage water attributable to infiltration is 53.1cm and the balance of 0.5cm came from the soil water extant in the root zone profile at the start of the season. It can be thus be shown based on Eq. 4, that the leaching fraction is 50.7%.

As noted earlier in *Section 3.2.2.e*, the inverse relationship between concentrations and depths given in Eq. 4 is not applicable here. In other words, with the current data leaching fraction can be calculated only based on the ratios of the drainage and irrigation water depths,

not based on concentrations. Note that the leaching requirement equation, Eq. 6, may not be directly applicable to the data presented here.

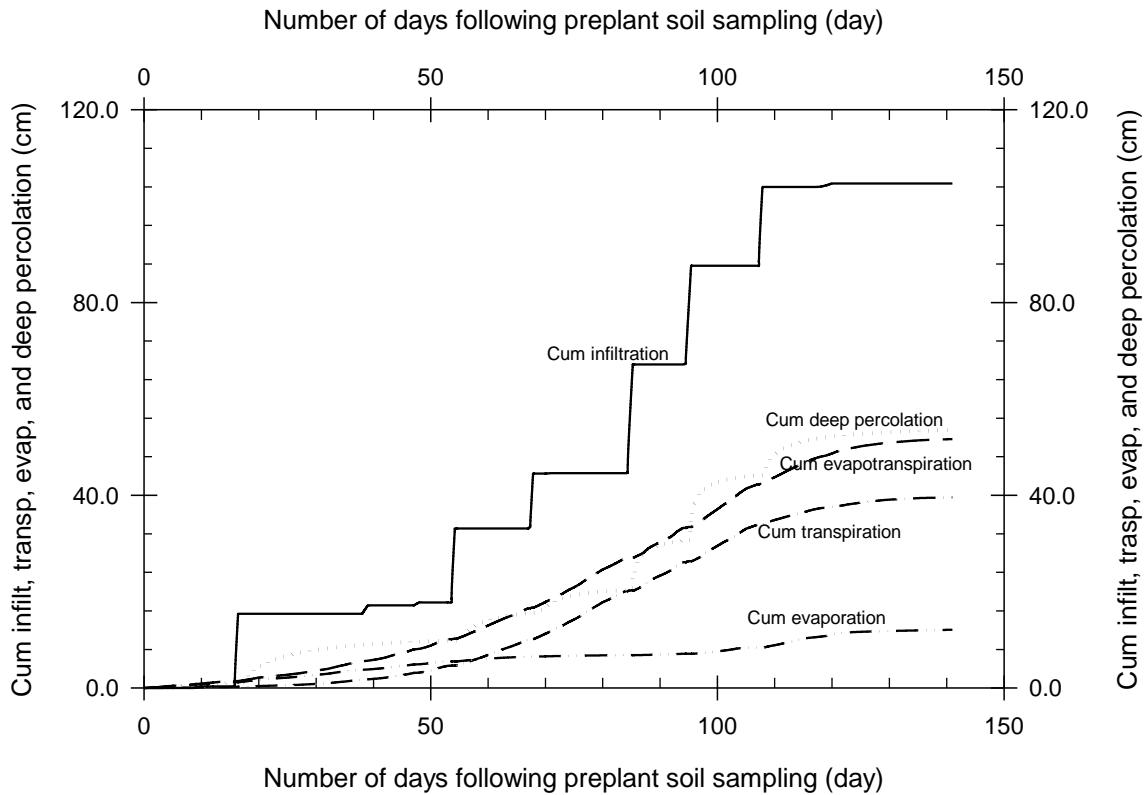


Figure 15: Cumulative (running sum of) infiltration, transpiration, evaporation, evapotranspiration, and deep percolation fluxes

3.3.2.f. *Cautionary note*

Results and observations presented here are only partly based on measured data and are not complemented by measured crop growth and yield data. Thus, they need to be treated only as useful insights that can be used to help identify potential problems and guide future studies. Furthermore, the current study is limited to point-scale analysis of root zone salinity and as such the results cannot be directly generalized for an entire field, without the assumption that the surface boundary conditions, initial conditions, and the soil physical and chemical properties observed at the sampling node used in the current analysis are replicated fully or substantially across the field.

Chapter 4. Concluding remarks, summary, and cautionary note

4.1. Background and objectives

Crop production in the Yuma area is almost entirely dependent on irrigation water supply from the Colorado river. With an average EC_{iw} of 1.1 to 1.3dS/m, the Colorado river water in Yuma is considered to be of medium salinity in terms of its suitability for crop production. Root zone concentration of salts generally increase in the course of cropping seasons due mainly to evapotranspiration effects. Increases in the salt concentration of the crop root zone in excess of some thresholds can lead to reduced root water uptake, poor soil permeability and tilth, and specific ion effects. Thus, salinity management that seeks to maintain the salt content of the crop root zone under a set threshold, required for optimal crop production, is a key component of an effective agronomic and irrigation management package in irrigated watersheds. Accordingly, intentional over irrigation aimed at effecting periodic leaching of salts from the crop root zone, is widely practiced in the Yuma area, to maintain a favorable salt balance for crop growth and yield. Effective salinity management is of particular significance in the Yuma area, because many of the crops grown in the area are sensitive to salinity.

Optimal salinity management in irrigated soils, in principle, requires monitoring the salt load of irrigation water and the time evolution of salt concentrations in the root zone soil solution over a suitable time frame, such as a cropping season. A salinity management strategy that is entirely reliant on field and laboratory studies is impractical, because the time and effort needed for field collection and laboratory analysis of required data and expenses incurred can be prohibitive. Mathematical models, on the other hand, represent more flexible and inexpensive salinity evaluation, management, and research aid.

The overall objective of the project reported here is, thus, to conduct a modeling study aimed at a preliminary evaluation of the effectiveness of current salinity management practices in fields that are under wheat crop in the Yuma Valley Irrigation Districts. Specifically, a simulation based point-scale analysis of the season-long evolution of root zone salinity under wheat crop was conducted for some selected fields in the Yuma Valley Irrigation Districts. In addition, the potential adverse effects of root zone salinity, if any, on crop yield and soil physical properties of agronomic significance was assessed.

4.2. Method and data description

A physically based mathematical model, HYDRUS-1D (which is widely used to simulate coupled soil water flow, solute transport-reaction, and heat transport through a variably saturated porous medium), was applied in the current study to simulate pertinent root zone soil processes. HYDRUS-1D inputs for a season-long simulation of the time-evolution of the root zone salinity of a cropped field consists of soils, crop, irrigation, meteorological, and events calendar data. Specifically, HYDRUS input data consists of model parameters, initial and boundary conditions for both soil water dynamics and solute transport-reaction simulations, and limiting surface fluxes. Model parameters include soil water retention and conductivity parameters, solute transport and reaction parameters, parameters of the crop response functions to water and salinity stresses and root water distribution function parameters. In addition, applicable surface and bottom boundary conditions for flow and transport-reaction simulations need to be specified. Furthermore, potential evaporation from the soil surface and potential transpiration through the crop canopy constitute the limiting surface fluxes.

Some model inputs were obtained based on field and laboratory measurements and other inputs were derived from literature sources, HYDRUS databases, or were determined based on measured data. The measured salinity data, used in the simulation study reported here, was derived from data sets collected in the Yuma Valley Irrigation Districts in the winter spring seasons of 2016 and 2017. Two of the data sets, labeled here as data sets I and II, were selected for use in the current analysis. Data set I is collected in a field located in the South Gila Valley and data set II is from a field in the Yuma Valley.

Both data sets I and II were collected in fields that were under (durum) wheat crop. Crop was grown in rectangular irrigation basins, measuring 650ft (198.1m) × 1250ft (381m) for data set I and 625ft (190.5m) × 895ft (272.8m) for data set II. The salinity simulation period, which overlaps with the cropping season, spans 143 and 141 days for data sets I and II, respectively. The soils of the study sites are loam for data set I and sandy loam for data set II. Precipitation in the study area is infrequent and it typically consists of light showers of limited depth. Hence, its contribution to the water balance of the study sites was considered negligible. Irrigation is, thus, the primary source of water for crop production. Crop water requirements were applied in five irrigation doses (for data set I) and six irrigations (for data set II), distributed across the cropping season.

For both data set I and II, the seasonal precipitation and reference evapotranspiration data were downloaded from the AZMET web portal for the weather stations that are closest to the study sites. The corresponding crop potential evapotranspiration was then deduced from reference evapotranspiration as a function of the crop coefficient, which varied from a minimum of 0.3 at season's end to 1.1 in the mid-season stage. The potential evapotranspiration was then partitioned into evaporation and transpiration components (which constitute separate input data streams of HYDRUS-1D) as a function of the crop leaf area index. Actual transpiration was computed as a function of the potential crop transpiration, the root water uptake distribution, and the crop's response to soil water and salinity stresses. Root water uptake distribution was assumed here to follow the trapezoidal model of Hoffman and van Genuchten and Feddes' formulation was used to describe the crop's response to soil water stresses. The crop response to salinity stresses was expressed in terms of the function proposed by Maas. Parameters of the soil water and salinity stress response functions were derived from HYDRUS-1D databases based on crop type.

4.3. Results, Soil water

Simulated seasonal soil water content profiles monitored at fixed observation points across the root zone show that, for both data sets I and II, irrigation events are marked by sharp rises in soil water contents, particularly in the upper soil layers of the profile. Soil water contents, of the upper soil layers, reached saturation (41cm/m for data set I and 38.8cm/m for data set II) at the end of each irrigation event. Between irrigation events, however, soil water contents generally declined with time due to the combined effect of crop transpiration, evaporation through the soil surface, and deep percolation through the bottom boundary of the root zone. The seasonal minima root zone soil water contents, which also occurred in the upper soil layers of the root zone profile, are 11.7cm/m for data set I and 12.2cm/m for data set II. For both data sets, relatively dry soil conditions were observed earlier in the cropping season and toward the end of the season. Desiccated soil conditions observed early in the cropping season are mainly related to relatively long irrigation intervals, while those that occurred toward the end of the season appear to be related to increased evapotranspiration (in fact, mostly evaporation) attributable to the warming spring weather. Overall, the simulated data suggests that soil water contents increased with depth from the soil surface.

To provide context to the observed seasonal root zone soil water content variability, in light of crop availability of soil water, the simulated soil water content data was compared with soil water constants of irrigation significance. The soil water constants considered here are field capacity, wilting point, and the lower limit of the readily available soil water content. The comparison reveals that, for both data sets I and II, the soil water contents through much of the cropping season fell within the readily available soil water range, which in practice is considered favorable soil water environment for crop growth and yield. However, relatively dry soil conditions that approximate wilting point water contents (of 12.5 and 10cm/m for data sets I and II, respectively) were observed in the surface soil layers over a period of weeks, early in the season and, prior to crop harvest.

The effect of the relatively low soil water contents on crop yield during the latter part of the cropping season is likely negligible, if any. On the other hand, the relatively low soil water contents of the upper soil layers in the early part of the cropping season (which are attributable to long irrigation intervals) and the resultant reduction in root water uptake may have some effect on crop growth, if not yield, and hence may need to be looked into in follow-up studies. This observation is mainly relevant to data set I than data set II. In data set II, however, potential adverse effects of limited water availability in the early part of the season appears to have been mitigated to a degree by infiltration fluxes attributable to relatively major precipitation events. Furthermore, the soil water content profile of data set II shows that, over a part of the cropping season, an appreciable fraction of the root zone soil profile has soil water contents that are well in excess of the field capacity water content, suggesting significant over irrigation.

The root zone soil water content profiles presented in this study are results of simulation and are only partly based on measurement data. Hence, it is important that the preceding observations in regard to limited crop availability of soil water (in parts of the growing season) and its potential adverse effects on crops and the excess deep percolation below the crop root zone should be viewed here only as cautionary notes.

4.4. Results, Soil salinity

Simulated seasonal salinity profiles monitored at preset observation points in the root zone show that, for both data sets I and II, the soil solution electrical conductivity, *EC*, at the near surface soil horizons decreased sharply during irrigation events. The decline in the *EC* of

the upper soil layers averaged over all irrigations of the season are 1.0 and 0.8dS/m for data sets I and II, respectively. Following irrigation events the soil solution *EC* of the upper soil layer, of data set I, fell to an average value of about 1.3dS/cm which is close to the *EC* of the irrigation water (1.2dS/m). For data set II, on the other hand, the soil solution *EC* of the upper soil layers fell to an average of about 1.0dS/m following irrigation events, which is less than the *EC* of the irrigation water. Note that for both data sets, the soil solution *EC*, observed right after each irrigation event, is less than the computed seasonal average root zone salinity of 2.8dS/m (data set I) and 1.8dS/m (data set II) by significant margin. The results also show that, for both data sets I and II, the soil solution *EC* increased with depth from the soil surface during irrigation events.

These results suggest that dilution of the soil solution in the upper soil layers with irrigation water and subsequent leaching to lower soil horizons appear to be important factors in explaining the observed root zone *EC* variability trends during irrigation events. However, the average soil solution *EC* of 1.0dS/m (observed in the upper soil layer of the data set II following irrigation events), which is less than the *EC* of the irrigation water, suggests that soil physicochemical processes also have a contribution.

On the whole, simulated data also shows that, between irrigation events, soil solution *EC* at each of the observation points increased with time for both data sets I and II. This observation is consistent with the overall trend of decreasing soil water contents noted earlier between irrigations. Generally, the time rate of increase in the soil solution *EC* is highest at the upper observation point and decreases with depth from the surface. In the upper soil horizons, the decrease in soil water contents between irrigations is driven mainly by evapotranspiration, a process that leads to increased salt concentration in the soil solution and hence increased *EC*. The data also shows that, for both data sets, the *EC* of the upper soil horizons is more sensitive to surface fluxes (irrigation, natural precipitation, and evaporation) and crop transpiration than those of the lower sections of the root zone profile. As a result, all root zone salinity extremes (a seasonal minimum of 1.2dS/m and maximum of 7.7dS/m for data set I and a minimum of 0.9 and a maximum of 4.2dS/m for data set II) were also observed at the upper soil layers. Overall, evapotranspiration between irrigation events appears to be the main driver of the observed increase in salinity in the upper soil layers of the root zone profile, while deep percolation is more influential in the salinity of the lower soil horizons. However, the effects of

evapotranspiration and to a degree deep percolation are modulated by soil physicochemical processes.

The effects of salinity on crop yield were evaluated based on the seasonal average root zone *ECs* and the crop salt tolerance threshold. The seasonal average root zone *EC* for data set I is 2.8dS/m, which exceeded the crop salt tolerance threshold of 2.1dS/m, for durum wheat, by a margin of 0.7dS/m. The corresponding relative yield is 98.3%. By comparison, the seasonal mean root zone salinity for data set II is 1.8dS/m, which is less than the crop salt tolerance threshold. This implies that, in data set II, salinity has no adverse effect on crop yield. Overall, these results suggest that the seasonal average root zone salinity had no measurable effect on crop yield in both fields.

4.5. Result, Sodium adsorption ratio

The seasonal variation of the root zone sodium adsorption ratio, *SAR*, data follows the same general trend with time as those of the *EC* data for both data sets I and II. Overall, *SAR* increased between irrigation events at each observation point in the root zone and the *SAR* of the near surface soil horizons increased at a much faster pace with time compared to the lower lying soil layers of the root zone and the rate of increase became more pronounced toward the end of the cropping season. As a result, the seasonal maximum *SAR* of 9.2 and 7.6meq^{0.5}/L^{0.5} for data sets I and II, respectively, occurred in the upper soil layer and were observed right before crop harvest. The results also show that the time rate of increase in *SAR* generally declined with depth. The simulated data shows that, for both data sets, the root zone *SAR* increased during the season.

The *SAR* of the upper soil horizon, of data set I, showed a slight decline during each irrigation event. However, it showed no discernible change over much of the lower section of the soil profile. By contrast, the *SAR* profile of the upper soil horizon, of data sets II, showed an appreciable increase during irrigation events. A closer look at the solid phase distribution of the cations, *Ca*, *Mg*, and *Na*, revealed that in both data sets precipitation of calcium as calcium carbonate, during irrigation, is the most significant soil physicochemical process in terms of its net effect on the liquid phase concentration of calcium. The concentration of *Mg* in the soil solution appears to be influenced to some extent by cation exchange. The effect of cation exchange on the soil solution concentration of *Na* is negligible. The results also show that

transport (advection and dispersion) processes have influence on the distribution of cations and on the resultant *SAR*.

The seasonal average root zone *SAR* are $6.2\text{meq}^{0.5}/\text{L}^{0.5}$ (for data set I) and $5.1\text{meq}^{0.5}/\text{L}^{0.5}$ (for data set II). Although the root zone average *SAR* for both data sets are not particularly high, it ought to be noted that sodic risks need to be evaluated taking into account not only the soil solution *SAR*, but also the corresponding *EC*. According to Essington, a soil is considered sodic if its *SAR* exceeds 13 to $15\text{meq}^{0.5}/\text{L}^{0.5}$ and the corresponding *EC* is equal or less than 4dS/m. Based on this criterion, it can be observed that the average root zone *SAR* of both data sets are well under the indicated upper limit. However, the seasonal average root zone *EC* of 2.8dS/m (data set I) and 1.8dS/m (data set II) are less than the 4dS/m lower bound by an appreciable margin. Evidently, this leads to a degree of uncertainty in regard to the determination of the potential sodic hazards of the soil solution salt composition of both data sets. Consequently, authors are unable here to characterize the potential effects of sodium on soil physical properties of the study sites.

4.6. Cumulative boundary fluxes, transpiration, and leaching fraction

Computed cumulative fluxes that leave the crop root zone through its upper and lower boundaries (i.e., infiltration, evaporation, deep percolation) and the crop canopy (i.e., transpiration) were examined to assess the seasonal leaching fraction. A close examination of the data shows that the seasonal cumulative infiltration fluxes accounted for 100 and 99.9% of the cumulative outgoing fluxes, from the root zone, of data sets I and II, respectively. The seasonal leaching fractions calculated based on these data were 27.1% for data set I and 50.7% for data set II. The large leaching fraction calculated for data set II is consistent with the relatively low seasonal average root zone *EC* of 1.8dS/m, which is not only about two-thirds of the root zone average *EC* of data set I, but is also well under the 2.1dS/m salt tolerance threshold of durum wheat.

4.7. Summary and cautionary note

4.7.1. Summary

4.7.1.a. Soil water

- For both data sets I and II, the results show that soil water contents through much of the cropping season fall within the readily available soil water range (23.8 to 35.0cm/m for data set I and 20.0 to 30.0cm/m for data set II), which in practice is considered favorable soil water environment for crop growth and yield.
- With deep percolation fractions of 27.1% (data set I) and 50.7% (data set II), irrigation amounts for both data sets exceed the crop water requirement by an appreciable/significant margin.
- The results show that the soil water contents of the upper soil layers, of both data sets, fell close to wilting point (12.5cm/m for data set I and 10.0cm/m for data set II) early in the cropping season and in the weeks that preceded crop harvest. The relatively dry soil conditions of the upper horizons, early in the season, may possibly have effects on crop growth, if not yield, and hence need to be looked into in follow-up studies.

4.7.1.b. Salinity

- The soil solution *EC* of the upper soil layers, of both data sets I and II, showed appreciable declines (average decrements of 1.0dS/m for data set I and 0.8dS/m for data set II) during irrigation events. By comparison, the observed changes in the *EC* of the lower section of the root zone profile were marginal.
- The results show that between irrigation events, root zone *EC* generally showed an increasing trend with time and typically peaked before irrigations. The time rate of increase in *EC* is typically highest in the surface horizons and showed a decreasing trend with depth.

- Computed root zone salinity varies between 1.2dS/m and 7.7dS/m for data set I and between 0.9 and 4.2dS/m for data set II. Notably, all salinity extremes were observed in the upper most soil layer.
- It appears that, between irrigations, the concentrating effect of evapotranspiration is the main factor responsible for the observed increases in the *EC* of the surface soil horizons of the root zone. On the other hand, solute transport effects appear to be more influential on the time evolution of salinity in the lower soil horizons. However, the effects of evapotranspiration and solute transport are, to a varying degree, modulated by soil physicochemical processes.
- The seasonal average root zone salinity are 2.8dS/m and 1.8dS/m for data sets I and II, respectively. The corresponding yield losses are 1.7% (for data set I) and 0% (for data set II). These results suggest that, in both fields, the seasonal average root zone salinity had no measurable adverse effect on crop yield.
- Root zone salinity varies with depth and crops are more sensitive to higher salinity levels in the near surface soil horizons than in the lower section of the root zone. Crop sensitivity to salinity also varies with the stage of growth of the crop. Thus, a follow-up study that compares the average salinity within the upper soil layers of the root zone, during the most sensitive crop growth stages, with crop salt tolerance thresholds may potentially yield useful insights that can complement the relative yield data reported here, which was determined based seasonal root zone average salinity.

4.7.1.c. Sodium adsorption ratio

- The *SAR* of the upper soil horizon of data set I showed a decreasing trend during each irrigation event, the average decrement across all irrigations being $0.18\text{meq}^{0.5}/\text{L}^{0.5}$ and the maximum decrement is $0.35\text{meq}^{0.5}/\text{L}^{0.5}$. By comparison, the *SAR* of the near surface soil horizon of data set II exhibited an increasing trend during irrigations, with an average increment of $0.35\text{meq}^{0.5}/\text{L}^{0.5}$ and a maximum increment of $0.82\text{meq}^{0.5}/\text{L}^{0.5}$.

- Root zone *SAR* generally showed an increasing trend between irrigation events and peaked right before irrigations. Typically, the *SAR* of the near surface soil horizons increased at a much faster pace with time compared to the lower lying soil layers of the root zone.
- Computed root zone *SAR* varied between 5.1 and 9.2meq^{0.5}/L^{0.5} for data set I and between 4.1 and 7.6meq^{0.5}/L^{0.5} for data set II. Notably, all but one of the salinity extrema were observed in the upper most soil layer.
- The average root zone *SAR* of 6.2meq^{0.5}/L^{0.5} (for data set I) and 5.1meq^{0.5}/L^{0.5} (for data set II) are not particularly high. However, a determination of the potential sodic risks, associated with the salt compositions of the soil solutions of both data sets, based on the more rigorous criterion that takes into account the effects of the root zone average *SAR* and *EC* could not be made here.

4.7.1.d. Fluxes and leaching fraction

- The root zone water balance of data set I showed that the computed cumulative infiltration over the cropping season is 66.1cm and the seasonal cumulative deep percolation depth attributable to infiltration is 17.9cm. Thus, the corresponding leaching fraction is 27.1%.
- The root zone water balance for data set II showed that the computed seasonal cumulative infiltration is 104.7cm and the fraction of the seasonal cumulative deep percolation attributable to cumulative infiltration is 53.1cm. Thus, the corresponding leaching fraction is 50.7%.

4.7.2. Cautionary note

- The results presented here are only partly based on measured data. In addition, they are not complemented by measured crop growth and yield data. Thus, they need to be treated only as useful insights that can help identify potential problems and guide future studies.

- The current study is limited to point-scale analysis of root zone salinity and as such the results cannot be directly generalized for an entire field, without the assumption that the surface boundary conditions, initial conditions, and the soil physical and chemical properties observed at the sampling node used in the current analysis are replicated fully or substantially across the field.

References

- Ayers, R.S. and Westcot, D.W., (1985). *Water Quality for Agriculture*. FAO Irrig. Drain. Paper 29.
- Cornel University (accessed March 2020). *Certified Crop Advisor Study Resources, Soil and Water Management*. <https://nrcca.cals.cornell.edu/soil/CA2/CA0212.1-3.php>.
- Corwin, D.L. (2003). Soil Salinity Measurement. *Encyclopedia of Water Science*, 10.1081/E-EWS 120010191.
- Corwin, D.L., Rhoades, J.D., and Simunek, J. (2007). Leaching Requirement for Soil Salinity Control: Steady-State Versus Transient Models. *Agric. Water Mangt.*, 90(2007):165-180.
- Deverel, S.J. and Fuji, R., (1990). *Chemistry of Trace Elements in Soils and Groundwater*. Chapter 4. *Agricultural Salinity Assessment and Management*, Tanji, K.K. (ed.), ASCE, ASCE Manuals and Reports on Engineering Practice No. 71.
- Essington, M. E. (2005). *Soil and Water Chemistry, an Integrative Approach*. CRC Press, New York, NY.
- Feddes, R.A., Kowalik, P.J., Zaradny, H. (1978). *Simulation of Field Water Use and Crop Yield*. John Wiley & Sons, New York, NY.
- Goncalves, M.C., Simunek, J., Ramos, T.B., Martins, J.C., Neves, M.J., Pires, F.P. (2006). Multicomponent Solute Transport in Soil Lysimeters with Waters of Different Quality. *Water Resour. Res.* 42, W08401, doi:10.1029/2005WR004802.
- Hanson, B.R., Grattan, S.R., and Fulton, A. (2006). *Agricultural Salinity and Drainage*. University of California Irrigation Program, University of California, Davis.

- Hoffman, G. J. and van Genuchten, M. TH. (1983). *Soil Properties and Efficient Water Use: Water Management for Salinity Control*. Taylor, H.M., Jordan, W.R., and Sinclair, T.R. (eds.). Limitations and Efficient Water Use in Crop Production, American Society, of Agronomy, Madison, WI, 73-85.
- Hunsaker, D.J., Fitzgerald, G.J., French, A.N., Clarke, T.R., Ottman, M.J., Pinter, P.J. (2017). Wheat Irrigation Management Using Multispectral Crop Coefficients: I. Crop Evapotranspiration Prediction. *Trans ASBE*, 50(6):2017-2033.
- Jurinak, J.J. (1990). *Chemistry of Salt Affected Soils and Waters. Chapter 3. Agricultural Salinity Assessment and Management*, Tanji, K.K. (ed.) ASCE, ASCE Manuals and Reports on Engineering Practice No. 71.
- Maas, E.V. (1990). *Crop Salt Tolerance. Agricultural Salinity. Chapter 13. Agricultural Salinity Assessment and Management*, Tanji, K.K. (ed.) ASCE, ASCE Manuals and Reports on Engineering Practice No. 71.
- Maas, E.V. (1993). *Testing Crops for Salinity Tolerance. Proc. Workshop on Adaptation of Plants to Soil Stresses*. Marienville, J.W., Baligar, B.V., Duncan, R.R., and Yohe, J.M (eds.). INSTROMIL. Pub. No. 94-2, Univ of NE, Lincoln, NE, August, 1993.
- Maas, E.V. and Hoffman, G.J. (1977). Crop Salt Tolerance – Current Assessment. *J. Irrig Drain. Div*, ASCE, 103(IR2):115-134.
- Maas, E.V. and Poss, J.A. (1989). Salt Sensitivity of Wheat at Various Growth Stages. *Irrig. Sci.* 10:29-40.
- North East Region Certified Crop Advisors (Accessed 2020). *North East Region Certified Crop Advisors: Study Resource, Soil and Water Management*, <https://nrcca.cals.cornell.edu/soil/CA2/CA0212.1-3.php>
- Oster, J.D., Letey, J., Vaughan, P., Wu, L., and Qadir, M. (2012). Comparison of Transient State Models that Include Salinity and Matric Stress Effects on Plant Yield. *Agric. Water Mangt.*, 103(2012):167-175.
- PC-Progress (Accessed 2020). Molding Salinity with the Standard and UNSATCHEM Modules of HYDRUS-1D. <https://www.pc-progress.com/en/Default.aspx?h1d-tutorials#k9>
- Ramos, T.B., Simunek, J., Goncalves, M.C, Martins, J.C., Prazeres, A., Castanheira, N.L., Pereira, L.S. (2011). Field Evaluation of a Multicomponent Solute Transport Model in Soils Irrigated with Saline Waters. *J. Hydrol.* doi:10.1016/j.jhydrol.2011.07.016.

- Rhoades J.D. (1974). *Drainage for Salinity Control. Chapter 16. Drainage and Agriculture. van Schilfhaarde, J. (ed.). Agronomy 17, American Society of Agronomy. 433-461.*
- Rhoades, J.D. (1982). *Reclamation and Management of Salt-Affected Soils after Drainage. Proceedings of the First Annual Western Provincial Conf., Rationalization of Water and Soil Res. and Management. Lethbridge, Alberta, Can., Nov. 27-Dec. 2; 123-197.*
- Rhoades, J.D. (1990). *Overview: Diagnosis of Salinity Problems and Selection of Control Practices. Chapter 2. Agricultural Salinity Assessment and Management, Tanji, K.K. (ed.), ASCE, ASCE Manuals and Reports in Engineering Practice No. 71.*
- Rhoades, J. and Loveday, J. (1990). *Salinity in Irrigated Agriculture In: B. A. Stewart and D. R. Nielsen, (eds.), Irrigation of Agricultural Crops, Vol. 30, Monograph, American Society of Agronomy, Madison, 1990, pp. 1089-1142.*
- Richards, L.A. (1954). *Diagnosis and Improvement of Saline and Alkali Soils. USDA, Agric. Handbook 60, Washington, D.C.*
- Robbins, C.W. (1990). *Field and laboratory Measurements. Chapter 10. Agricultural Salinity Assessment and Management, Tanji, K.K. (ed.), ASCE, ASCE Manuals and Reports in Engineering Practice No. 71.*
- Robbins, C.W., and Carter, D.L. (1983). Selectivity Coefficients for Calcium-Magnesium-Sodium-Potassium Exchange in Eight Soils. *Irrig. Sci.* 4:95-102.
- Robbins, C.W., Jurinak, J.J., and Wagenet, R.J. (1983). Calculating Cation Exchange in Salt Transport Model. *Soil Sci. Soc. Am. J.*, 44:1195-1200.
- Sanchez, C.A. and Silvertooth, J.C. (1996)
- Simunek, J., Sejna, M., Saito, H., Sakai, M., and van Genuchten M.Th. (2013). *The HYDRUS-1D Software Package for Simulating the One-Dimensional Movement of Water, Heat, and Multiple Solutes in Variably-Saturated Media. Ver. 4.17.* Depart. of Env. Sci. University of California Riverside, Riverside, CA.
- Simunek, J. and Suarez, D.L. (1996). Sodic Soil Reclamation Using Multicomponent Transport Modeling. *J. Irrig. Drain Eng.*, ASCE, 123(5):367-376.

- Simunek, J., Suarez, D.L., and Sejna, M. (1996). *The UNSATCHEM Software Package for Simulating One-dimensional Variably Saturated Water Flow, Heat Transport, Carbon Dioxide Production and Transport, and Multicomponent Solute Transport with Major Ion Chemistry*. Version 2.0, Res. Rep. 141. US Salinity Lab., ARS, River side, CA, 186 pp.
- Tanji, K. (1990). *Nature and Extent of Agricultural Salinity. Chapter 1. Agricultural Salinity Assessment and Management*, Tanji, K.K. (ed.), ASCE, ASCE Manuals and Reports on Engineering Practice No. 71.
- University of California Committee of Consultants (1974). "Guidelines for Interpretation of Water Quality for Agriculture." *University of California, Davis*, 13p.
- Wesseling, J. G., Elbers, J.A., Kabat, P., and van den Broek, B.J. (1991). *SWATRE: Instructions for Input, Internal Note*. Winand Staring Centre, Wageningen, the Netherlands.